2
8-30-79

LA-7734-PR
Progress Report

Collective Ion Acceleration

October 1977—September 1978

University of California

LOS ALAMOS SCIENTIFIC LABORATORY
Post Office Box 1663 | Los Alamos, New Mexico 87545

LA-7734-PR
Progress Report

Special Distribution
Issued: July 1979

Collective Ion Acceleration

October 1977—September 1978

R. J. Faehl
B. B. Godfrey
W. R. Shanahan

CONTENTS

COLLECTIVE ION ACCELERATION
OCTOBER 1977 - SEPTEMBER 1978

by

R. J. Faehl, B. B. Godfrey, and W. R. Shanahan

ABSTRACT

Numerical and analytic studies of collective ion acceleration in intense relativistic electron beams are presented. Investigation of autoresonant acceleration has shown that radial beam inhomogeneities distort the slow cyclotron wave into a surface-localized mode. Variation of linear wave fields in inhomogeneous magnetic fields is strongly affected by this. Numerical studies of self-consistent cyclotron waves show the persistence of linear characteristics even at large amplitudes. Propagation of large amplitude waves has been observed over moderate distances in simulations without significant attenuation or nonlinear disruption.

Ion acceleration in virtual cathodes has also been studied. Insights into both formation and late time dynamics have been gained. Increased virtual cathode understanding is being pursued toward defining optimal configurations.

Future plans are outlined.

I. SUMMARY

Collective ion acceleration in intense relativistic electron beams is one of the most promising and ingenious applications yet proposed for pulsed power technology. It is also still highly conjectural. Successful generation of significant currents of heavy or light ions to energies of several hundred MeV per nucleon in a compact and relatively inexpensive system would find ready uses in electronuclear breeding, inertial confinement fusion, basic nuclear

science, medical and materials research. In fact, the extent of its applications is difficult to gauge because no source has ever combined the energy and current which these devices promise to yield. Continuing research is needed to bring any collective acceleration concept to fruition, however. At Los Alamos Scientific Laboratory (LASL), we are engaged in an intense theoretical effort to understand and evaluate several of the most promising schemes.

The autoresonant accelerator, conceived by Austin Research Associates (ARA),[1] is a proposal to trap ions in large cyclotron waves carried by a relativistic electron beam. Acceleration is achieved by spatially varying the magnetic field in a waveguide. Although this is conceptually simple, there are extensive unresolved questions about wave coherence, propagation in unneutralized beams, and nonlinear phenomena, all of which seem capable of disrupting the cyclotron fields. Conventional, charge-neutral plasmas are so rich in wave-wave and wave-particle interactions that large-amplitude monochromatic waves have little trouble spreading their energy over broad wave and/or particle spectra. This experience had induced initial pessimism on the prospects for a scheme requiring narrow band propagation for up to 10 meters. Extensive numerical simulation at both LASL and ARA has shown the feasibility of growing such waves, however. LASL studies have furthermore indicated that extraction from the amplifier can be accomplished with little difficulty and that propagation over moderate distances induces only minimal attenuation.[2] The reason why long coherence scales can occur is intimately tied to the nature of unneutralized electron beams. The single species medium does not possess low-frequency modes to facilitate wave and particle scattering, while the wave phase velocity is too far removed from particle velocities ($v_e \cong c$) to permit direct wave-particle interactions. The only other sources of wave decay are three- and four-wave couplings and intrinsic phase mixing, which are fairly weak in high-density beams. Consequently, the required beam wave coherence does not automatically mitigate against collective traveling wave accelerators.

The importance of beam nonneutrality must be emphasized when considering collective accelerator characteristics. Large self-fields, for instance, lead to uniquely determined equilibria with significant radial gradients in energy and rotation. Self-consistent cyclotron waves have been demonstrated to be much more surface localized than previously believed. Further investigations at LASL indicate that this strongly affects the wave accelerating fields in both homogeneous and spatially varying magnetic fields.[3] One result of this is

that smaller fields will be available but that they will not depend as strongly on cyclotron wavelength.

Other collective acceleration mechanisms have also been investigated at LASL. One of the more interesting involves formation of a virtual cathode in the vicinity of a plasma sheath. Virtual cathodes form when beam current is greater than can be sustained by the waveguide. The ensuing beam disruption effectively transforms beam kinetic energy into locally intense axial fields. These have been proposed as the source of collectively accelerated ions measured in many experiments, where ions at 2-3 times the beam energy occur. Numerical simulation of representative configurations yielded the ion energy spectra, but without the electrostatic characteristics commonly taken to be the accelerating source mechanism. These continuing investigations promise to yield entirely new interpretations for this class of experiments, with concomitant insights into their optimization.

Methods have also been suggested for moving the virtual cathode to accelerate negative ions.[4] Numerical simulations have demonstrated this under somewhat artificial conditions. There are still questions as to the viability of this scheme, but enough progress has been made to warrant continued investigation, albeit at a low level.

Study of the complex, self-consistent dynamics of nonneutral relativistic beams requires sophisticated numerical tools. We have developed an exceptionally powerful and flexible code for treating relativistic charged particle beams, CCUBE. CCUBE is a two-dimensional, fully electromagnetic, relativistic particle-in-cell simulation code. Its implementation in generalized orthogonal curvilinear geometry is especially useful in simulation of complex configurations which frequently arise in collective acceleration schemes. This capability is further enhanced through employment of a Galerkin particle algorithm. With suitable density weighting, the algorithm simplifies calculation of complicated boundaries.[5]

II. PROGRESS DURING FY78

Computational and analytic research on collective ion acceleration at LASL during the past year has concentrated on understanding the physics of the Autoresonant Acceleration concept, while supporting the feasibility experiment of it being conducted by ARA. We had previously demonstrated self-consistent wave growth relevant to autoresonant acceleration in numerical simulations. During

the past year, we have studied the extraction, propagation, and nonlinear characteristics of self-consistent cyclotron waves suitable for autoresonant acceleration. We continued numerical studies of small-amplitude waves to infer properties during inhomogeneous propagation, and unexpected results were obtained. To complement our previous helical wave-growth studies, we undertook a detailed linear study of an alternative growth mechanism, the inductive loop. Several alternate collective acceleration mechanisms were also considered at LASL during the last year. Further study has shown the traveling virtual accelerator may yet be feasible. Studies directed toward understanding experimentally observed acceleration associated with virtual cathodes was also initiated. Finally, a low-level effort was continued on the LASL-originated concept of a temporally phase-modulated accelerator.

A. Autoresonant Accelerator

Previous LASL studies of the autoresonant accelerator have shown that large-amplitude cyclotron waves can be grown in a helical waveguide, that relativistic beams can propagate in spatially decreasing magnetic fields, and that collective acceleration of a small number of ions is possible in such fields. The waves employed in this last effort were introduced artificially. Extensive numerical analysis of the linearized cyclotron waves, conducted in conjunction with the full simulations, however, shows that the radial structure of true eigenmodes is highly localized on the beam surface. Careful examination of the artificially excited waves in the simulation indicated that they probably contained large continuum, as opposed to discrete, mode components. Thus, while the simulation waves propagated in satisfactory agreement with linear theory, there were large uncertainties as to whether their overall behavior was representative of self-consistent laboratory waves. To address this problem, we extended our linear theory calculations to investigate the effects of inhomogeneous propagation on realistic small-amplitude cyclotron waves.

Numerical analysis of linear eigenmodes in intense relativistic electron beams has revealed the importance of using self-consistent beam equilibria. Inclusion of radial variations in γ, due to space-charge effects, and rotation can radically distort modes, especially the slow-beam cyclotron one in which we are mainly interested. This can be seen clearly by considering certain characteristics, such as the ratio of radial beam modulation to axial electric field. It should be remembered that while absolute magnitudes have no meaning in linear theory, the relative magnitudes are fixed and highly characteristic of

the wave. The above-mentioned ratio, moreover, is singularly relevant to collective acceleration, for it relates the amount of beam surface modulation to the accelerating electric field. For typical beam and wave parameters, the difference between including radial γ-variations and assuming constant γ is a reduction of the axial electric field by a significant factor, i.e., 1/3 to 1/4, for a given surface modulation. The correct equilibrium is important for accurate calculation of cyclotron wave properties. As the wave propagates along a decreasing magnetic field, it is, therefore, crucial that self-consistent equilibrium changes are accounted for.

The numerical approach used by us started with determination of a self-consistent eigenmode for a given homogeneous magnetic field, current, and density profile. Then a new magnetic field was chosen and the corresponding beam equilibrium calculated, under assumption of constant current, angular momentum, and energy. The original wave information was included through the above conservation laws, plus conservation of wave energy flux. In cases of only spatially varying fields, the frequency is also a constant of the motion. For sufficiently weakly varying quantities, this procedure allows calculation of local dispersion and eigenmode structure. The results of such calculations differ significantly from simpler heuristic estimates of inhomogeneous propagation. Taking a wave which is initially in a high field region (short wavelength) and following it in a decreasing field, we find that its phase velocity, v_{ph}, does not depart markedly from simple linear expectations, i.e.,

$$v_{ph} = v_0/(1 + \Omega/\gamma\,\omega_0) \quad , \tag{1}$$

where $\Omega = eB_0/mc$. However, in regard to its wavefield, the simple guess was that the potential of the wave would remain constant, so that

$$E_z \propto k\phi_0 \quad , \tag{2}$$

that is, the field would decrease linearly with the magnetic field. This does not account for the nature of a beam cyclotron wave, however. Our detailed calculations indicate that E_z remains virtually constant as long as $kR_B \gtrsim 1$. When the wavelength becomes longer, Eq. (2), in fact, is reasonably good. This more accurate treatment also shows that a much larger beam modulation is required to produce the accelerating E_z field, however. Since stability limits

the effective relative modulation to roughly one-half the beam radius, or $\Delta R/R_B \cong 1/2$, there is a practical limit to the cyclotron wave magnitudes which can be used. Both factors must be included in designing the axial magnetic field variation, such that acceleration is accomplished in minimum distance with neither beam disruption nor particle de-trapping. These considerations are discussed in detail in Appendix A for typical solid beams and field parameters.

The above considerations were predicated on the validity of linear theory in realistic, radially inhomogeneous beams. Since the self-consistent results differ so quantitatively from those of simple model theory, it is important to determine which, if either, theory actually describes nonlinear, physical cyclotron waves.

We have previously demonstrated the simulation ability to grow large-amplitude cyclotron waves in a helical waveguide, so studying self-consistent waves was only a matter of extracting them into a smooth-walled guide. The advantage of employing a realistically terminated growth section was that the amplitude of the waves could be controlled by varying the length of the section. This also facilitated extraction. The primary concern over cyclotron wave extraction, and the reason matched terminations help, is that the unstable, growing eigenfields are modified by interaction with the helical waveguide fields. Thus, when the wave leaves a growth section, it must relax toward its stable state. It was feared that this nonadiabatic relaxation might distort or disrupt the coherent wave. With matched terminations, however, the waveguide fields are damped smoothly to zero by the end of the growth section. Residual fields not terminated on the helix were "soaked up" by a ring of resistive material outside the helix. With this arrangement, waves were observed to propagate freely from the growth section, with little distortion of the cyclotron fields. High-frequency electromagnetic noise was enhanced by extraction but at least part of this had a purely numerical origin. Even if physical, however, such noise could probably be controlled experimentally. The significant point is that the cyclotron fields remained quiescent and narrowband.

After extraction, we followed the wave relaxation for distances on the order of one meter. This is probably further than would occur in the proof-of-principle experiments, since the beam would pass into an adiabatic magnetic field compresser as soon after growth as practical. In the interest of studying the nonlinear structure of the waves, however, these and longer propagation studies are useful.

One of the first observations made about the relaxation process is that the fields suffer relatively little attenuation, only of order 10-20%. Self-consistent linear theory predicts that the ratio of beam modulation to axial electric field, $\Delta R/E_z$, is smaller for helically unstable cyclotron waves than it is for stable waves. Preliminary estimates had assumed that the modulation would remain constant, so transition to smooth-walled propagation would result in significant reductions in accelerating field. In fact, it is the field which is roughly invariant and the modulation which increased. This is beneficial in that larger fields are obtained, but worrisome with respect to wave contact with the walls. The observation is also consistent with self-consistent linear theory.

The ultimate test of linear theory consists of measurement of the radial wave profiles. Simple theory predicts a relatively flat, bulk perturbation while self-consistent theory gives a highly surface-localized wave. Since behavior of the wave in an acceleration section is quite different for the two theories, it is important to determine which describes large-amplitude cyclotron waves. Careful diagnosis of the simulations shows that the large-amplitude cyclotron waves are in good qualitative agreement with self-consistent theory. In fact, since measured uncertainties are magnified when one forms ratios, the magnitudes are in remarkably good quantitative agreement with linear theory. The major surprise is that nonlinear cyclotron waves, in these high-density beams at least, differ so little from their small-amplitude counterparts. Appendix B describes this work in more detail.

Attention has been focused on the $m = 0$ cyclotron wave in a solid beam because it is the desired acceleration mode and the projected beam configuration. However, in the growth section studied most exhaustively at LASL, the helical waveguide, various nonaxisymmetric modes ($m \neq 0$) are also destabilized. We have numerically examined nonaxisymmetric waves for stability with GRADR and found that the $m = 1$ possesses the largest growth increment of all $m \neq 0$ waves (Ref. Appendix C). In fact, for the current ARA experimental parameters, the $m = 1$ instability is significantly stronger than $m = 0$. Variation of the parameters, such as increase in magnetic field, can preferentially reduce $m = 1$ with respect to $m = 0$, but no high-current regime has been discovered yet in which $m = 0$ is the stronger of the instabilities. None of these studies can address the problem of nonlinear competition between the modes or give information about the final wave state, both of which may prove interesting topics for future

investigation. Until these are conducted, however, one must assume that linear theory will govern wave growth in the helix. This implies that care must be taken in designing the initial wave exciter so that excitation of $m = 1$ modes occurs at orders of magnitude lower level. Consideration should also be given to design of a spatial filtering network that will highly distort the unstable $m = 1$ waves while leaving the desired modes largely unaffected.

One of the more effective means found for suppressing the $m = 1$ instability was to use a hollow electron beam. This has also been suggested as a way of obtaining larger fields for a given modulation, ΔR. It will be remembered that self-consistent space-charge and rotation effects reduce the axial electric field by a significant factor compared with simple linear theory. The space-charge fields and rotation, however, are known to be much smaller in hollow beams than in solid beams with the same current and energy. It was, therefore, hoped that cyclotron eigenmodes in hollow beams would more nearly exhibit the behavior of simple linear theory.

GRADR studies of suitable cyclotron waves were made in hollow beams as a function of aspect ratio, that is $(R_{out} + R_{in})/(R_{out} - R_{in})$. Appendix C contains the description of this work. As this ratio was increased from 1 (solid beam) up to almost 10, it was observed that the ratio of modulation to field on the inner radius, $\Delta R/E_z|_{in}$, remained almost invariant. The total variation of this ratio was on the order of 30%, and the trend was toward increasing values (undesirable) with the highest aspect ratios. As disappointing as this result was, however, it was even worse when one considered that the E_z field fell off roughly at e^{+kr} as the axis was approached. The ratio of modulation to axial field was, therefore, considerably worse in hollow than in solid beams. It appears that the only advantage of hollow beams is reduction of $m = 1$ growth rates in the helix, while disadvantages include reduced accelerating field on axis and lack of radial containment for ions.

The helix is not the only slow-wave structure which has been considered for cyclotron wave growth. Inductive loop structures have also been studied, primarily by ARA. Their analysis, however, modeled the actual nonaxisymmetric structure with an effective impedance given in terms of lumped circuit parameters. There is nothing intrinsically wrong with this approach, and it is certainly a powerful technique for obtaining qualitative information about complicated structures. Its accuracy though depends on the expression used for impedance; low-frequency expressions can be quite different from high-frequency

ones. We, therefore, sought to check the earlier results by undertaking a more explicit, detailed study of this growth mechanism. The complex three-dimensionality of this structure eventually thwarted us, but not before we had been able to draw some interesting conclusions.

In Appendix D, we outline our explicit model of an inductive loop. The primary feature added to this analysis was that the coupling E_θ fields were zeroed out on the metallic loop, and finite only in the capacitive gaps on the loops. This is in contradistinction to the lumped parameter model, where it is distributed uniformly around the loop. Because the azimuthal localization of the E_θ field can impose a periodicity on the solutions, there was reason to believe that certain nonaxisymmetric modes ($m \neq 0$) would be distorted, others enhanced, while in general modes with different m could be coupled. To implement this numerically in GRADR, it was necessary from a practical standpoint to treat loops with infinitesimal radial extent. This significantly reduced the capacitance, which was then compensated by filling the space outside the loop with a dielectric material (ε = 30-60). While the dielectric served to slow the guided waves down to desired velocities, it must be noted that it did not completely replicate the cavity-like field structure of a true capacitative plate structure. Nevertheless, with a waveguide structure spanning z, θ, and r dimensions, a fully three-dimensional treatment would be required, and such numerical tools are not available at present. The numerical model described in Appendix D can be said to more accurately model the azimuthal structure of the ARA-envisioned waveguide, while being less accurate in treating the coupling.

Comparison of numerical growth results are given in Appendix E. The distributed parameter model yields much larger growth rates than our periodic gap one. This is not unreasonable, since correct treatment of the three-dimensional fields in the region outside the loops is probably not represented with the high dielectric medium employed by us. The E_θ field on the loop is the characteristic field for this instability. It is 4-5 times larger with the low-frequency boundary conditions than with the azimuthally periodic ones, thus the larger growth rate. Since the calculations were otherwise identical, we conclude that the lumped parameter model can, at least under some circumstances, overestimate the strength of the loop-driven instability. Our calculations, however, suffer from not being completely self-consistent and three-dimensional. The possibility of writing a three-dimensional numerical linear code is being pursued at a low level by us, but until it, or a similar numerical tool is

developed, accurate evaluation of inductive loop structures can only be accomplished empirically.

Cyclotron wave amplifiers are needed by an autoresonant accelerator for the same reason collective acceleration is being pursued in the first place: external power supplies can not excite RF traveling waves much larger than 10^4 V/cm. Since ARA hopes to conduct proof-of-principle experiments with wave magnitudes of 2.5×10^5 V/cm, it is apparent that cyclotron waves excited to their largest level by external sources must still be grown. While numerical studies at LASL and ARA indicate that such a beam wave amplifier can probably be built and operated as required, the need to amplify wave powers by up to four orders of magnitude leads to high-gain problems, such as feedback, amplification of unwanted modes, and power handling on the structure. These would all be ameliorated if larger waves could be excited initially. Toward this end, the suggestion has been advanced that self-fields of the beam might be used to self-excite a suitable cyclotron wave.

Various structures have been numerically evaluated at LASL for use as self-driven antennas. These are described in Appendix F. The most successful examined to date consists of a right circular cavity one-half wavelength long connected with a similar length of "unterminated" helix. This structure excites a narrow band cyclotron wave signal with a magnitude on the order of 5×10^4 V/cm. The excitation is due to zero-order "grounding current" which rings for a long period because of improper termination of the helix, (Ref. Appendix H of 1977 LASL Annual Report). Such a configuration is also very efficient at exciting zero-frequency, nontraveling waves, as have been all "self-driven antennas" to date. Although self-excitation of cyclotron waves has been shown to be feasible, the concept will have only academic interest until means of removing zero-frequency disturbances are found.

Finally, flashover problems with the ARA beam machine have resulted in delays with operating at 3 MeV. As an interim measure, experiments will be conducted with reduced parameters, such as beam energy of 2.0-2.25 MeV and current 15-20 kA. We have reformulated our linear wave studies consistent with these new parameters. The results, reported in Appendix G, indicate that not only can programmatic goals be achieved; they may actually be improved if both beam and guide radius are reduced by a factor of 2.

B. Alternative Collective Acceleration Approaches

Most of the LASL effort has been devoted to studying autoresonant ion acceleration, but a low-level effort has also been expended on alternative collective acceleration mechanisms. This work has focused on three particular schemes. The bulk of the effort has been devoted to study of virtual cathode acceleration in vacuum waveguides. While this has yielded best results to date, large uncertainties still exist about the acceleration mechanism. New results have also prompted re-examination of the traveling virtual cathode accelerator. While this scheme is still marginal, certain deleterious characteristics, which had mitigated against it, have been successfully resolved. The third scheme was the phase-modulated accelerator, originated at LASL and described in the FY77 annual report. This was pursued at a very low level during this year. Present indications are that its primary role may be in heavy ion fusion or as an injector into a high β accelerator.

Collective acceleration produced by forming a virtual cathode in vacuum is an attractive, simple configuration which has been experimentally demonstrated at many institutions. Performance typically involves acceleration of large numbers of ions (10^{12}-10^{14}) to roughly 1.5 times the beam energy, with a high energy tail out to 10 times the electron beam energy. While these are useful parameters for light-ion-driven inertial confinement pellets, they do not satisfy requirements for a medium-energy accelerator at present. Nevertheless, higher energy beam machines may soon be possible, and compact generation of, say, 200-MeV protons would find ready applications. The problem with this mechanism is that, despite widespread speculation, no quantitative model for the observed ion spectrum exists. Allusion is often made to a deep, steady potential, derived by Poukey and expanded upon by Olson. In many space-charge limiting simulations conducted both at LASL and at the Air Force Weapons Laboratory, however, no such well has even been calculated. Work was, therefore, undertaken to simulate a model configuration for collective ion acceleration. Since any acceleration results would be closely tied to virtual cathode dynamics, a detailed numerical study was decided upon to gain better understanding of this state.

The key results garnered from simulation of virtual cathodes were that (1) no steady potential well with depth greater than $mc^2(\gamma_0 - 1)$ was observed, (2) fluctuating potentials in excess of $mc^2(\gamma_0 - 1)$ were indeed measured, up to 1.7 $mc^2(\gamma_0 - 1)$, and (3) the magnitude of the peak potential correlates quite

well with a macroscopic recurrence period for the motion of the entire virtual cathode. This last is further associated with onset of electron reflection and possibly with the flux of potential fluctuations on the beam. A quantitative model for these results is still being formulated by us, but it is apparent that since no steady anomalous well exists, simple trapping arguments cannot be advanced to explain even the low-energy ion spectra.

The second phase of this numerical study consisted of using the virtual cathode to accelerate ions from a pre-existing plasma. A dense plasma slab ($n_p = 35.0\ n_0$) was initially located adjacent to the injection plane. Since it was much denser than the beam, space-charge fields were essentially neutralized in the plasma. To prevent charge depletion, however, the slab was made moderately thick, roughly 2-3 cm. This model configuration may be regarded as a crude analogue of the plasma formed from a Luce diode. The differences are appreciable, though, and it is possible that key features of the experiment are not represented here. More sophisticated plasma configurations are being considered at present, but no data is yet available on these. When the beam with supercritical current was injected through such a slab, it propagated freely until leaving the slab. Immediately upon exiting the plasma, it formed a virtual cathode. As expected, this virtual cathode possessed an average potential depth of only $|e\phi| \cong mc^2(\gamma_0 - 1)$. One possibly significant difference between these calculations and the metallic anode ones treated earlier was that the beam was highly two-stream unstable with the plasma. The plasma length was too short for beam disruption, but it certainly resulted in an enhanced fluctuation level on the beam. Whether this or interaction of ions with the well was responsible, the virtual cathode did not exhibit the regular oscillations which were correlated with potentials greater than $mc^2(\gamma_0 - 1)$.

Ions were found to be accelerated quite rapidly ($\Delta t \cong 100\ \omega_p^{-1}$) and over short distances ($\Delta z \cong 10\ c/\omega_p$) to energies of order $\varepsilon_{ion} \cong 1.5\ mc^2(\gamma_0 - 1)$. This was followed by a slower period of acceleration which was not localized to the virtual cathode. The virtual cathode evolution was furthermore different from previous, moving well models. Instead of charge neutralization occurring near the back of the potential well, enough ion current was accelerated to force neutralize the beam. Thus, the ion density need be only $n_i \cong n_0/\gamma^2$ rather than $n_i \cong n_0$. In consequence, the back edge of the potential exhibited little motion, but because propagation was facilitated by the ions, the potential possessed a flat bottom, extending from the original back edge out to the front

edge of the accelerated ions. While this does not enhance the electrostatic potential, ϕ, it can contribute significantly to the electromagnetic vector potential $\bar{A}$. In fact, ion acceleration in excess of $\varepsilon_{ion} = mc^2(\gamma_0 - 1)$ scales, though not linearly, with the measured quantity, $\partial\langle A_z\rangle/\partial t$, brackets indicating average over the fast time scale.

The mere fact that a monotonic increase in $\langle A_z\rangle$ occurs for constant current injection indicates that additional current must be flowing, and this is possible only because sufficient numbers of ions are accelerated to allow propagation. Velocity of the ions is not a major factor as long as $v_{ion} << c$. Motion of the partially neutralizing ion bunch, however, is important insofar as it increases the integral

$$\int_V J dV \quad ,$$

where

$$J = \sum_j n_j q_j v_j \quad .$$

For similar current configurations, the same current carrying volume will eventually be attained regardless of the velocity of the ions. This argument suggests the simulation result that ions with different masses reach the same energy as a function of distance. More analysis will be needed to understand the apparent numerical scaling with ion charge, Z, however. Both these results and the calculated ion energy spectrum are in agreement with experiments. Moreover, since the peak electrostatic potential is only of order the beam kinetic energy, the mechanism for ion acceleration to 2-3 times the beam energy, which we measure in the simulations, is clearly <u>not</u> a deep, steady electrostatic well. Inductive forces, neglected in previous analyses, are responsible for the excess acceleration above the beam kinetic energy. The role these may play in so-called "Luce geometry" experiments, where acceleration to ten times beam energy is commonly seen, is still moot at this time. The combination of inductive and electrostatic forces appears to be the mechanism for the bulk acceleration of ions $\varepsilon_{ion} = 1\text{-}3\ mc^2(\gamma_0 - 1)$, but to date no high-energy tail has been observed in our simulations. Pursuit of possible synchronous mechanisms to

explain the tail will continue at a low level. More detail on these studies can be found in Appendix H.

Further work on the Traveling Virtual Cathode mechanism conducted again in collaboration with the Air Force Weapons Laboratory is reported in Appendix I. This mechanism was discussed in the FY77 annual report (Appendix L). At the time of the previous report, only constant current injection had been simulated. Those calculations showed that a virtual cathode could be formed in the waveguide interior, but that it was subject to large irregular fluctuations in both position and magnitude. Subsequent simulations with linear current risetime, however, have demonstrated that those undesirable characteristics were not intrinsic features of the virtual cathode. On the contrary, increasing the current at a sufficient rate yields smooth, monotonic motion of the virtual cathode toward the metallic foil. The observed acceleration was too high to trap realistic ions, but simulations with unphysically low mass-to-charge ratios showed almost complete negative ion capture by the virtual cathode fields from an initially neutral plasma slug. Though ion acceleration under artificial conditions has been numerically demonstrated, extrapolation to physically realizable conditions requires further study. Specifically, while acceleration of the virtual cathode can be reduced by increasing the current risetime, it is not certain that turbulent fluctuations will not reappear with the slower velocity. Analysis is also required to determine whether the virtual cathode fields ($E \cong 2 \times 10^5$ V/cm) will strip negative ions to a neutral state.

The final alternative acceleration scheme, phase-modulated acceleration, has received only nominal attention during the past year. Preliminary investigations indicated the concept should be most viable at ion velocity, $v_i \lesssim 0.5$ c. In the low-velocity regime, however, it seemed quite competitive with other collective acceleration schemes. These considerations strongly suggest applications in heavy ion fusion. Since the initial heavy ion velocity, moreover, is extremely small, the possibility of dephasing zero-frequency cyclotron waves was examined. These are extremely easy to excite in a relativistic electron beam, at magnitudes of $1\text{-}2 \times 10^5$ V/cm. Calculations on the test particle code NOVA indicated promise, but accurate evaluation of this particular mode of acceleration must await full, self-consistent simulation. Those calculations are planned for the coming year.

C. Code Development

Numerical studies form a significant element of collective acceleration research at LASL. As a complement to analytic studies, these permit treatment of both self-consistent nonlinear states and more generalized linear ones with boundary conditions. The changing status of evolving research calls for flexible, general-purpose codes and smaller, more specific codes to address particular problems or conditions.

CCUBE, a two-dimensional relativistic particle simulation code written for the express purpose of studying electron beam physics, is the primary numerical tool for our investigations. Although it has been discussed previously, projected research efforts have dictated a series of significant modifications. During the past year, the "particle pushing" routines have been completely rewritten to employ an arbitrary order Galerkin algorithm. This employs only fields, so potentials are no longer needed in the code. By incorporating magnetic field forces in a series of microsteps, electromagnetic effects are more accurately treated. This permits omission of current corrections needed to preserve the continuity equation. In the process, a unique particle weighting scheme has been implemented which greatly simplifies treatment of complicated boundaries. Diode design calculations, conducted within a different context, have ably demonstrated the flexibility of this new version of CCUBE. The code changes are described in Appendix J.

While many new classes of problems can now be studied with CCUBE, this version does exhibit a higher level of longitudinal fluctuations. The magnitude seems acceptable at present but can probably be reduced by incorporation of higher order weighting splines. Such a course, however, would make boundary treatments more difficult. In short, a series of innovative changes have been made in CCUBE which should facilitate simulation of geometrically complex autoresonant accelerator configurations, but which have also degraded certain noise characteristics. Colloquially, one does not get something for nothing. Other modifications can probably be made to improve those characteristics if it should appear necessary. For the coming year, though, no problems are anticipated and a stable code format is expected.

The GRADR code has proved highly useful for studying linear phenomena on self-consistent beam equilibria. In the past year, improvements have been made to it for examination of non-axisymmetric ($m \neq 0$) helix modes, non-axisymmetric boundaries (for loop drivers), hollow beams, and inhomogeneous

wave propagation within a WKB framework. These topics are discussed in more detail in the appropriate appendices.

Such a code is essential for mapping out linear parameter regimes which can then be followed nonlinearly in CCUBE simulations. Nevertheless, certain problems are intrinsically three-dimensional. The ARA loop drive geometry is one such example. In a search for more general numerical tools, we discovered an overall paucity in this area. Since the need is evident, it appears that we shall have to devise a code for treating three-dimensional boundaries and/or beam equilibrium. The time scale for this undertaking, however, is difficult to estimate. Until such a code has been written and debugged, analytic expressions and estimates must suffice.

Other smaller codes are commonly written to address specific problems, but do not have general applicability. While the list of these is extensive, most are never documented and quickly fade into obscurity. The ability to efficiently produce such programs nevertheless does aid in overall study of collective acceleration problems.

III. PLANS FOR FY79

The Autoresonant Accelerator feasibility experiment has begun to generate preliminary data. During the coming year, these data will be used to resolve questions of beam propagation and quality, wave growth and extraction, and ion loading. We at LASL intend to conduct analytic and numerical studies on these same issues in such a manner as to provide support for the experiment without neglecting key basic physics questions. Additional work will also be performed, as time permits, on alternative acceleration approaches. Elucidation of these mechanisms may later permit their employment in conjunction with autoresonant acceleration, such as using virtual cathodes for ion injection. CCUBE, GRADR, and other smaller codes will undergo continuing minor modifications, but will be essentially stable. Conversion from the CHAT compiler to a more standard Extended FORTRAN one (FTN) should reduce execution times and enhance code portability.

In the previous year, work was concentrated on wave growth and extraction. We will exploit this experience to investigate propagation of beam and waves into spatially varying magnetic fields. Two parallel efforts will be conducted. In the first, we will employ beams of high quality to study compression and compression-induced modifications to laminar and wave-carrying beams. The other

line of research will study nonideal beams and their effect on wave-growth and propagations.

If an electron beam propagates into magnetic field gradients which are long compared to its larmor radius, beam characteristics will change smoothly and adiabatically. This implies that the product of field times beam radius squared Ba^2, will remain constant, and also that the ratio of transverse energy to field strength will be invariant. While cold beams should remain cold, zero-frequency modulations will increase in magnitude. If these latter become too peaked, they may phase mix and enhance the random scatter on the beam. The first investigations will, therefore, examine compression of equilibrium beams to determine scale lengths needed to obtain minimum beam heating.

Compression of cyclotron waves may present more problems than simple laminar compression since the waves possess both intrinsic radial and axial scale lengths. Self-consistent linear studies of cyclotron waves have already shown that wave modulation becomes progressively more surface-peaked as wavelength is decreased. Simulation of nonlinear waves show this trait in good agreement with linear theory. The relative modulation is, therefore, expected to increase during compression. Coherence can not be lost during this stage, however, and field magnitudes must show minimal attenuation. Degraded wave quality will exacerbate any problems with ion loading, which is planned to follow immediately after the compression. Goals here are to characterize waves during compression and determine most favorable conditions.

The above studies presuppose good beam quality at the onset. Before entering the compression stage, however, the beam must be extracted from a diode, propagate through a zero-frequency suppression section, then a wave growth section, and finally be extracted from the growth section. Beam quality in the later phases of an accelerator can be significantly degraded by the earlier stages. Some estimate of this can be obtained from static diode codes through analysis of individual trajectories. The full noise spectrum though requires treatment of electromagnetic as well as electrostatic fluctuations, so we intend to study beam quality effects with self-consistent two-dimensional simulations.

The first effect experienced by the beam as it passes through a metallic anode ground plane is radial pinching. This is followed by expansion as the beam bounces around its radial equilibrium position, that is, zero-frequency cyclotron bouncing. The magnitude of bouncing depends on waveguide radius and guide magnetic field as well as mean beam radius, energy, rotation, angular

divergence and temperature. Experimental conditions dictate the field, waveguide radius and total beam energy. Diode design and foil scattering determine the other quantities, but these are not known precisely a priori and are subject to shot-to-shot variation. Unless beam characteristics satisfy all equilibrium conditions when entering the waveguide, bouncing will result, and bouncing is undesirable. This has resulted in design of a nonadiabatic field transition section near the anode to suppress it. It is reasonable that success of such a section will depend on ability to match the field variation with actual beam parameters. Propagation of a laminar beam, for instance, through the nonadiabatic section will certainly induce bouncing. The sensitivity of a given field design to beam conditions will be one of the first projects undertaken in this study. For a given energy and current, we will examine the resulting beam state as a function of both initial divergence and beam scatter (i.e., temperature). If necessary, new field configurations will be examined. As a sidelight, previous studies at LASL have indicated the viability of certain self-driven antenna configurations, subject to the condition that zero-frequency waves can be removed from the beam afterward. This will also be pursued if manpower is available.

Once beam characteristics leaving the transition section are determined, they will be used for helical wave growth simulations. The effects of nonideal beam quality will be inferred from amplifier performance. Reduced extraction efficiency, if any, will also be measured. Experimental parameters will be used to provide touch points between calculation and measurement.

After the above objectives have been satisfied, preliminary studies will be undertaken to determine feasibility of different schemes for loading ions into the troughs of cyclotron waves. This project will tie in directly with planned simulations of an alternate mechanism, the Temporal Phase Modulation accelerator. Becuase its conceptual simplicity translates into calculational simplicity, there should be little problem in simulating this configuration. If it is viable, a background plasma will be initialized at a location conducive for ion trapping. An interesting question should be resolved when the local beam energy is large enough so that $n_i \cong n_e/\gamma^2$, that is, Budker's condition for force-free equilibrium is satisfied. Beam disruption may occur under those conditions due to localized pinching. Results of these calculations will apply directly to autoresonant acceleration in the high ion density limit. This

project should be nearing completion by the end of the second quarter of this fiscal year.

Several CCUBE developments are scheduled to be completed during the coming year, though none of the magnitude of conversion to an entirely new algorithm which was accomplished in the previous year. Continuing characterization of this algorithm is occurring as new types of calculations are undertaken. At this point, however, it appears that CCUBE is stable and will undergo only minor changes in the foreseeable future. One change which should not affect CCUBE usage is conversion to CDC-Extended FORTRAN and the FTN compiler. Laboratory estimates are that computer throughput will increase by 30% with this compiler. While such figures neglect variations from code-to-code, we hope to realize some reduction in problem run time. Conversion will also facilitate CCUBE usage on the CRAY-1 computer and at other facilities. Finally, low-level efforts in pursuit of three-dimensional calculation will continue during the coming year. Unexpected problems arising from the ARA experiments will be addressed as time and manpower permits.

A tentative schedule for LASL activities in FY79 is depicted on the following page. The serial and exploratory nature of the planned research is such that changes may be made, as required on the basis of evolving results. The manpower for this schedule is estimated to be between 2.0 and 2.5 man years.

ACKNOWLEDGMENTS

This document describes research performed during FY78 on collective ion acceleration in intense relativistic electron beams by Group T-15, Intense Particle Beam Theory, of the Los Alamos Scientific Laboratory . The work was sponsored by the U. S. Army Ballistic Missile Defense Advanced Technology Center and by the U. S. Department of Energy. We are indebted to these agencies for their support.

Special thanks is due to Dr. Larry Havard, who supervised the Advanced Technology Center's program and provided both technical and administrative guidance. Funding from DOE's Division of Military Applications was provided through the LASL Supporting Research program.

Within the Los Alamos Scientific Laboratory, Thomas Hayward coordinated efforts supported by the Ballistic Missile Defense Advanced Technology Center. This report was prepared with the assistance of Nathana Haines, Group Secretary.

TENTATIVE WORK PLAN FOR FY79

Oct. - Dec.	Jan. - Mar.	Apr. - Jun.	Jul. - Sep.

Beam Compression/Expansion ——————→

Cyclotron Wave Deceleration ——→

Zero-Frequency Suppression ——→

Scattered Beam Effects ——→

Temporal Phase Modulation ——→

Virtual Cathode Acceleration Studies ——→

Ion Loading ——→

REFERENCES

1. M. L. Sloan and W. E. Drummond, "Autoresonant Accelerator Concept," Phys. Rev. Lett. 31, 1234 (1973).

2. R. J. Faehl, W. R. Shanahan, and B. B. Godfrey, "Nonlinear Characteristics of Cyclotron Waves in an ARA Configuration," to appear in Proc. 3rd Int. Conf. on Collective Methods of Acceleration, Laguna Beach, California, May 22-25, 1978.

3. B. B. Godfrey and B. S. Newberger, J. Appl. Phys., to be published.

4. R. B. Miller, R. J. Faehl, T. C. Genoni, and W. A. Proctor, "Collective Ion Acceleration in a Traveling Virtual Cathode," IEEE Trans. Nucl. Sci. NS-24, 1648 (1977).

5. B. B. Godfrey, "Application of Galerkin's Method to Particle-in-Cell Plasma Simulation," Proc. 8th Conference on Numerical Simulation Plasmas, Monterey, California, June 28-30, 1978.

APPENDIXES

This section contains eleven appendixes describing in detail various aspects of collective ion acceleration. Each is self-contained. Section II of the report summarizes the appendixes, pointing out significant features and tying the results together.

APPENDIX A

WAVE AMPLITUDE VARIATION AND ENERGY FLOW IN AUTORESONANT COLLECTIVE ION ACCELERATION

To be published in the Journal of Applied Physics
August 1979

WAVE AMPLITUDE VARIATION AND ENERGY FLOW IN AUTORESONANT COLLECTIVE ION ACCELERATION

by

Brendan B. Godfrey and Barry S. Newberger

ABSTRACT

An expression for the energy of small amplitude waves in a radially inhomogeneous, cold fluid, unneutralized, relativistic electron beam is obtained in terms of the wave amplitudes. The result is employed together with conservation of wave energy to determine how the axial electric field strength and beam edge modulation associated with slow cyclotron waves change with position in an electron beam propagating along the adiabatically spatially decreasing magnetic guide field of an autoresonant collective ion accelerator. The resulting axial profiles are found to depart markedly from those of earlier, radially homogeneous beam calculations. Possible impacts of these findings on a planned autoresonant acceleration feasibility experiment are discussed.

I. INTRODUCTION

Autoresonant collective ion acceleration[1,2] is among the most thoroughly investigated proposals for utilizing the intense fields of high-current relativistic electron beams to accelerate light or heavy ions to energies of hundreds or, perhaps, thousands of MeV per nucleon.[3] Autoresonant acceleration employs an electron beam propagating in vacuum along a magnetic guide field which slowly diverges spatially (and thereby decreases in magnitude) from the input to the output end of the ion acceleration region. Linear theory predicts that slow cyclotron waves launched at the input end will increase in phase velocity as they move into regions of weaker magnetic field. Provided the guide field strength is appropriately tailored axially, ions trapped by the electrostatic fields of the cyclotron waves can be expected to accelerate with the waves up to quite high energy.

Since efficient trapping of the ions depends on a balance between the axial electric field of the cyclotron wave and the rate of wave phase velocity change, it is important to understand the adiabatic variation of cyclotron wave amplitude down the ion accelerator. This problem is intrinsically nonlinear due to the large amplitudes of the cyclotron waves, radially inhomogeneous due to the equilibrium fields and finite extent of the electron beam, and axially inhomogeneous due to variation of axial magnetic field strength and beam parameters tied to it. Detailed answers probably require extensive multidimensional computer simulations, and such work is in progress.[4-6] Nonetheless, one can expect to obtain valuable insight by investigating the properties of small amplitude, linearized waves in an axially uniform beam equilibrium and relating wave amplitudes at different magnetic field strengths by the requirement that wave energy be conserved as the wave moves down the ion accelerator. Until recently, the further approximation that the beam equilibrium be radially uniform out to a sharp edge was required so that homogeneous plasma linear theory could be applied. In this limit the axial electric field of the slow cyclotron mode was found to vary linearly with magnetic guide field.[7]

In order to obtain the properties of small-amplitude waves in more realistic, radially inhomogeneous equilibria, we have developed a computer program to solve numerically the fourth-order system of radial differential equations for eigenmodes of any cold fluid relativistic particle beam equilibrium which depends on radius only.[8] A particularly striking conclusion of studies based on this computer code is the strong effect of beam radial kinetic energy inhomogeneity, caused by space-charge, on the radial structure of cyclotron waves. Particle motion and most field components associated with the waves are highly localized to the beam surface. This contrasts with the homogeneous model, which has both the perturbed fluid and the perturbed field components as Bessel functions in radius. With such a disparity between the eigenmode structures from the two models, it would be surprizing not to find differences in their predictions for the adiabatic variation of wave amplitude as cyclotron waves move through the ion accelerator. In this paper we show that, for realistic solid beam equilibria, the slow cyclotron wave axial electric field strength is nearly constant in the strong guide field region, and only approaches the linear dependence of the homogeneous model where the magnetic guide field is sufficiently weak that the cyclotron wavelength much exceeds the beam radius.

A cyclotron wave train appears in space as a periodic modulation of the beam envelope.[2] It is desirable to know the variation in amplitude of the modulation throughout the accelerator in order to design a vacuum cavity of minimum radius. Having the metal wall close to the beam enhances stability and reduces space-charge effects. Here too we find that the axial profile of beam modulation is modified strongly by radial inhomogeneity. Moreover, the degree of modulation required to produce a given axial electric field is systematically larger for the inhomogeneous equilibrium.

In Sec. II we derive a general formula for wave energy in an axisymmetric, radially strongly inhomogeneous cold fluid relativistic electron beam. This expression is employed along with the usual definition of wave energy conservation to obtain in Sec. III the variation with guide field strength of wave phase velocity, group velocity, axial electric field, and beam modulation for parameters of interest to the ion acceleration experiments soon to begin at Austin Research Associates, Inc.[9] From these quantities an optimal magnetic guide field axial profile is determined. Section IV discusses both the potential impact of these results on autoresonant collective ion acceleration and the limitations of the present model from neglect of nonlinearities and thermal effects.

II. WAVE ENERGY IN A RADIALLY INHOMOGENEOUS BEAM

Let the small-amplitude eigenmodes of a weakly inhomogeneous nondissipative plasma be defined locally by the matrix equation

$$A \cdot X = 0 , \tag{1}$$

where X is a vector of wave components such as perturbed electric fields, magnetic fields, and fluid velocities. The generalized dielectric tensor A depends only on equilibrium quantities. Weinberg[10] has shown that under quite general conditions wave energy can be defined as

$$U = \tfrac{1}{2} X \cdot \left(\frac{\partial}{\partial \omega} A \right) \cdot X , \tag{2}$$

provided that A is symmetric. Moreover, an energy conservation equation exists,

$$\frac{\partial}{\partial t} U + \nabla \cdot (v_g U) = 0 \quad . \tag{3}$$

Here, ω, k, and v_g are the local frequency, wavenumber, and group velocity,

$$v_g = \nabla_k \omega \ . \tag{4}$$

The problem at hand differs from Weinberg's only in that (1) the beam is strongly inhomogeneous radially and (2) we care solely about axial flow of wave energy. Reproducing his analysis with these two modifications, we find that Eq. (1) holds if A is taken as a matrix operator containing radial derivatives. The appropriate quantity corresponding to Eq. (2) is energy per unit length,

$$U = \frac{1}{2} \int_0^R X \cdot (\frac{\partial}{\partial \omega} A) \cdot X \, r \, dr \ , \quad . \tag{5}$$

with the requirement now that A be self-adjoint.[11] Energy flow is described by

$$\frac{\partial}{\partial t} U + \frac{\partial}{\partial z} (v_g U) = 0 \ . \tag{6}$$

The group velocity is treated as a scalar, since only the axial component is meaningful.

The matrix operator A is given in Table II of Ref. 8, but not in self-adjoint form. Recasting it requires considerable algebra. The end product is presented in Table I, which gives A and X, and Table II, which defines the transformed dependent variables $\bar{B}$ and $\bar{u}$ and certain special symbols. As in Ref. 8, E, B, and u represent the perturbed electric and magnetic fields and the fluid relativistic momentum. Equilibrium quantities carry a zero superscript. Equations are normalized such that the electron charge and mass and the speed of light are unity. Boundary conditions consistant with self-adjointness are (1) fields are regular on axis, and (2) tangential electric fields vanish at the outer boundary, $r = R$. Accuracy of the transformations has been verified by solving numerically the equations and comparing the results to those of Ref. 8.

TABLE I

MATRIX REPRESENTATION OF RADIAL EIGENMODE EQUATIONS IN SELF-ADJOINT FORM. DIFFERENTIAL OPERATORS IN A_{ij} END IN A CENTERED DOT. NULL ELEMENTS ARE OMITTED. SEE TABLE II FOR SPECIAL SYMBOLS.

$A_{ij} =$

$\omega\left(1+\frac{n^o u_z{}^{o2}}{\Omega^2}\right)$	$\omega\frac{n^o u_z{}^o u_\theta{}^o}{\Omega^2}$	-	-	$\frac{1}{r}\frac{d}{dr}r\cdot$	$-\frac{m}{r}$	$-\omega\frac{n^o\gamma^o}{\Omega}$	-	-
$\omega\frac{n^o u_z{}^o u_\theta{}^o}{\Omega^2}$	$\omega\left(1+\frac{n^o u_\theta{}^{o2}}{\Omega^2}\right)$	-	$-\frac{d}{dr}\cdot$	-	k	-	$-\omega\frac{n^o\gamma^o}{\Omega}$	-
-	-	ω	$-\frac{m}{r}$	k	-	-	-	$-\omega\frac{n^o\gamma^o}{\Omega}$
-	$\frac{1}{r}\frac{d}{dr}r\cdot$	$-\frac{m}{r}$	ω	-	-	-	-	$\omega\frac{n^o u_\theta{}^o}{\Omega}$
$-\frac{d}{dr}\cdot$	-	k	-	ω	-	-	-	$-\omega\frac{n^o u_z{}^o}{\Omega}$
$-\frac{m}{r}$	k	-	-	-	ω	$\omega\frac{n^o u_\theta{}^o}{\Omega}$	$-\omega\frac{n^o u_z{}^o}{\Omega}$	-
$-\omega\frac{n^o\gamma^o}{\Omega}$	-	-	-	-	$\omega\frac{n^o u_\theta{}^o}{\Omega}$	$\omega n^o\left(1+\frac{n^o u_\theta{}^{o2}}{\Omega^2}\right)$	$-\omega n^o\frac{u_z{}^o u_\theta{}^o}{\Omega^2}$	$\omega n^o\frac{\eta_z}{\Omega}$
-	$-\omega\frac{n^o\gamma^o}{\Omega}$	-	-	-	$-\omega\frac{n^o u_z{}^o}{\Omega}$	$-\omega n^o\frac{n^o u_z{}^o u_\theta{}^o}{\Omega^2}$	$\omega n^o\left(1+\frac{n^o u_z{}^{o2}}{\Omega^2}\right)$	$\omega n^o\frac{\eta_\theta}{\Omega}$
-	-	$-\omega\frac{n^o\gamma^o}{\Omega}$	$\omega\frac{n^o u_\theta{}^o}{\Omega}$	$-\omega\frac{n^o u_z{}^o}{\Omega}$	-	$\omega n^o\frac{\eta_z}{\Omega}$	$\omega n^o\frac{\eta_\theta}{\Omega}$	$\omega n^o\frac{\eta_z{}^2+\eta_\theta{}^2+n^o\gamma^{o2}+\Delta}{\Omega^2}$

$X_j =$

E_z	E_θ	$-i\,E_r$	$i\,\bar{B}_z$	$i\,\bar{B}_\theta$	$\bar{B}_r$	$i\,\bar{u}_z$	$i\,\bar{u}_\theta$	$\bar{u}_r$

TABLE II

DEFINITIONS OF SPECIAL SYMBOLS AND TRANSFORMED VARIABLES USED IN TABLE I.
NOTE THAT THE ZEROES OF Ω AND Δ ARE SINGULAR POINTS OF THE RADIAL EIGENMODE EQUATIONS.

$$\Omega = \omega\gamma^o - k\,u_z^o - \frac{m}{r}\,u_\theta^o$$

$$\Delta = \Omega^2 - n^o - \xi_z\,\eta_z - \xi_\theta\,\eta_\theta$$

$$\xi_z = \frac{d}{dr}\,u_z^o - B_\theta^o$$

$$\xi_\theta = \frac{1}{r}\frac{d}{dr}\,ru_\theta^o + B_z^o$$

$$\eta_z = E_r^o\,\frac{u_z^o}{\gamma^o} - B_\theta^o$$

$$\eta_\theta = E_r^o\,\frac{u_\theta^o}{\gamma^o} + B_z^o + \frac{2}{r}\,u_\theta^o$$

$$i\bar{B}_z = iB_z - \frac{u_\theta^o}{\Omega}\,n^o u_r$$

$$i\bar{B}_\theta = iB_\theta + \frac{u_z^o}{\Omega}\,n^o u_r$$

$$i\bar{u}_z = iu_z + \frac{\eta_z - \xi_z}{\Omega}\,u_r$$

$$i\bar{u}_\theta = iu_\theta + \frac{\eta_\theta - \xi_\theta}{\Omega}\,u_r$$

$$\bar{B}_r = B_r + \frac{n^o}{\Omega}\left[i\left(u_z^o u_\theta - u_\theta^o u_z\right) + \frac{1}{\Omega}\left(u_\theta^o\,\frac{d}{dr}\,u_z^o - u_z^o r\,\frac{d}{dr}\,\frac{1}{r}\,u_\theta^o\right)u_r\right]$$

$$\bar{u}_r = u_r$$

With the equations in self-adjoint form, it is straightforward to construct equivalent variational integrals. Variational integrals can, in turn, be used for Rayleigh-Ritz eigenvalue estimates and for construction of finite element difference schemes.[12] We shall address the first of these applications in a subsequent publication.

Inserting Table I into Eq. (5) gives the desired wave energy density,

$$
\begin{aligned}
U = \frac{1}{2}\int_0^R \Bigg\{ & |E|^2 + |\bar{B}|^2 \\
& - n^o \Bigg[\left(1-2\,\frac{\gamma^o\omega}{\Omega}\right)\left(|\bar{u}|^2 - \frac{|u^o\cdot E|^2}{\Omega^2}\right) \\
& + \frac{n^o |(u^o x \bar{u})_r|^2}{\Omega^2} + \frac{\eta_z^2+\eta_\theta^2+n^o\gamma^{o2}+\Delta-\Omega^2}{\Omega^2}\,\bar{u}_r^{\,2} \\
& + \left(2\ 1-\frac{\gamma^o\omega}{\Omega}\right)\frac{\eta_z i\bar{u}_z+\eta_\theta i\bar{u}_\theta}{\Omega}\,\bar{u}_r \Bigg] \Bigg\} r\ dr\ .
\end{aligned}
\tag{7}
$$

Attempting to simplify the integrand analytically is futile. Instead, we solve Eq. (1) as in Ref. 8 for the eigenmode and eigenfrequency, and then integrate Eq. (7) numerically.

For low-frequency slow cyclotron waves in an ultrarelativistic, radially uniform beam filling the drift tube, an approximate but much simpler expression exists,[7]

$$
U \cong -\omega \int_0^R \frac{n^o\gamma^o}{B_z^o} |E|^2\ r\ dr\ . \tag{8}
$$

We have evaluated Eq. (7) and Eq. (8) for a uniform beam with $\gamma^o = 20$ and find that they agree quite well for $\omega^2 << n^o$, as expected. We also performed the comparison for the physically more realistic equilibrium treated in Ref. 8, for which the current density and particle energy (kinetic plus potential) are specified to be uniform in radius, and the remaining beam profiles are computed

self-consistently. Here too, agreement is fairly good, suggesting that Eq. (8) may have a wider range of applicability than originally expected. Incidentally, agreement in the case of the non-self-consistent rigid rotor beam model[13] is poor. As Sloan has observed,[14] a self-consistent equilibrium is necessary for the meaningful definition of wave energy.

III. APPLICATION TO AUTORESONANT ACCELERATION

The Austin Research Associates, Inc. experiment[9] employs a 3-MeV, 30-kA electron beam. At the generator diode the electron beam is approximately uniform radially in current density and, of course, energy. The beam has a reasonably sharp outer edge at 3.0 cm. The diode is embedded in a 2.5-kg guide field. Leaving the diode region, the beam propagates into a 3.4 kg guide field, where a 300-MHz slow cyclotron wave is excited. The beam is further compressed until the guide field reaches about 25 kg, and ions are added. Adiabatic expansion of the beam as the guide field drops to about 2 kg provides the ion acceleration. It is hoped that several amps of 30-MeV protons can be obtained with this apparatus.

To represent these parameters in dimensionless form, we normalize the beam density to its value in the 3.4-kg field. The beam plasma frequency there is $\omega_p = 3 \cdot 10^{10}$ sec^{-1}. The guide field is then expressed as the cyclotron frequency scaled to ω_p. Thus, $B_z^o = 2.0$ in the wave growth section and 1.47 in the diode. Other field components are scaled similarly. The cyclotron wave (angular) frequency relative to the reference value of ω_p is $\omega = 0.06$. At the diode $\gamma^o = 7.0$ and $\nu = 1.75$. (Budker's dimensionless current parameter ν is defined as the axial line density of electrons in the beam, multiplied by the classical electron radius.[15]) Since the length scale c/ω_p is one centimeter, the dimensionless beam radius at the diode is $a = 3$.

To estimate the spatial variation of the cyclotron wave amplitude in the experiment, we employ conservation of wave energy flux, Eq. (6), together with the fact that wave energy is proportional to the square of the wave amplitude, Eq. (5). Because the actual calculations are entirely numerical, we give here only an outline of the procedure and then turn to a discussion of the results. Conceptually, five steps are required to obtain the wave amplitude as a function of applied magnetic field strength:

(1) Specify the injected beam profile and applied magnetic field strength at the anode plane of the diode. To agree with the planned experiment, we

choose a nonrotating, axisymmetric, $\nu = 1.75$, $\gamma^o = 7.0$ electron beam radially uniform in energy and in current density out to a sharp edge, $a = 3.0$; B_z^o is 1.47.

(2) Compute corresponding self-consistent axisymmetric beam equilibria within a metalic drift tube for different guide field strengths. Within the drift tube away from the diode, the beam expands or contracts radially and rotates in order to achieve force balance. Beam kinetic energy is reduced by space charge effects, with γ^o at the beam axis depressed relative to its value at $r = a$ by roughly ν. Equilibria are found numerically by solving the standard set of four equilibrium equations[8] together with equations expressing conservation of total energy, canonical angular momentum, and particle flux along stream lines. These latter equations relate the beam equilibria to the injection conditions of step one. Details of this procedure and characteristic equilibrium profiles are given in Ref. 16. The drift tube radius must be specified to solve the field equations. We set $B_z^o R^2$ constant with $R = 3.8$ when $B_z^o = 2$. Since $B_z^o a^2$ is expected to be approximately constant, this choice of $R(B_z^o)$ has the desirable property that R/a is fairly constant at about 1.4.

(3) For each equilibrium and a fixed frequency of $\omega = 0.06$, compute the axial wavenumber k and the cyclotron wave radial profiles, as in Ref. 8. In other words solve Eq. (1) with A and X defined in Tables I and II as an eigenvalue problem in k. Wave amplitudes are now determined as a function of B_z^o up to an overall multiplicative constant $\sigma(B_z^o)$. In addition, the wave phase velocity is known.

(4) Repeat the eigenvalue calculations of step three at a slightly different frequency $\omega + \delta\omega$ to obtain the shifted wavenumber $k + \delta k$. The group velocity is $\delta\omega/\delta k$.

(5) Integrate Eq. (7) using equilibrium and wave profiles from steps two and three. This gives the wave energy up to the factor σ^2. The wave energy is, of course, time independent in the present problem, so that Eq. (6) reduces to $v_g U$ constant throughout the accelerator independent of B_z^o. Thus, the dependence of σ on B_z^o is determined. Specifying the cyclotron wave amplitude at the beginning of the accelerator, we know it throughout the system.

The calculations just described have been carried out for a range of B_z^o values from 0.65 to 20.0, or 1.1 kg to 34.0 kg. For fields below the lower limit, no equilibrium exists. Throughout the range the axial wave number determined numerically is well approximated by the simple expression

$$kv_z^o = \omega + B_z^o/\gamma^o \ , \tag{9}$$

with γ^o, v_z^o, and B_z^o evaluated at r = a; $v_z^o \equiv u_z^o/\gamma^o$. The group velocity is given to within a few percent by

$$v_g = v_z^o \ . \tag{10}$$

Neither result is unexpected.

Figure 1 presents the axial electric field strength on axis of the slow cyclotron wave as a function of applied magnetic field strength, with E_z normalized to unity (i.e., 0.51 MV/cm.) at $B_z^o = 2$. Note that E_z is proportional to k for B_z^o small but becomes flat for B_z^o large. For reasons to be discussed below, the transition value depends on wavelength, occuring for ka a bit larger than one. In contrast, analytic estimates of E_z in the radially uniform beam model give E_z proportional to k,[7] the dashed line in Fig. 1. Because that analysis is, strictly speaking, valid only for long wavelengths, we have carried out a numerical study for the uniform beam, performing steps three, four, and five above on a radially homogeneous, charge and current neutral beam ($E_r^o = B_\theta^o = 0$) of radius specified by $B_z^o\ a^2$ constant. Beam energy in the model is taken as the injection energy reduced by $2\nu\ \ell n\ R/a$. This physically reasonable value of γ^o leads to values of k and v_g in close agreement with the self-consistent beam results. For E_z, on the other hand, the uniform beam model predicts much larger values at large B_z^o. Note that both curves in Fig. 1 avoid the "wave breaking region" indicated. One expects disruption of the electron beam for electric fields of order $k\nu$ or greater for a $\nu/\gamma \sim 1/4$ beam.[2]

Some qualitative understanding of the difference in results of the two cases can be developed from Eq. (8). Because in equilibrium beam particles tend to stay on magnetic flux surfaces, $n^o\gamma^o/B_z^o$ is approximately constant. In addition, the slow cyclotron wave is predominately electrostatic, which means that

$$kE_r \cong \frac{d}{dr} E_z \tag{11}$$

and $E_\theta \cong 0$. Finally, v_g is nearly constant. Combining all these gives

$$\int_0^R [(kE_z)^2 + (\frac{d}{dr} E_z)^2] rdr \propto k^2 \quad . \tag{12}$$

In the uniform beam model the radial profile of E_z is representable piecewise by Bessel functions,[17] and Eq. (12) reduces to

$$E_z^2 \propto k^2/(1+\alpha k^2 a^2) \quad . \tag{13}$$

The factor α is on the order of 0.17, but depends weakly on the beam and wave parameters. For ka small the E_z radial profile for the self-consistent solid beam equilibrium does not differ greatly from its form in the uniform beam model.[8] Hence, the two plots of E_z on axis in Fig. 1 lie close together for small B_z^o. As ka exceeds one, however, the radial profile of E_z becomes rather flat out to near the beam radius, where it abruptly decreases in value. The dominance of dE_z/dr near r = a in Eq. (12) decreases significantly the variation of E_z with B_z^o relative to the uniform beam model. A quantitative analytic expression in this case has not yet been derived.

We next compute the optimal dependence of B_z^o on axial location z in the accelerator. To do this we employ the ion equation of motion

$$\frac{dv}{dt} = \frac{Q}{M} E \tag{14}$$

and require that the ions move in phase with the slow cyclotron waves so that they experience the maximum accelerative field at all times. The v in Eq. (14) is then the wave phase velocity, and E is the maximum axial electric field E_z. The ions are treated nonrelativistically. Q/M is the ion charge to mass ratio. Rearranging terms in Eq. (14) yields

$$z = \frac{M}{Q} \int v\, E_z^{-1}\, dv \quad . \tag{15}$$

Since we know both v and E_z as functions of B_z^o, we have B_z^o as an implicit function of z. The optimal axial magnetic field at the beginning of the acceleration region out to z = 4 is displayed in Fig. 2 for each of the three curves in Fig. 1. In all three cases the total accelerator length is about 83 with $B_z^o = 1$ at the termination. The total length is approximately the same for the three

quite different E_z curves because throughout most of the accelerator the ions are in a weak B_z^o region. Nonetheless, it is important to know the proper magnetic field variation at the beginning of the acceleration region. Too steep a decrease in B_z^o would dump the ions from the electrostatic wells of the cyclotron waves.

To make contact with the planned experiment, we recall that the length scale for these calculations is 1 cm. Thus, the total acceleration length is only 83 cm provided $E_z = 1$, or 0.51 MV/cm, at $B_z^o = 2$, or 3.4 kg. As we shall see, however, $E_z = 0.08$ at $B_z^o = 2$ seems to be about the largest axial electric field practical. This choice of E_z leads to an accelerator stretched by a factor of 12 to 1000 cm.

The practical limitation referred to comes from consideration of the beam radius modulation associated with a given wave amplitude,

$$\delta a = -u_r/\Omega \ , \tag{16}$$

with u_r and Ω evaluated at the beam edge, $r = a$. Plotted in Fig. 3 is the relative modulation $\delta a/a$ for the self-consistent beam equilibrium and for the uniform beam model. The curves are normalized to the E_z values of Fig. 1. Thus, for the self-consistent beam equilibrium, a relative modulation of 2.8 is required to produce $E_z = 1$ at $B_z^o = 2$. Of course, $\delta a/a > 1$ is impossible, and computer simulations indicate $\delta a/a > 0.5$ is undesirable.[18] This limits E_z to less than 0.2 at $B_z^o = 2$, the magnetic field in which the cyclotron wave is initially to be excited. Demanding that $\delta a/a$ remain less than 0.5 throughout the accelerator further restricts E_z at $B_z^o = 2$ to less than 0.08.

In contrast, the radially uniform beam model predicts that $\delta a/a$ of order 0.5 is sufficient to give $E_z = 1$ at $B_z^o = 2$. The disparity arises because, as mentioned in the Introduction, the slow cyclotron wave in the self-consistent, radially inhomogeneous equilibrium is a surface mode, while in the uniform beam model it is a body mode. Only the outermost electrons participate strongly in the former, and so much larger beam modulation is required to produce the same axial electric field strength. In order to test these predictions of linear theory, we are performing a series of fully self-consistent, nonlinear, two-dimensional, axisymmetric computer simulations using the PIC code CCUBE.[18,19] To date, attention has been restricted to $B_z^o = 2$, but work at stronger guide fields is planned.[18] The results of two typical computations $\delta a/aE_z$ are

indicated by "X" in Fig. 3. (Dividing $\delta a/a$ by E_z has the effect of normalizing the simulation data to $E_z = 1$.) The point labeled "S" is a small amplitude wave $E_z = 0.06$; the point labeled "L" a large amplitude wave $E_z = 0.2$. Uncertainty in the data is about 15%. Agreement between the self-consistent beam linear theory and the simulation results is good. The reduction in $\delta a/aE_z$ of about 1/3 for the large amplitude wave relative to the small is due to nonlinear effects. For progressively larger wave fields the beam particles are more tightly coupled in their oscillations, and the cyclotron wave begins a transition from a surface to a body wave. In the simulations this change, while small for $E_z = 0.2$, is directly observable in the electron streamlines.

IV. CONCLUSIONS

We have obtained a general expression for the energy density of a small amplitude wave in an axisymmetric, relativistic particle beam equilibrium with a self-consistent but otherwise arbitrary radial profile. Using this expression together with conservation of wave energy flux, we examined the adiabatic variation of the slow cyclotron wave as it propagates through the autoresonant accelerator device in order to obtain guidance for an experiment soon to be performed by Austin Research Associates, Inc. Two models were employed, a radially uniform cold beam without equilibrium self-fields and a more realistic model for a cold solid beam including self-field effects. The radially uniform model has been used extensively in analytic studies.[1,7,9] We found first that the uniform model predicts a more or less linear variation of the accelerating field E_z with the guide field B_z^o, while the self-consistent model gives E_z essentially constant for $ka > 1$ and linear with B_z^o only at long wavelengths. The difference is important only in the first 5% of the accelerator region, however. Of greater impact is our second finding, that the self-consistent model requires a beam radius modulation by the cyclotron wave that is four to ten times that required by the uniform beam model to produce a given value of E_z. This result has been corroborated for small B_z^o by computer simulation.

Applying the predictions of the self-consistent beam equilibrium model to the planned experiment suggests that E_z be excited to no more than 40 kV/cm at $B_z^o = 3.4$ kg, so that the relative radial modulation of the beam can remain below about 0.5. For this excitation amplitude, E_z ranges between 80 kV/cm and 20 kV/cm as B_z^o decreases from 34 kg to 1.7 kg. Total acceleration distance is 1000 cm for an optimal magnetic field profile but probably should be increased

about 20% to improve ion phase stability in the face of real-world electron beam irregularities. (Reducing the maximum field from 34 kg to 25 kg would not shorten the accelerator significantly.) The expected proton energy is 35 MeV. Ion current, an extremely important issue, is not addressed by this analysis. Because the upcoming experiment was designed quite conservatively, the accelerator parameters suggested here can be accomodated without difficulty. Our findings do, however, raise important questions regarding scaling to larger devices.

The present study has two limitations: It assumes small amplitude waves and a cold beam. The latter assumption is, we believe, very good in that finite Larmour radius effects large enough to modify the results presented here also are large enough to damp significantly the cyclotron waves. A hot electron beam clearly must be avoided experimentally. We hope to quantify this observation at a later date.

Testing the validity of the small amplitude approximation is a primary goal of our continuing simulation effort. As noted in Sec. III, reasonable agreement between simulation results and linear theory has been demonstrated at small B_z^o. We expect that nonlinear effects will increase allowed accelerating field strengths by no more than about 50%. To obtain still larger fields at a fixed electron beam current probably will require hollow beams.

V. ACKNOWLEDGEMENTS

It is a pleasure to acknowledge the helpful comments and suggestions of R. J. Faehl, W. R. Shanahan, M. L. Sloan, and L. E. Thode. We wish also to thank Faehl for providing us with the unpublished results of his computer simulation studies.

This work was performed under the auspices of the U. S. Department of Energy.

REFERENCES

1. M. L. Sloan and W. E. Drummand, "Autoresonant Accelerator Concept, "Phys. Rev. Lett. 31, 1234 (1973).

2. B. B. Godfrey, "Langmuir Wave Phase Velocity in Unneutralized Beams," IEEE Plasma Sci. 4, 223 (1977).

3. Norman Rostoker, Editor, Proc. 3rd Int. Conf. Collective Methods of Acceleration, Laguna Beach, California, May 22-25, 1978, to be published.

4. R. J. Faehl, B. B. Godfrey, B. S. Newberger, and W. R. Shanahan, L. E. Thode, "Computer Simulation of Collective Ion Acceleration by Discrete Cyclotron Modes," IEEE Nucl. Sci. 14, 1637 (1977).

5. B. B. Godfrey, R. J. Faehl, B. S. Newberger, W. R. Shanahan, and L. E. Thode, "Relativistic Electron Beam Cyclotron Wave Growth in Helical Slow Wave Structures," Proc. 2nd Int. Top. Conf. High Power Electron and Ion Beam Research and Technology (Cornell, 1977), Vol. II, p. 541.

6. R. J. Faehl, B. S. Newberger, and B. B. Godfrey, "Simulation of Cyclotron Wave Growth in a Helical Slow Wave Growth," submitted to Phys. Fluids.

7. W. E. Drummond, G. I. Bourianoff, D. E. Hasti, W. W. Rienstra, M. L. Sloan, and J. R. Thompson, "Preliminary Design Parameters for the Auto-Resonant Acceleration of Protons using the FX-25 or FX-100 Electron Beam Sources," AFWL-TR-74-343 (Air Force Weapons Laboratory, Albuquerque, 1975), Sec. II.

8. B. B. Godfrey, "Linear Theory of Radially Inhomogeneous Unneutralized Relativistic Electron Beams," submitted to IEEE Plas. Sci.

9. W. E. Drummond, Ed., "Proof of Principle Auto-Resonant Accelerator Experiment," Report I-ARA-78-U-36 (Austin Research Associates, 1978).

10. S. Weinberg, "Eikonel Method in Magnetohydrodynamics," Phys. Rev. 126, 1899 (1962).

11. E. L. Ince, Ordinary Differential Equations (Dover, New York, 1956), Ch. IX.

13. R. C. Davidson, Theory of Nonneutral Plasmas (Benjamin, Reading, 1974), Ch. 2.4.

14. M. L. Sloan, "Proof of Principle Auto-Resonant Accelerator Experiment," Austin Research Associates report I-ARA-78-U-36, App. U (1978).

15. G. I. Budker, "Relativistic Stabilized Electron Beam," Atom. Ener. 1, 9 (1956).

16. L. E. Thode, B. B. Godfrey, and W. R. Shanahan, "Vacuum Propagation of Solid Relativistic Electron Beams: Correlations Among Experiment, Simulation, and Theory," submitted to Phys. Fluids.

17. M. Abramowitz and I. A. Stegun, Handbook of Mathematical Functions (U.S. Government Printing Office, 1965), Sec. 9.1.28, 9.1.30, and 11.4.5.

18. R. J. Faehl, private communication.

19. B. B. Godfrey, "Application of Galerkin's Method to Particle-in-Cell Plasma Simulation," in Proc. 8th Conf. Num. Sim. Plas. (Monterey, 1978).

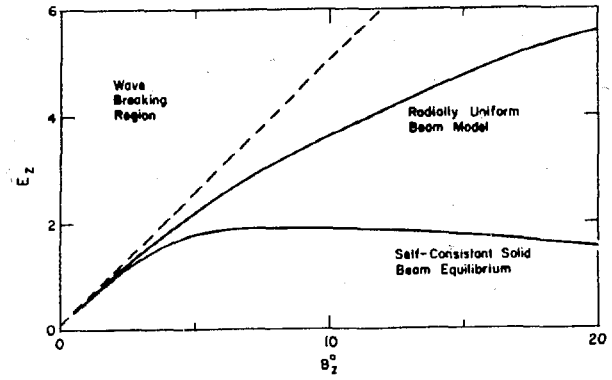

Fig. 1

Adiabatic variation of the axial electric field with changing magnetic guide field for a slow cyclotron wave in the radially uniform and the self-consistent solid beam equilibria. Curves are normalized to $E_z = 1$ at $b_z^o = 2$.

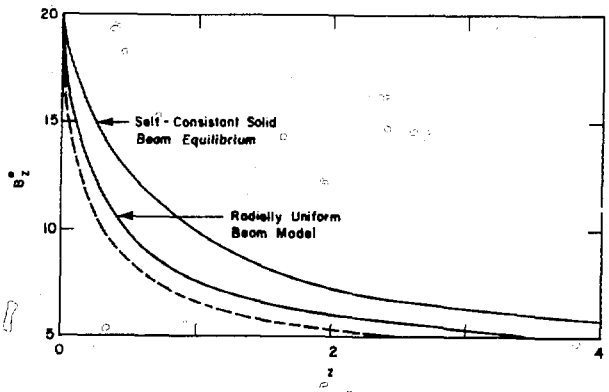

Fig. 2

Optimal axial variation of the magnetic guide field of an autoresonant accelerator for the axial electric fields plotted in Fig. 1.

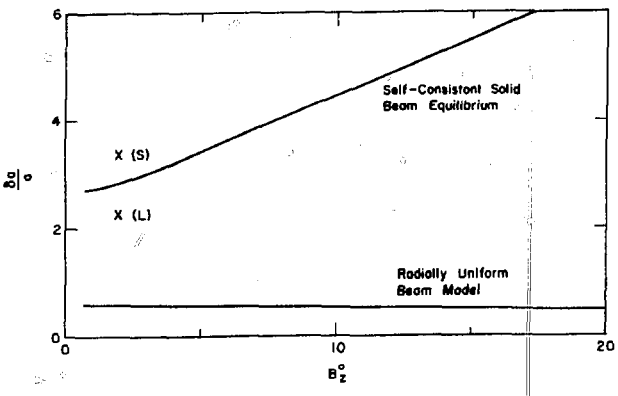

Fig. 3

Relative modulation of the beam surface by a slow cyclotron wave with axial electric fields as plotted in Fig. 1.

APPENDIX B

NONLINEAR CHARACTERISTICS OF CYCLOTRON WAVES IN AN ARA CONFIGURATION

To be published in the Proceedings of the Third International Conference on Collective Methods of Acceleration

NONLINEAR CHARACTERISTICS OF CYCLOTRON WAVES IN AN ARA CONFIGURATION

by

R. J. Faehl, W. R. Shanahan, and B. B. Godfrey

ABSTRACT

The Autoresonant Accelerator (ARA) offers great promise for collective ion acceleration provided large amplitude cyclotron waves can be generated with long coherence scales and controllable propagation characteristics. Numerical simulations have been performed to examine cyclotron wave growth in a helical slow-wave structure. No inhibition of growth was observed, short of an intrinsic space charge limitation. Extraction of such waves from the amplifying section through realistic terminations has been performed. The radial structure and propagation of these large, extracted cyclotron waves has been studied and comparisons with linearized waves have been drawn. The effect of nonlinear wave properties on ARA designs are presented.

I. INTRODUCTION

Ion acceleration in collective wave fields of relativistic electron beams has been studied energetically in recent years.[1-5] The Auto-Resonant Accelerator (ARA), which utilizes a slow cyclotron mode, is probably the best analyzed and furthest developed of such collective wave schemes. In these conceptually simple schemes, ions are trapped in a beam-supported wave, which is then accelerated in some fashion. There are implicit assumptions here, however, namely that nonlinear waves (a) remain coherent for long distances and times and (b) behave, at least approximately, like linear waves. These fundamental questions have motivated us to study finite-amplitude cyclotron waves such as are needed in the ARA. We have studied the nonlinear wave characteristics with emphasis on radial wave structure, field strength, and possible deviations from

linear dispersion. Large two-dimensional particle simulations were used to grow waves self-consistently and then follow their subsequent propagation. These results have been augmented by numerical studies of radially inhomogeneous linear theory and analysis of nonlinear waves.

The overall structure of this paper is as follows. Linear theory and the equations from which it is derived are examined briefly. Origin of the axial electric field, the component responsible for ion acceleration, is discussed. Also, qualitative examination of the equations suggests possible nonlinear effects. The simulations themselves are then described. Finally, simulation results are given in which slow cyclotron waves are grown from small amplitude signals and stable propagation is observed over modest scale lengths. Analysis of the simulations is performed to obtain data that can be compared directly with linear theory.

II. LINEAR THEORY AND NONLINEAR CYCLOTRON WAVES

Before discussing "nonlinear waves", it is proper to define what we mean by "nonlinear". The term is used in this context simply to distinguish finite amplitude waves from the results of first-order perturbation analysis. This is complicated since unique equilibrium conditions make even linear analysis of unneutralized relativistic electron beams nontrivial. A brief analysis of the linear equations shows this clearly.

Relativistic electron beam equilibrium during vacuum propagation in a smooth-walled drift tube requires a large, external axial magnetic field, B_z. Since the beam is unneutralized, significant radial electric and azimuthal magnetic fields are present with magnitudes determined by total beam current, beam and drift tube dimensions, and radial density distribution. For these to be self-consistent, the beam must rotate, giving a zero-order v_θ. Finally, since there are large equilibrium potentials, injection of even a monoenergetic beam into a finite radius drift tube results in radial variations in γ, given by

$$mc^2(\gamma_0 - 1) = mc^2(\gamma(r) - 1) - e\phi(r) \quad , \qquad (1)$$

where $\gamma = [1 - (v/c)^2]^{-1/2}$ and ϕ is the electrostatic potential. Linearization around a <u>self-consistent</u> beam equilibrium leads to equations which, to the best of our knowledge, do not possess closed-form solutions. Consequently, analytic

efforts have often neglected beam rotation, density inhomogeneity, and/or radial γ-variations. As we show below, the consequences can be significant vis-à-vis collective ion acceleration.

The dispersion of beam cyclotron waves can be quite accurately described with a reduced set of linearized cold fluid and field equations, which for azimuthally symmetric modes (m = 0) are

$$\frac{\partial \tilde{p}_r}{\partial t} + v_z \frac{\partial \tilde{p}_r}{\partial z} - 2v_\theta \frac{\tilde{p}_\theta}{r} = -\frac{e}{m}\left(\tilde{E}_r + \tilde{v}_\theta B_z - v_z \tilde{B}_\theta\right) \tag{2}$$

$$\frac{\partial \tilde{p}_\theta}{\partial t} + v_z \frac{\partial \tilde{p}_\theta}{\partial z} + v_\theta \frac{\tilde{p}_r}{r} = -\frac{e}{m}\left(\tilde{E}_\theta + v_z \tilde{B}_r - \tilde{v}_r B_z\right) \tag{3}$$

$$\frac{\partial \tilde{n}}{\partial t} = -\frac{\partial \tilde{n} v_z}{\partial z} - \frac{1}{r}\frac{\partial}{\partial_r} r\, n_0 \tilde{v}_r \tag{4}$$

$$\frac{\partial^2 \tilde{A}_i}{\partial t^2} - c^2 \frac{\partial^2 \tilde{A}_i}{\partial z^2} - c^2 \frac{1}{r}\frac{\partial}{\partial r} r \frac{\partial \tilde{A}_i}{\partial r} = 4\pi e c (n_0 \tilde{v}_i + \tilde{n} v_i) \quad , \tag{5}$$

where tildes refer to perturbed quantities, $\underset{\sim}{v}_r = 0$, $\tilde{p}_i = \gamma_0 \tilde{v}_i$, $i = r,\theta$, and A is the vector potential, such that $\underset{\sim}{B} = \nabla \times \underset{\sim}{A}$. Numerical solution of the full fluid and field equations on <u>self-consistent</u> equilibria provide confidence in the viability of Eqs. (2)-(5) for modeling cyclotron waves.[6,7] Aside from their utility in deriving dispersion relations, this reduced set can yield information directly about nonlinear waves.

In writing the model equations (2)-(5), the $\tilde{p}_z$ and $\tilde{E}_z$ equations were omitted. Although they could be included for the sake of accuracy, they effectively decouple from cyclotron waves of interest to ARA. In fact, they arise almost as by-products. The v_r- and v_θ-induced motions characterize the wave, leading to periodic radial modulations of the beam. Figure 1, taken from a wave growth simulation, clearly shows this. In Fig. 1(a), the configuration space (r - z) of the beam exhibits this beam modulation after a section of convective wave growth. Figure 1(b) shows the corresponding constant contours of ϕ, the electrostatic potential. The potential troughs are associated with the modulations. This is the source of the E_z field that traps and accelerates the ions; the radial modulation causes density compressions and rarefactions.

Thus, the cyclotron wave always possesses some E_z field, but its magnitude is determined by the depth of radial modulation. To be more precise, it is the radial integral of the density modulation which determines E_z, and this depends on the structure of v_r, since $\delta r \approx v_r/(\Omega/\gamma)$, $\Omega = eB_z/mc$. If the radial perturbation is distributed broadly across the beam, the integrated density modulation will be greater than if it were, say, localized on the surface. Since there is only a finite beam-to-wall separation, the magnitude of modulation on the outside of the beam is limited. Maximizing the axial electric field, therefore, depends sensitively on the radial eigenmodes.

Other information deducible from Eqs. (2)-(5) is more qualitative. Examination of the first order equations shows the terms neglected in this order, but which in general need not be small. A prime example is the radial convective term, $v_r(\partial p_i/\partial_r)$, $i = r,\theta$. These terms are clearly not first order. However, when the waves become finite, perturbation schemes become dubious and actual magnitudes must be considered. In this case, lack of an axially homogeneous ($k = 0$) v_r component indicates that, for large waves at k_0, the convective terms contribute most strongly at $2k_0$, the spatial second harmonic. (Since the $2k_0$ contribution is not resonant, however, only forced oscillations are induced.) More directly applicable terms are those involving v_z. In the reduced equations, only the $k = 0$ component was retained. The self-field $B_\theta(k = 0)$ can be quite large, however, so finite values of $v_z(k = k_0)$ can contribute significantly to the k_0 mode. While one can argue that these should be included in linear theory, v_z is coupled <u>nonlinearly</u> with wave amplitude, through

$$\tilde{v}_z \cong c(\gamma^2 - 1 - \tilde{p}_r^2 - \tilde{p}_\theta^2)^{1/2}/\gamma \quad . \tag{6}$$

This nonlinear term can directly alter the cyclotron dispersion. Linear results are of little value in estimating $\tilde{v}_z$ since there is no guarantee á priori that the nonlinear ratio of wave quantities remains fixed. One of our primary objectives, in fact, is to determine the <u>relative</u> magnitudes of nonlinear wave quantities. To do this, more powerful numerical tools are required.

III. DESCRIPTION OF CYCLOTRON WAVE GROWTH SIMULATIONS

The study of relativistic slow cyclotron waves requires self-consistency. Two-dimensional relativistic particle simulations were therefore conducted to

amplify small amplitude cyclotron-like perturbations. The large amplitude extracted signals were then allowed to propagate for moderate distances in a smooth-walled guide. A more complete discussion of the cyclotron wave growth has been reported elsewhere,[7] but a brief outline will now be given to place that work in perspective.

Wave growth in a helical slow wave structure has been widely employed for many years, for example, as the basis for traveling wave tubes. The principle of operation is that in a helix waveguide structure, the phase velocity of the electromagnetic mode is reduced to $V_{ph} \cong c \sin \psi$, where ψ is the helix pitch angle. It is, in fact, lowered to the point where resonance with a slow beam mode is achieved. Only slow modes can be resonant since, by definition, they alone possess phase velocities slower than the medium velocity, in this case $v_0 \cong c$. In traveling wave tubes, the beam mode is a Langmuir wave. ARA applications call for unstable growth of the slow cyclotron wave, however. This mode is quite dissimilar from the space charge wave. Previous theoretical and experimental experience was therefore inapplicable. This led to a number of unpleasant surprises in the simulations before certain fundamentals of electrical engineering were rediscovered and successful stable amplification was achieved.

Figure 2 depicts the simulation configuration used in these studies. A sheath helix with pitch angle ψ and radius R_H, illustrated with the dashed line in the figure, was attached to perfectly conducting flanges on either end, shown as crosshatching. An outer conducting wall with radius R_W existed outside the helix. The relativistic electron beam was injected on the left simulation boundary and propagated to the right, downstream boundary, where it was "smoothly" extracted. Once the space charge fields reached the grounded helix, they induced a charge flow on it. This "charging current" is quite physical and in a nonresistive helix, it rang for an unacceptably long period. More gentle risetimes would have ameliorated this condition, for helix dispersion eventually smooths the charging pulse. Although the helix current smoothed, however, the residual current flow resulted in a strong, finite width diamagnetic region. The total B_z field experienced by the beam was therefore discontinuous at the flange/helix boundaries. This stationary discontinuity excited zero-frequency cyclotron waves with wavenumber $k \cong \Omega_0/\gamma_0 v_0$. These waves did not interfere with growth of the coupled helix/cyclotron waves, but beating of the two finite-amplitude cyclotron modes yielded a potential distribution unsuitable for long-term trapping. Removal of the helix current without

disturbing helix charge distributions was found to be highly desirable, and accomplished in the simulations, as in the laboratory, by terminating the helix with matched impedances. After the initial transients decayed away, the current and charge distributions were quiescent and suitable for introduction of a small amplitude signal at the most unstable frequency upstream of the helix. Our "generator" was directly tied to the helix, but other more physical antennas have been examined. When the signal generator was "turned on", steady cyclotron wave amplification occurred, in close agreement with linear theory. To prevent oscillation, rather than amplification, large volumetric resistances were added outside the helix at the far end of the growth section. These were sufficiently large that they inhibited amplification, but such magnitudes were required to prevent oscillation. After the resulting large amplitude cyclotron wave reached the end of the helix, it was found to propagate into the smooth-walled drift tube with only nominal (10-20%) attenuation of the wave.

IV. DISCUSSION AND ANALYSIS OF NUMERICAL CALCULATIONS

The model configuration described above was successfully employed to grow large amplitude cyclotron waves. Since growth is due to coupling with the helical waveguide mode, however, the finite amplitude wave possessed a different radial structure from a stable cyclotron wave. Relaxation toward a stable configuration is thus expected after the wave leaves the growth section. This is, in fact, the dominant behavior observed in simulations. A small fraction of the wave energy is nevertheless converted into high-frequency noise. This noise seems to couple into resonant TE and TM wave guide modes with moderate efficiency. These are only tentative conclusions, since there are indications that the coupling may be enhanced by purely numerical effects. Even if the simulations overestimate the magnitude of electromagnetic noise, however, the combination of high frequency with incoherence in this field make it unlikely to interfere with the cyclotron accelerating fields. The low frequency field itself showed only weak attenuation or loss of coherence as it propagated for distances of order $L = 100\ c/\omega_p$ beyond the growth section. The only wave coupling effect observed was a tendency toward generation of harmonics, which never amounted to more than a few percent of the primary wave energy.

Demonstration of long coherence lengths for nonlinear cyclotron waves was accomplished with the numerical simulations. Beyond this, however, a primary objective was to characterize the finite-amplitude wave state. How then should

a nonlinear wave be characterized? Linear waves are completely described once a dispersion relation and the eigenfunctions are determined. The situation is much more complicated for finite-amplitude waves. For one thing, linear superposition of modes is no longer strictly valid; a nonzero coupling between all modes exists in general. Therefore, while it is still important to determine the relation between ω and k, i.e., the dispersion, one also needs to specify the spectrum. Spectral characteristics are a self-consistent aspect of a nonlinear wave state. The radial wave structure in our case is also a valid indicator, insofar as it can be compared with a linear eigenfunction. As mentioned earlier, it can be directly correlated with the E_z field of the wave. Finally, linear theory allows us to predict ratios of eigenfunctions, for instance, $v_{r\ max}/E_{z\ max}$. Similar ratios can be determined directly from simulations. In this fashion, the degree to which nonlinear waves resemble linear ones can be inferred quantitatively. To make these concepts more concrete, we will consider a typical simulation.

A series of simulation calculations was performed in a geometry similar to that in Fig. 2. In units of c/ω_p*, the helix and the inner flange radii were $R_H = 3.8$, the outer flange radius was $R_W = 5.7$, and the beam radius, $R_B = 2.65$. This last dimension corresponds to a Budker parameter of = 1.75, or 30 kA. The helix extended from z = 15.0 to 115.0, with a pitch angle $\psi = -15°$. The helix was excited directly at z 30, giving a total growth length $L_{grow} = 85$. For these conditions, the growth rate was $\Gamma = 0.020\ \omega_p$ and the group velocity v_{gr} 0.6 c, giving almost 3 e-foldings, in the absence of resistive terminations. These simulations were designed for conservative performance, with a maximum power amplification of only about a factor of 260. In fact, addition of various resistive elements to inhibit feedback shortened the effective growth length, so that the observed amplification factor was on the order of 130. Our purpose here was not maximum amplification; in specifically designed wave growth simulations, amplification factors almost 10 times larger have been measured.[7] The large amplitude cyclotron waves which were grown, however, proved very suitable for studying the nonlinear characteristics.

The magnitude of the E_z field on axis is plotted in Figure 3, as a function of axial position. The electric field is observed to reach its maximum value

---

*For comparison purposes note that when $n_0 \cong 3 \times 10^{11}$ cm^{-2}, $c/\omega_p \cong 1$ cm.

near the end of the helix. More significant, however, is that, while some fluctuations in amplitude are observed, the average field of the extracted wave is only about 10% lower than the peak.

The E_z values shown in Fig. 3 were obtained by setting numerical "probes" at various positions along the axis. Figure 4 shows a typical "probe" trace, near the end of the growth section, and its associated power spectrum. The dashed line indicates the frequency expected from linear theory for this configuration. There is virtually no detectable frequency shift, even though the magnitude is over 2×10^5 V/cm, assuming $n_0 = 10^{12}$ cm^{-3}. Since this probe was still within the region dominated by the linear helix, this is perhaps not surprising. Figure 5, however, compares that power spectrum with one obtained almost 90 c/ω_p further down the propagation path, well beyond the helix. Although the total noise content at high frequencies is quite different, the low frequency cyclotron signal is hardly affected at all.

With the aid of computer-generated movies, a point of constant phase can be observed directly. The phase velocity of finite amplitude waves determined in this fashion was remarkably close to that of infinitesimal linear waves. As an example, a series of wave crests were followed for a distance $L = 50\ c/\omega_p$ and times on the order of $t = 300\ \omega_p^{-1}$. Wave modulation was such that $\Delta r/R_B = 0.23$. (The beam-to-wall separation for this calculation corresponded to $\Delta r/R_B = 0.43$). The average phase velocity was measured to be $V_{ph} = 0.275$ c, while linear theory predicted $V_{ph} = 0.269$ c.

One of the few nonlinear spectral effects observed so far has been harmonic generation. This is registered to varying degrees on probes of E_z, B_θ, and E_θ fields, and seems to be correlated with the wave magnitude. The specific origin of this apparent nonlinearity has not yet been identified but is under investigation.

Figure 6 shows the beam envelope under typical conditions of steady cyclotron wave amplification. Radial beam modulations increase through the growth section but are <u>not</u> attenuated on leaving it. In fact, they increase to somewhat larger values. Surprisingly, this behavior is explicable on the basis of inhomogeneous linear theory. Figure 7 shows the radial eigenfunctions for v_r derived on self-consistent radial profiles, with the same wavelength. These are related to the radial modulation by $\Delta r = \tilde{v}_r/(\omega - kv_0)$. Figure 7(a) depicts the radial velocity structure within the growth section; the frequency is $\omega = 0.124 \pm 0.020i\ \omega_p$. In Fig. 7(b), we show the eigenfunction under identical

conditions, except that a smooth waveguide wall is at the helix radius; for constant frequency, the relative wavenumber shift is less than 1%. Both scales are normalized to the maximum value of E_z. Since Fig. 3 indicated that the E_z magnitude did not decrease significantly, it is evident that the radial modulation must increase substantially as the mode relaxes toward its stable configuration.

We have repeatedly referred to inhomogeneous linear theory. The reason is well illustrated by the above example. To obtain the expected ratio, linearization was performed around the radially inhomogeneous equilibrium. If the same calculation is conducted, except with a constant, averaged value of γ, i.e.,

$$\langle\gamma\rangle = \int_0^{R_B} \gamma \, dr/R_B \quad ,$$

qualitatively and quantitatively different eigenfunctions result. Figure 8 gives a comparison between the v_r and E_z eigenfunctions computed with $\langle\gamma\rangle$, Figs. 8(a,b) and those with $\gamma(r)$, Figs. 8(c,d). The difference is quite significant, for it indicates that, if linear theory is relevant to finite amplitude waves, over 4 times the density modulation is required to induce a given E_z magnitude than would be expected on the basis of the simpler $\langle\gamma\rangle$ analysis. Since the beam modulation is effectively limited to the beam-to-wall separation, this implies relatively small upper limits on the obtainable wave acceleration fields. Although the magnitude is still large compared with conventional fields, it is much smaller than originally anticipated. The self-consistent equilibrium employed here depends on a specific current distribution, of course, and this is certainly not unique. Tailoring the radial current distribution may yield more propitious field/modulation ratios. The important point is that linear theory at least should be based upon realistic, not idealized, beam states.

Eigenfunctions of the radial velocity were also compared with linear theory. These were obtained numerically by measuring the root-mean-square radial velocity of the beam at various axial slices as a function of the original stream lines, i.e.,

$$\langle v_r(r_0)\rangle = [\int_0^T v_r^2(r_0)dt/T]^{1/2} \quad .$$

The time interval for averaging was chosen large enough so that uncertainties in quantities at the desired wave frequency were less than 2%. Figure 9 shows the linear eigenfunction as a solid line, and the nonlinear as a dashed line, both normalized to the axial E_z magnitude. The structure is qualitatively the same, though the nonlinear wave exhibits less modulation. This is significant in that it indicates less modulation is required to produce a given E_z-field on axis. Compared with Fig. 8, however, it is apparent that inhomogeneous linear theory is more applicable to nonlinear waves than is simple linear theory.

The ratio of beam modulation to induced axial electric field is a very important accelerator parameter, due to finite beam/wall separation. Simulation derived values of $(\Delta r/E_z)_{max}$ are plotted in Fig. 10 as a function of z. It is clear that the ratio approaches the inhomogeneous linear values in both the unstable growth section and the stable propagation section.

Finally, note that finite transverse oscillations occur at the expense of the original beam energy, which was predominantly longitudinal. A simple model for the effect on longitudinal motion is

$$v_z(r_0) = c[\gamma_0^2(r_0) - 1 - p^2(r_0)]^{1/2}/\gamma_0(r_0) \quad . \tag{7}$$

Since we measured the RMS eigenfunctions of p_r, Eq. (7) can be estimated directly. Figure 10 shows the relative mean change in v_z as a function of z, for a typical wave growth/propagation simulation, with $\delta_r/R_B \lesssim 23\%$. This v_z not only induces frequency modulations through terms like $v_z B_\theta$ in Eq. (2), but also in the basic Doppler shift, kv_z. If frequency shifts on the order of $k\Delta v_z$ are not compensated by wavelength shifts, the nonlinear phase velocity should have been reduced. Phase velocity changes of this size would have been seen in simulation movies, however, but the measured values, as discussed above, were not reduced. It is not clear at this time why such effects have not been observed in the simulations.

V. CONCLUSIONS

Cyclotron waves suitable for use in an Autoresonant Accelerator have been self-consistently grown to nonlinear levels in numerical simulations, and thereafter propagated for moderate distances without significant attenuation. While

the investigation of these nonlinear wave states has not been completed yet, certain important observations can still be made.

The primary conclusion must be that cyclotron waves possessing relative radial modulations of 20% or less are not violently unstable, and in fact exhibit coherence lengths at least on the order of the simulations, i.e., $\Delta L \cong 10^2\ c/\omega_p$. Larger amplitude waves will be simulated in the near future. Comparisons with inhomogeneous linear theory revealed quantitative differences in nonlinear waves but no qualitative changes.

Finite amplitude cyclotron waves were also found to be highly localized on the beam surface, which is consistent with inhomogeneous linear theory. The interior of the beam does not "actively" participate in the oscillation. Therefore, a relatively large radial surface modulation, much larger than simple linear theory predicted, is needed to produce a given magnitude field on axis. Previous work[7] has shown that an upper limit on the amplitude is that the total potential, equilibrium plus wave, must not exceed the space charge limit, roughly

$$\phi_{total} \lesssim (mc^2/e)(\gamma_0 - \gamma_0^{1/3}) \quad .$$

This in turn limits both the allowable beam-to-wall separation and the radial modulation. Although nonlinear cyclotron waves are not quite so surface-peaked as linear ones, the linear picture is still qualitatively correct. If these results prove to be valid over a broad range of magnetic field, they impose real limits on ARA performance, for the linear results indicate that propagation in a decreasing field will not reduce the E_z field, but rather increase the relative beam modulation. Conclusive results must await either experiments or simulations of cyclotron wave propagation in inhomogeneous fields. We are actively pursuing the latter.

A final observation of considerable interest is that the phase velocity of finite amplitude waves is very accurately given by linear theory, at least at the simulated wave strengths. Since a nonlinear frequency shift on the order of $k\Delta v_z$ plays a significant role in cylotron waves in low density beams,[8,10] measurable changes in the phase velocity should have been detectable for waves seen in the simulation. Larger amplitude waves, however, should prove a more stringent test on any nonlinear phase velocity modifications.

This work is currently being extended to larger amplitude waves, propagation in axially varying magnetic fields, and longer propagation distances. If present trends, consistent with inhomogeneous linear theory, persist, significant alterations will be needed in the design of an Autoresonant accelerator. Possible improvements may result from reshaping the acceleration section, giving smaller acceleration gradients, finding an optimum radial current profile, or employing a higher energy electron beam.

ACKNOWLEDGMENT

This work was supported under the auspices of the U. S. Department of Energy.

REFERENCES

1. M. L. Sloan and W. E. Drummond, "Autoresonant Accelerator Concept," Phys. Rev. Lett. 31, 1234 (1973).

2. R. J. Faehl and B. B. Godfrey, "Collective Ion Acceleration Through Temporal Modulation of Relativistic-Electron-Beam Energy," Phys. Rev. Lett. 40, 1137 (1978).

3. P. Sprangle, A. T. Drobot, and W. M. Manheimer, "Collective Ion Acceleration in a Converging Waveguide," Phys. Rev. Lett. 36, 1180 (1976).

4. V. V. Velikov, A. G. Lymer,, and N. A. Khizhnyak, "Acceleration of Ions by a Modulated Electron Beam," Sov. Phys.-Tech. Phys. Lett. 1, 276 (1975).

5. S. V. Yadavalli, "Synchronous Slow Space-Charge Wave Accelerator (SSWA)," to appear in Nucl. Instru. Methods.

6. B. B. Godfrey, "Linear Theory of Radially Inhomogeneous Unneutralized Relativistic Electron Beams," submitted to IEEE Trans. Plasma Sci.

7. R. J. Faehl, B. S. Newberger, and B. B. Godfrey, "Simulation of Cyclotron Wave Growth in a Helical Slow Wave Structure," submitted to Phys. Fluids.

8. H. V. Wong, "Nonlinear Theory of Instability Due to Coupling of Electron Cyclotron Beam Mode and Sheath Helix Eigenmode," Austin Research Associates, Inc. report I-ARA-77-U-47 (ARA-273), p. 185 (1977).

9. R. C. Davidson, Theory of Nonneutral Plasmas (W. A. Benjamin, Inc. Reading, Massachusets, 1974).

10. G. I. Bourianoff, B. N. Moore, and B. R. Penumalli, "Computer Simulation of Linear and Non-Linear Wave Growth Phenomena," 3rd Int. Conf. on Collective Methods of Acceleration, Laguna Beach, California, May 22-25, 1978.

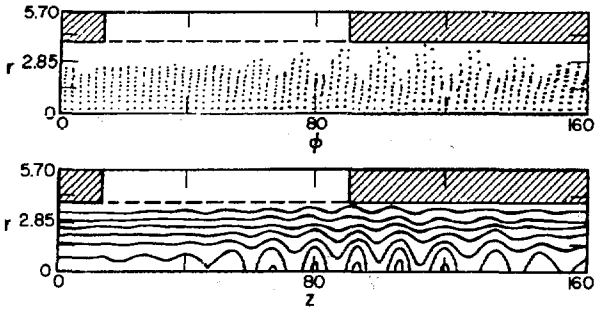

Fig. 1

Convectively grown cyclotron wave in particle simulation, (a) configuration space (r - z) and (b) constant contours of electrostatic potential.

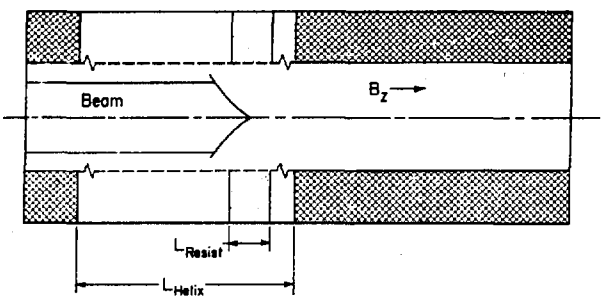

Fig. 2

Schematic representation of the simulation configuration employed to grow cyclotron wave.

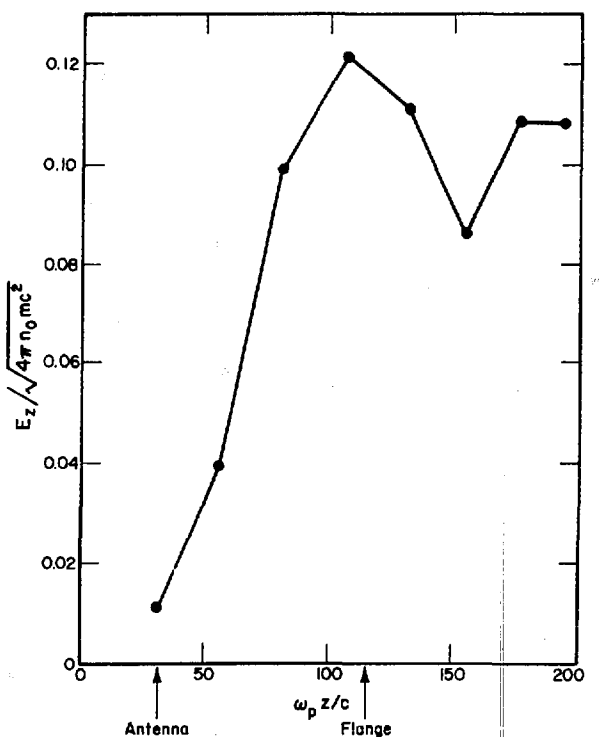

Fig. 3

E_z as a function of axial position, z; r = 0.35 c/ω_p, R_B = 2.65, R_H - 3.8, R_W = 5.7/3.8, ψ = -15°, eB_o/mc = 2.0 ω_p, L = 200 c/ω_p, L_{grow} = 100 c/ω_p.

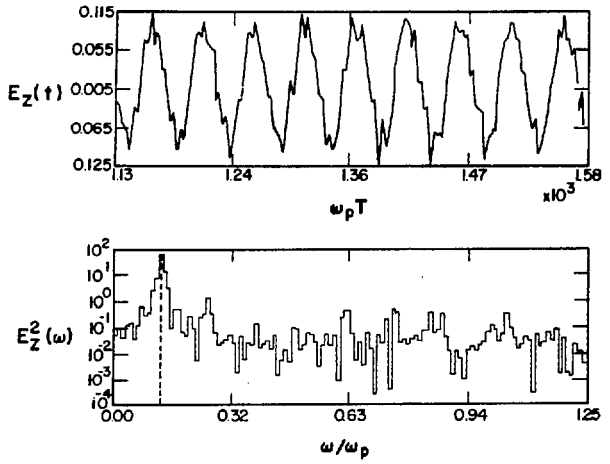

Fig. 4

(a) Typical E_z "probe" trace; r = 0.35, z = 106; (b) power spectrum derived from probe trace. Dashed line indicates frequency of original antenna signal.

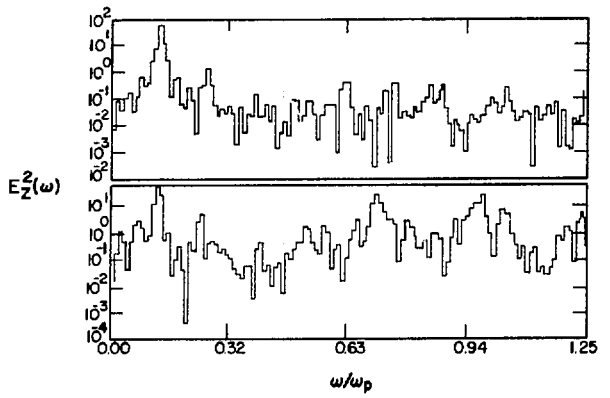

Fig. 5

Comparison of E_z power spectra at z. (a) z = 106 and (b) z = 193. Enhanced high frequency components at z = 193 may be due to numerical effects.

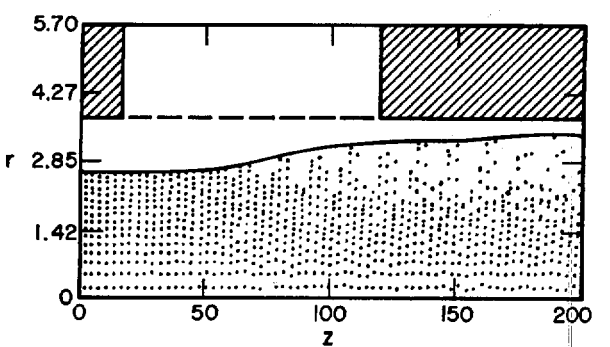

Fig. 6

Typical beam envelope in a wave growth run. Growth section extends from z = 15 to z = 115.

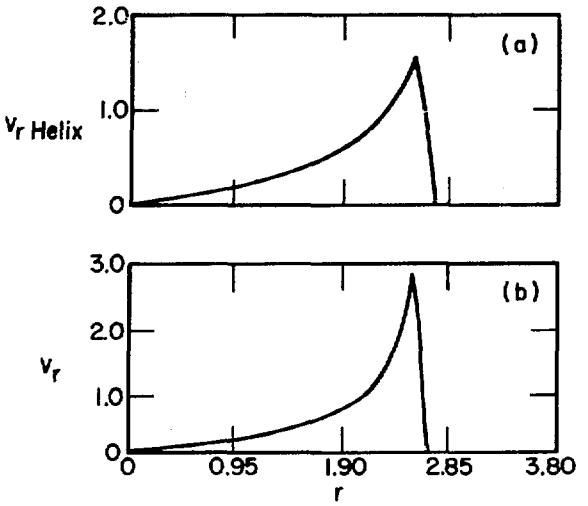

Fig. 7

Comparison of linear eigenfunctions of v_r derived numerically on a self-consistent equilibrium, R_B=2.65, Ω_o=2.0 ω_p. (a) v_r versus r within growth section, R_H=3.8, R_W=5.7, ψ=-15°, ω=0.124±0.020 i ω_p, k=0.46 ω_p/c; (b) v_r versus r in smooth-walled waveguide, R_W=3.3, ω=0.122 ω_p, k=0.46 ω_p.

Fig. 8

Comparison of v_r and E_z linear eigenfunctions, R_B=2.65, R_W=3.8, k=0.46 ω_p/c. (a) v_r versus r derived from equilibrium with $\langle\gamma\rangle$=4.9, (b) E_z versus r, same as (a); (c) v_r versus r derived from self-consistent equilibrium, $\gamma(R_B)$=5.8, $\gamma(0)$=4, (d) E_z versus r, same as (c).

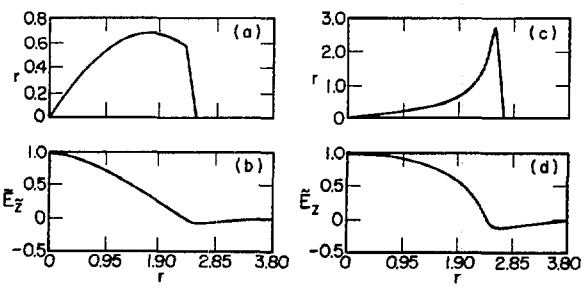

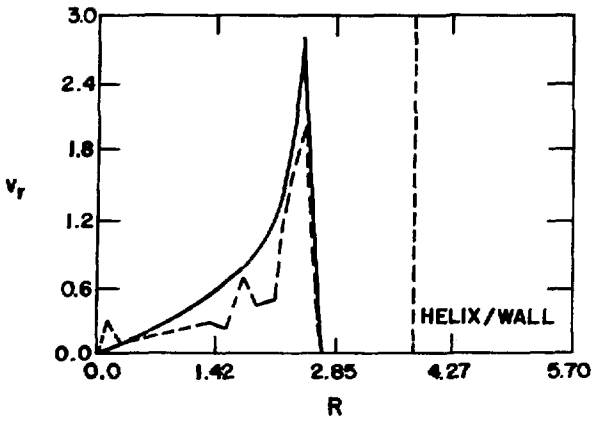

Fig. 9

Comparison of v_r linear eigenfunction (solid line) with RMS $v_r(r_o)$ derived from simulation (dashed line), R_B=2.65, R_W=3.8, $\delta r/R_B$=23%.

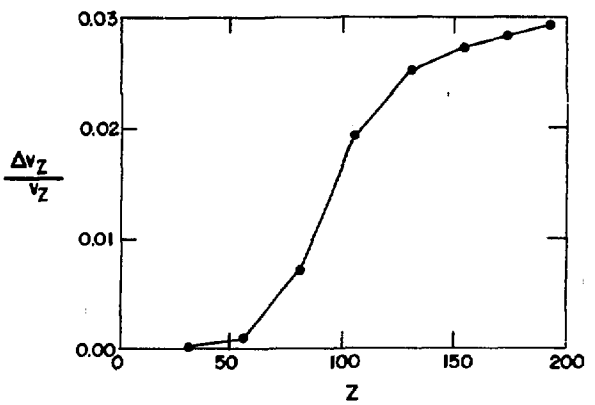

Fig. 10

Tabulated estimate of v_z shift as a function of z using Eq. (7) and simulation data, for parameters of Fig. 3.

APPENDIX C

NONAXISYMMETRIC BEAM/HELIX INSTABILITY AND NONSOLID BEAMS

NONAXISYMMETRIC BEAM/HELIX INSTABILITY AND NONSOLID BEAMS

by

R. J. Faehl

ABSTRACT

Beam/helix growth rates of nonaxisymmetric modes are examined numerically for parameters appropriate to autoresonant ion acceleration. These are compared with $m = 0$ growth rates in both solid and hollow beams. Hollow beams reduce $m = 1$ growth with respect to $m = 0$, but overall offer few advantages for ion acceleration.

In the FY77 annual report, a fairly detailed discussion was given of linear theory for the helix-beam coupling instability. This discussion was based on analytic theory and numerical solution of linearized cold fluid/electromagnetic equations of self-consistent equilibria. Although the potential importance of nonaxisymmetric modes ($m \neq 0$) was noted, we confined our attention at that time to the $m = 0$ mode in a solid beam. We have since extended the numerical results to hollow beams and the $m \neq 0$ modes.

All nonaxisymmetric helix modes ($m \neq 0$) possess moderately high phase velocity, since $\omega_{Helix} = -qc\,(\tan\psi + mk/R_H q^2)$, where ψ is the pitch angle, R_H is the helix radius, and $q = (k^2 - \omega^2/c^2)^{1/2}$. The axial electric field for these waves, furthermore, vanishes on axis (i.e., $E_z(r=0) = 0$), so that ion acceleration in an $m \neq 0$ mode could only be achieved far from the axis. While this is an undesirable characteristic of all modes, $m = 1$ is probably the most deleterious. Not only is it of little use for ion acceleration, it can be strongly disruptive by kinking the beam into the wall. Growth of the $m = 1$ beam/helix mode is, therefore, particularly undesirable. To examine it, and other nonaxisymmetric modes, we extended the $m = 0$ dispersion calculation to the case of arbitrary m.

TABLE I

HELIX/BEAM INSTABILITY AS A FUNCTION OF GUIDE B_z FIELD

Ω_0	m = 0		m = 1	
	Γ_{max}	k_{max}	Γ_{max}	k_{max}
2.0	0.024	0.46	0.121*	0.24
2.5	0.025	0.59	0.082	0.86
3.0	0.025	0.71	0.076	1.075
4.0	0.021	0.96	0.059	1.38

The summary of a series of calculations for m = 0 and m = 1 helix induced beam instabilities is shown in Table I, as a function of magnetic field, where $\Omega_0 = eB_0/mc$, $R_H = 3.8$, $R_B = 2.65$, $\nu = 1.75$, and $\psi = -15°$. (All distances are in units of c/ω_p.)

The magnetic field variation had little effect on the helix dispersion, but it shifted the cyclotron branch to higher k (short wavelength). Since the instability occurs roughly at resonance of the two modes, this shifts peak growth to shorter wavelength. As the table shows, the m = 1 growth rate is much larger than m = 0, for parameters of interest here. However, it is apparent that for these parameters the effect of magnetic field on the m = 0 mode is considerably less than on m = 1. Other parameter searches have also shown propitious scaling of m = 0 versus m = 1, but no parameter or combination of parameters yet examined has reduced the magnitude of m = 1 to less than m = 0.

For parameters examined so far, magnitude of the m = 1 growth in a helix is so much larger than m = 0 that active measures are probably required to suppress it. There are several possibilities for achieving this.

(1) One can excite the m = 0 cyclotron mode at sufficiently large magnitude that little or no amplification is required to raise it to a programmatically satisfactory level. This requires a clean excitation mechanism which will not simultaneously excite m = 1. The self-driven antenna concept discussed in another appendix has shown promise for large excitation levels, but further analysis would be required to determine the full composition of excited waves. (The simulations cannot provide useful information here, for they are axisymmetric and thus show only m = 0 waves.)

(2) Selective nonlinear suppression of the m = 1 waves, if possible, would facilitate free growth of both m = 0 and m = 1 perturbations. Austin Research Associates has had some success in studying nonlinear saturation mechanisms in low-density and/or weakly coupled beams. It is not clear that this work can be extended to the high-current regime, or if it can, that a mechanism can be found to suppress m = 1 without affecting m = 0. Further analysis appears necessary to determine the viability of this approach.

(3) Spatial filtering can be accomplished by loading a waveguide such that certain wavelengths are highly distorted while others are virtually unaffected. By distorting the portion of k-space in which m = 1 is unstable, but not m = 0, it should be possible to reduce m = 1 to manageable levels. Unfortunately, this is only possible where unstable regions in k-space are well separated. We can crudely estimate the width of unstable waves by noting that the instability is a resonance effect. It, therefore, peaks at roughly the intersection of the two dispersion curves and is effective until the linear frequency mismatch becomes too great. We find that the maximum mismatch is approximately equal to the peak growth rate,

$$\Delta\omega = |kv_0 - \Omega_0/\gamma_0 - kc \sin\psi| \cong \Gamma_{max} \quad , \tag{1}$$

which can be simplified by noting that the resonance, and hence, peak growth occurs at

$$k_{max}\, c = \Omega_0/(\beta_0 - \sin\psi)\gamma_0 \tag{2}$$

so that the unstable wave regions are defined by

$$\left| \frac{k}{k_{max}} - 1 \right| \leq \gamma_0\Gamma_{max}/\Omega_0 \quad .$$

Another resonance occurs for helix intersection with Langmuir (space-charge) waves, which gives

$$\left| \frac{k}{k_{Lmax}} - 1 \right| \leq \gamma\Gamma_{Lmax}/\omega_p \quad .$$

For m = 0, the Langmuir resonance occurs at very long wavelengths, i.e., $k_{Lmax} << 1$. The m = 1 Langmuir resonance is shifted to considerably shorter wavelengths, however. The situation is depicted schematically in Figs. 1 and 2, for m = 0 and m = 1 modes. The m = 1 Langmuir instability is so much stronger than its m = 0 counterpart, at moderate magnetic field (for instance, $\Omega_0 = 2.0\ \omega_p$) that the combined range of m = 1 Langmuir and m = 1 cyclotron completely overlaps the m = 0 band. For spatial filtering to be effective, a parameter regime must be chosen so that the m = 0 cyclotron wave is more unstable than any m = 1 mode. If one neglects higher order interactions, i.e., $m \geq 2$, it appears that the necessary separation can be achieved by going to sufficiently large magnetic field (compare to Table I).

The above results were all obtained in solid beams. It has been suggested that hollow beams may yield more propitious results. Toward this end, we have employed the GRADR code to numerically calculate stable and helically unstable cyclotron waves with a hollow beam. As with the solid beam calculations, only sharp radial boundaries were studied.

There are several characteristics of cyclotron waves which can be used to compare the effect of hollow beams versus solid ones. The axial electric field, for instance, is produced by radial modulation of the beam. It is, therefore, important to know how much modulation is needed to produce a desired field

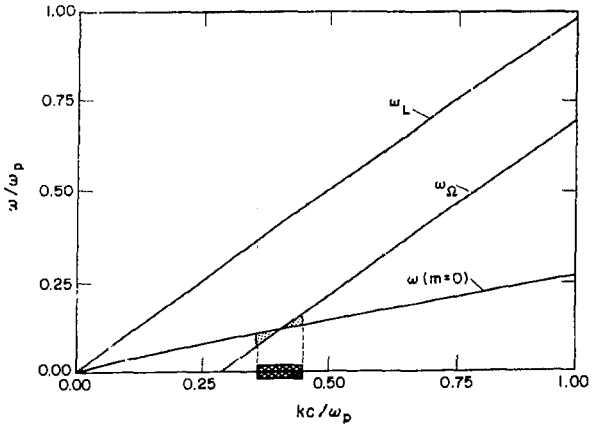

Fig. 1.

Dispersion of m=0 helix (ω), cyclotron (ω_Ω), and space-charge or Langmuir (ω_L) waves. Crosshatching shows approximate width of unstable interaction.

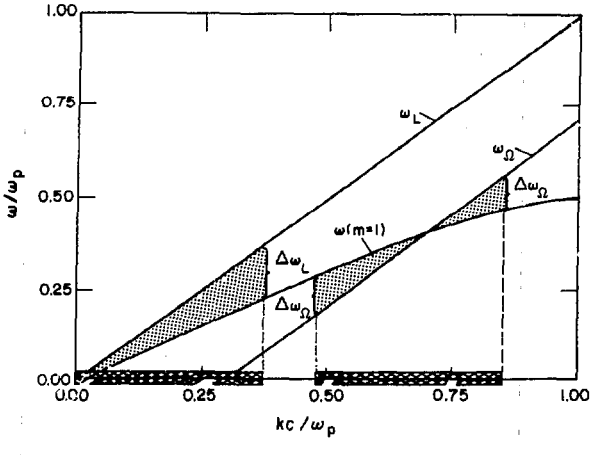

Fig. 2

Dispersion of m=1 helix (ω), cyclotron (ω_Ω), and space-charge (ω_L) waves. Crosshatching shows width of unstable interaction.

magnitude. Studies on the effect of radial γ variations described in Appendix B indicate that the eigenmode is highly surface-localized, so that roughly four times the modulation is required.

The peak growth rate for the m = 0 and m = 1 modes is shown as a function of beam aspect ratio R_B/Δ, where $\Delta = R_{out} - R_{in}$, in Table II. The beam-to-helix distance was maintained at a fixed value, $R_H - R_B = 1.15$, and the helix angle was $\psi = -15°$. A slight shift to lower k with increasing aspect ratio is expected due to smaller potential depression across the beam. (Reduced space-charge means larger γ.) The m = 1 space charge instability weakens significantly as the beam becomes more hollow, thus eliminating overlap with the m = 0 cyclotron growth. Overall, however, the "hollowness" of the beam seems to have little effect on the cyclotron instability.

The other reason advanced for employing hollow beams is that the wave would not be so localized on the surface. The space-charge variation of γ across a solid beam leads to highly peaked m = 0 cyclotron eigenmodes. Consequently, the E_z field on axis is much smaller (factor of four for typical ARA parameters) than one would expect from a constant γ analysis, for the same modulation. Since the modulation amplitude is limited by the finite beam-to-wall separation, this places a smaller upper bound on accelerating fields than had been anticipated (compare to Appendix A). With a hollow beam, the γ-variation across the beam is smaller, and thus, it was hoped, something more akin to the constant γ case would result. Table III, however, shows the $v_r(R_B)/E_z(R)$ ratio

TABLE II

HELIX/BEAM INSTABILITY GROWTH RATES AS A FUNCTION OF ASPECT RATIO

$R_H - R_B = 1.5$, $\nu = 1.75$, $\psi = -15°$, $\Omega_0 = 2.0\ \omega_p$, $\gamma_0 = 7.0$

R_B/Δ	m = 0		m = 1	
	Γ_{max}	k_{max}	Γ_{max}	k_{max}
1.0	0.022	0.46	0.121[a]	0.24[a]
2.5	0.026	0.44	0.107	0.64
4.0	0.025	0.42	0.090	0.62
10.0	0.024	0.42	0.064	0.57

[a]Peak growth for m = 1 space charge wave; approximate peak growth for cyclotron wave is $\Gamma_{max} = 0.098$ at $k_{max} = 0.67$.

TABLE III

MODULATION-TO-FIELD RATIO AS A FUNCTION OF BEAM ASPECT RATIO

$\nu = 1.75$, $\gamma_0 = 7.0$, $\Omega = 2.0\ \omega_p$, $R_W - R_B = 1.15$, $k = 0.45$

R_B/Δ	$v_r(R_B)/E_{z\ max}$	$v_r(R_B)/E_z(0)$
1.0	2.66	2.66
1.6	2.05	2.36
1.8	2.00	2.36
2.1	1.91	2.30
2.5	1.87	2.36
4.0	2.13	3.14
10.0	2.97	8.57

as a function of aspect ratio, for constant beam-to-wall separation and total current of 30 kA ($\nu = 1.75$).

Typical v_r and E_z eigenmodes are shown in Fig. 3. There is very little systematic enhancement of the modulation-to-field ratio with hollow beams, and the fact that peak E_z fields occur on the inner beam surface, and not on axis, implies that there will be little radial confinement of any ions and correspondingly poor ion beam quality.

In conclusion, we find little advantage for using a hollow, rather than solid beam. There are minor advantages and disadvantages for both, but to the extent we have studied that hollow beams ($R_B/\Delta R \leq 10$), we find no distinct programmatic advantages for changing to a hollow beam at this time.

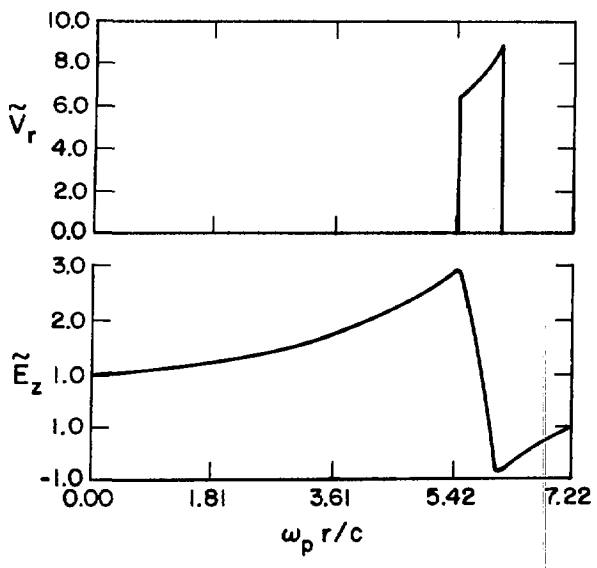

Fig. 3

Radial velocity ($\tilde{V}_r$) and axial field ($\tilde{E}_z$) eigenfunctions for hollow beam with R_{in}=5.45, R_{out}=6.07, γ_0=7, Ω_0=2.0 ω_p, and ν=1.75 (30 kA).

APPENDIX D

SLOW CYCLOTRON WAVE GROWTH BY PERIODIC INDUCTIVE STRUCTURES

To be published in the Proceedings of the Third International Conference on Collective Methods of Acceleration

SLOW CYCLOTRON WAVE GROWTH BY PERIODIC INDUCTIVE STRUCTURES

by

William R. Shanahan, Brendan B. Godfrey, and Rickey J. Faehl

ABSTRACT

The Auto-Resonant Accelerator concept of collective ion acceleration is critically dependent for its success upon the availability of an effective means with which to grow the relevant slow cyclotron wave. We present a preliminary study of such growth via a two-dimensionally periodic slow wave structure. This structure consists of a z-slotted waveguide about which are placed conducting straps axially and azimuthally interrupted by capacitive gaps. Appropriate boundary conditions are derived without reference to concepts borrowed from low-frequency circuit theory. These boundary conditions have been incorporated into a numerical code which performs linear normal mode analyses about self-consistently generated nonneutral relativistic electron beam equilibria. This same code may also be employed to examine the purely vacuum modes, which exhibit expected behavior. Questions of structure tuning are discussed. Initial results concerning wave growth are presented, and future activities indicated.

In the travelling-wave class of collective ion acceleration schemes, ions are placed in the trough of a large-amplitude plasma wave that has been produced on a relativistic electron beam. The ion-wave system is then accelerated by increasing the phase velocity of the wave through suitable spatial[1,2] or temporal[3] variation of system parameters. Crucial to the success of such schemes is the availability of an effective method with which to grow such large amplitude waves. For the Auto-Resonant Accelerator, where one is concerned with the slow cyclotron mode, several such methods have been investigated in the past. In one approach[4] explicit advantage is taken of the negative-energy nature of

the slow cyclotron mode to grow the wave through the introduction of a dissipative element, such as a resistive liner. In another, perhaps more familiar method, growth is achieved by permitting the electron beam to interact with a slow-wave structure. The use of such structures is particularly attractive in this context, inasmuch as their spatial structuring offers at least the possibility of growing modes with prescribed desirable properties while discriminating against less favorable waves. In particular, the slow-wave structure consisting of a metallic helix surrounding the relativistic electron beam has hitherto been extensively investigated from this point of view.[4,5] In this report, we present preliminary results of an investigation of another, quite different, slow-wave structure.

The system considered here consists of a z-slotted wave-guide around which are placed conducting straps. These straps are interrupted both axially and azimuthally by capacitive gaps to give rise to a two-dimensionally periodic structure. The entire system is enclosed within an outer cylindrical conducting wall. This structure, the resonant loop-drive, is depicted in Fig. 1. Interaction of an electron beam with such a structure may be viewed in two quite conceptually distinct, but physically equivalent, ways. Firstly, the periodic structure may be considered to be an effective LC-circuit with the electron beam serving as a source of electromotive force. The various geometric features of the slow-wave structure, such as the axial and azimuthal periodicities and corresponding strap lengths and widths, may then be adjusted to provide the effective LC-circuit with a resonant frequency appropriate to the beam mode whose growth is desired. Energy is consequently extracted from this mode; and since it is negative energy in character, the amplitude of the mode grows.

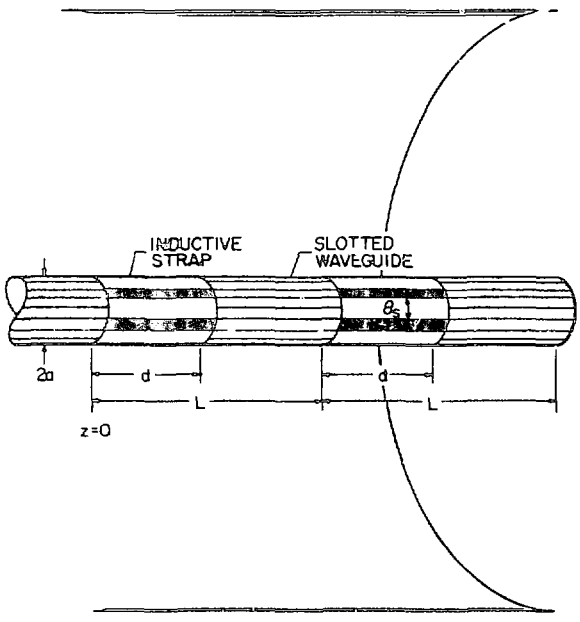

Fig. 1
Resonant loop-drive slow-wave structure.

The second, perhaps more satisfying, way of viewing the interaction

between the electron beam and the slow-wave structure being considered here is as being the solution of a boundary-value problem involving Maxwell's equations and a periodic boundary. In this view, the dispersion relation of the relevant vacuum mode mirrors in w-k space the periodicity in real space introduced by the boundary conditions. This mode is consequently highly distorted from its periodicity-free form and may be expected to intersect the less affected slow-cyclotron mode, the position and strength of the intersection being controlled by the geometric properties of the slow-wave structure. Of course, this is also the conventional view of the slow-wave structure interaction with nonrelativistic electron beams.[6]

Austin Research Associates, Inc. the inventors of the Auto-Resonant Accelerator principle, have presented a very useful analytic discussion of the slow-wave structure under consideration from the point of view of lumped-element circuit theory.[7] Such an analysis is essential for obtaining an intuitive grasp of the dynamics of slow-cyclotron wave growth by this method. However, this approach makes a number of assumptions whose limits it would be desirable to delineate. Firstly, a treatment strictly from the perspective of Maxwell's equations is desirable in determining those regions of frequency and wave-number where the more tractable lumped-element circuit theory is applicable. Such a determination should provide greater confidence in future analytic studies. Secondly, earlier analysis assumed that the capacitative gaps were so numerous that their capacitance could be assumed to be uniformly distributed in the azimuthal direction. In reality, the capacitance is concentrated at various points about the circumference of the conducting straps, thereby introducing a periodicity in this direction. Such a periodicity can have a marked effect on the relevant mode structure, linking together modes of different azimuthal quantum number. The analysis to be presented below addresses this question. Lastly, previous investigators employed a model beam profile which essentially ignored all radial variations. Numerical investigation has revealed that such a profile is not always appropriate for an electron beam with parameters suitable for collective ion acceleration.[8] An investigation of the effect of a more realistic profile on the growth mechanism is clearly desirable.

The purpose of this paper is to report on some preliminary results of an investigation designed to address these issues. We begin by deriving boundary conditions suitable to the slow-wave structure described above. No recourse is made during this derivation to concepts borrowed from low-frequency circuit

theory. These boundary conditions have been incorporated into a numerical code designed earlier to investigate the equilibrium and eigenmodes of a relativistic electron beam propagating in a nonperiodic geometry. This same code may be employed to examine the vacuum modes, an understanding of which is essential to a full appreciation of the cyclotron wave growth mechanism. Finally, we turn to some initial results regarding cyclotron wave growth on a relativistic beam.

The boundary conditions to be applied are simply those that the tangential electric field component $E_\theta(r = a)$ be continuous everywhere and vanish identically on the conducting straps. Further, the radial derivatives are required to be continuous at the gaps. The tangential electric field component $E_z(r = a)$ is, of course, forced to be zero by the presence of the z-slotted waveguide. The usual metallic boundary-value conditions are assumed to be applicable at the outer conducting wall. These conditions may be summarized conveniently as

$$\sum_{hj}\{E_\theta(r = a)S(\theta - j\theta_0)S(j\theta_0 + \theta_s - \theta)S(z - hL)S(hL + d - z)$$

$$+\left(\frac{\partial E_\theta^{(1)}}{\partial r}\Big|_{r=a} - \frac{\partial E_\theta^{(2)}}{\partial r}\Big|_{r=a}\right)S\left[\left(j + 1\right)\theta_0 - \theta\right]$$

$$\times S(\theta - j\theta_0 - \theta_s)S(z - hL - d)S(hL + L - z)\} = 0 \quad , \tag{1a}$$

and

$$E_{\theta,z}^{(2)}(r = b) = 0 \quad . \tag{1b}$$

Here L is the axial periodicity length, θ_0 is the corresponding azimuthal quantity, while d and θ_s are, respectively, the axial length and angular width of the conducting straps. The superscripts (1,2) refer to the regions interior and exterior to the slow-wave structure. We have also introduced the standard unit step function:

$$S(x) = \begin{cases} 1 & x > 0 \\ \\ 0 & x < 0 \end{cases} \quad .$$

The rather unsightly expression (1a) may be somewhat simplified to yield

$$\frac{\partial E_\theta^{(1)}}{\partial r} - \frac{\partial E_\theta^{(2)}}{\partial r} + \left[E_\theta^{(1)} - \frac{\partial E_\theta^{(1)}}{\partial r} - \frac{\partial E_\theta^{(2)}}{\partial r}\right] \mathrm{Str}(z,\theta) = 0 \qquad (2)$$

where $\mathrm{Str}(z,\theta)$ is that combination of step functions defining the positions of the straps:

$$\mathrm{Str}(\theta,z) = \sum_{hj} S(z - hL)S(hL + d - z)S(\theta - j\theta_0) \times S(j\theta_0 + \theta_s - \theta) \quad . \qquad (3)$$

The numerical code into which the above boundary conditions are to be incorporated solves for the eigenfrequencies and radial eigenfunctions of a mode of the beam-waveguide system, which has a specified axial wave number k_z and a particular azimuthal quantum number ℓ. Consequently, Equation (2) must be put into a form consistent with such a scheme. The two-dimensional periodicity of the present slow-wave structure implies that the fields will have the form of Bloch functions

$$\underline{E}^{(1,2)}(r,z,\theta) = \sum_{\substack{k\,\ell \\ n\,p}} E^{(1,2)}(r)\, e^{i(k+pk_0)z+i(\ell+nm_0)\theta} \quad . \qquad (4)$$

The desired form may be obtained by substituting (4) into (2), multiplying by the usual Fourier exponentials, and effecting the necessary elementary integrations. The result is

$$\bar{E}_\theta^{(1np)} + \frac{1}{\theta_0 L} \sum_{n'p'} \left[\theta_s d - \frac{2\pi L}{\mu_0} \delta_{nn'}\delta_{pp'} + \theta_s \frac{\sin(p' - p)k_0 d/2}{(p' - p)k_0 2} \delta_{nn'} + \frac{d\sin(n' - n)m_0\theta_s/2}{(n' - n)m_0/2} \delta_{pp'} + \frac{\sin(n' - n)m_0\theta_s/2 \sin(p' - p)k_0 d/2}{(n' - n)m_0(p' - p)k_0/2}\right]$$

$$\times \left[\left(1 + A_{p'}^{n'}\right) \bar{E}_\theta^{(1n'p')}(r = a) - \frac{\partial \bar{E}_\theta^{(1n'p')}(r)}{\partial r}\Big|_{r=a}\right] = 0 \quad , \qquad (5)$$

where we have defined

$$\bar{E}_\theta^{(lnp)}\ (r = a) = e^{i(pk_0 d/2 + nm_0\theta_s/2)}\ E_\theta^{(lnp)}\ (r = a) \tag{6}$$

and

$$A_p^n = \Big[\Big(I'_{\ell+nm_0+1}\ (k_p a) + I'_{\ell+nm_0-1}\ (k_p a)\Big)$$

$$\times \Big(K_{\ell+nm_0+1}\ (k_p b) + K_{\ell+nm_0-1}\ (k_p b)\Big)$$

$$- \Big(I_{\ell+nm_0+1}\ (k_p b) + I_{\ell+nm_0-1}\ (k_p b)\Big)$$

$$\times \Big(K'_{\ell+nm_0+1}\ (k_p a) + K'_{\ell+nm_0-1}\ (k_p a)\Big)\Big] \Big/ D \quad . \tag{7a}$$

$$D = [I_{\ell+nm_0+1}\ (k_p a) + I_{\ell+nm_0-1}\ (k_p a)]$$

$$\times [K_{\ell+nm_0+1}\ (k_p b) + K_{\ell+nm_0-1}\ (k_p b)] - [a \leftrightarrow b] \quad . \tag{7b}$$

$$k_p^2 = \frac{\varepsilon\omega^2}{c^2} - \left(k_z + \frac{2\pi p}{L}\right)^2 \quad . \tag{7c}$$

Equation (7) is derived from a consistent application of boundary condition (1b), together with that deriving from the continuity of the tangential electric field. Here $k_0 = 2\pi/L$ and m_0 is the analogous, but integral, quantity, which is in fact the number of azimuthal gaps employed. The prime on the summation symbol denotes, as usual, the omission of terms which would give rise to singularities through the vanishing of denominators. The quantity ε is the dielectric constant of the material which fills the region between the slow wave structure and the outer conducting wall. This material has been introduced for numerical tuning, as will be elaborated further below.

Equation (5) could perhaps be made the basis of analytic study of slow cyclotron wave growth. Such a study would require several assumptions and approximations whose validity in parameter regimes of experimental interest is not always clear. Our immediate objective has been rather to employ Eq. (5) to conduct numerical investigations, which are not limited by such assumptions and approximations. Previously,[8] a numerical code, GRADR, was written, which constructs self-consistent beam equilibria and performs a normal mode analysis of linear perturbations made about such equilibria. The code produces both the eigenfrequency and the corresponding radial eigenfunctions of a given mode. The equilibria examined have a number of features not shared by the model equilibria generally employed in analytic studies. In particular, the radial variation of the relativistic factor induced by the presence of the space charge is automatically included. This variation has a profound effect, both on the form of the radial eigenfunctions and on the overall appearance of the dispersion diagram. While the dispersion properties of the slow cyclotron wave under discussion are but little modified, the radial eigenfunctions are considerably modified from the Bessel function form characteristic of uniform radial profiles. Particularly striking is the peaking of the relevant eigenmode about the edge of the beams. In addition, discrete modes which appear in the uniform theory are replaced by bands of continuous modes. These features can have significant consequences for cyclotron wave growth mechanisms, leading, for example, to the necessity of greater radial modulation than that predicted by the uniform theory and to the shifting of relevant discrete modes into the regions of continua. These questions have been extensively investigated for growth by helical slow-wave structures[5] but are yet to be addressed for the loop drive.

The numerical code described above has been modified to include the periodic boundary conditions displayed in Eq. (5).

The code may also be used to examine the purely vacuum modes of the slow-wave structure. Such an examination is necessary for a full understanding of the interaction when a beam is present. Study of the vacuum modes is also useful in assessing the accuracy of various truncations which must be effected when using Eq. (5). We expect that the vacuum mode will be relatively flat and that it will exhibit a periodicity in w-k space given by k_0. The degree to which this periodicity is observed may be taken as a measure of the accuracy of a given truncation scheme. These expectations have been fully realized. Runs

with $k_0 = 1$ and d/L = 0.5-0.9 have revealed modes which vary in frequency by approximately 15 percent throughout a Brillouin zone. With three axial zones the frequency was periodic to within 2 percent, while with five it was periodic to within a tenth of a percent. These results were but little changed when azimuthal periodicity was included.

A further question, which may be addressed through a study of the vacuum modes, is that of tuning the slow-wave structure. One would like to achieve the growth of waves with phase velocities roughly in the range of 0.1-0.25. For parameters typical of Auto-Resonant Accelerator operation, this corresponds to a resonant frequency for the slow-wave structure of $w_0 = 0.06\text{-}0.1\ \omega_p$. This frequency is, of course, a function of the various geometrical factors involved, and one might believe that a judicious choice of these quantities would lead to the desired value. Actually, it was found difficult to reduce this frequency much below 0.2 without losing significant coupling between the various components. This difficulty can probably be traced to our idealization of the gaps as having no radial extent. The inclusion of a finite radial width would presumably lead to a greater effective capacitance in the equivalent circuit of the slow wave structure and, consequently, a lower resonant frequency. In the analysis of such a system one must recognize that the azimuthal and axial dependencies of the fields within the gaps are not identical to those occurring in the interior and exterior regions. Consequently, several important simplifications which occurred in the derivation of Eq. (5) do not appear, and the calculation rapidly becomes unwieldy. Rather than pursue this course, we have instead resorted to the simple expedient of filling the region between the slow-wave structure and the exterior wall with a substance of constant dielectric constant $\varepsilon \cong 30\text{-}60$. This quantity can now be adjusted to yield the desired resonant frequency. It is to be stressed that although the dielectric is being introduced here

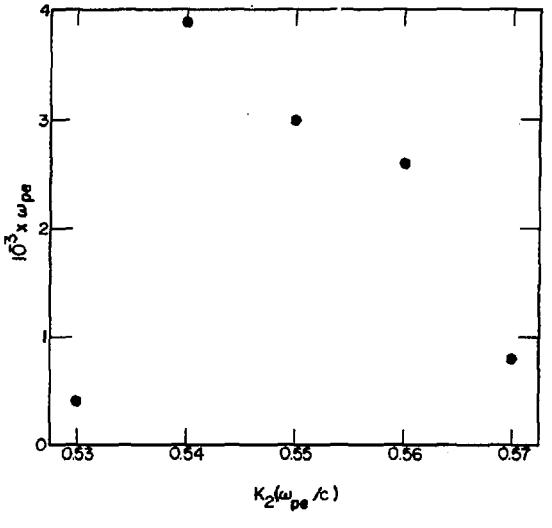

Fig. 2
Cyclotron wave growth with $\gamma = 7$, $R_{beam} = 2.65\ c/\delta_p$, $a = 3.8\ c/\omega_p$, $b/a = 10$, $\Omega_c = 2.0\ \omega_p$.

purely to achieve the desired tuning, it is not altogether clear that the presence of such a substance is not possible or desirable in the actual system. This issue must await the resolution of dielectric breakdown questions. Nevertheless, using this procedure with dielectric constants in the range 30-60, we have been able to produce vacuum modes of the desired frequency. Cyclotron wave growth at the desired phase velocity has not, however, yet been achieved.

Preliminary results for cyclotron wave growth at a somewhat higher phase velocity are exhibited in Fig. 2. Although the parameters chosen to generate this graph do not necessarily optimize the growth rate, examination of the results of this run reveal a number of features which are likely to persist under more favorable circumstances. Firstly, as is clear from the graph itself, the region of growth is very narrow in w-k space. This is in marked contrast to the case of the helical structure, which is a broad-band amplifier. Such sharpness of the resonance may prove an important advantage from the point of view of coherence, provided that it does not seriously militate against initial excitation of the desired mode. Further examination reveals significant coupling between the principal mode and those lying immediately adjacent diffraction zones, the ratio of amplitudes being roughly 0.25. Coupling to more distant zones is much less. Some concern may therefore arise that unwanted modes will experience significant growth. Actually, such concern is unwarranted in the present case, since the relevant modes lie in bands of the continuous modes referred to above. Previous investigation has revealed that such modes, if excited, tend to phase-mix away in a secular fashion.

Further study along the lines sketched here is clearly required to ascertain whether this slow-wave structure will provide an effective growth of the slow-cyclotron waves for Auto-Resonant Acceleration. The linear theory code described above will be used in the near future to determine those beam and structure parameters which lead to optimal phase velocity and growth rate. The important question of the growth of modes with higher principal azimuthal quantum numbers will also be addressed. All the information thereby gained will be used to choose parameters with which to perform cylindrical, relativistic, fully electromagnetic particle computer simulations[9] of slow cyclotron wave growth by the resonant loop drive.

ACKNOWLEDGMENTS

We wish to thank B. Newberger for helpful discussions. This work was supported under the auspices of the U.S. Department of Energy.

REFERENCES

1. M. L. Sloan and W. E. Drummond, "Autoresonant Accelerator Concept," Phys. Rev. Lett. 31, 1234 (1973).

2. P. Sprangle, A. T. Dobrot, and W. M. Mannheimer, "Collective Ion Acceleration in a Converging Waveguide," Phys. Rev. Lett. 36, 1180 (1976).

3. R. J. Faehl and B. B. Godfrey, "Collective Ion Acceleration through Temporal Variation of Relativistic-Electron-Beam Energy," Phys. Rev. Lett. 40, 1137 (1978).

4. W. E. Drummond et. al., "A Theoretical Investigation of Auto-Resonant Acceleration," Air Force Weapons Laboratory report AFWL-TR-296 (1976).

5. R. J. Faehl, B. S. Newberger, and B. B. Godfrey, "Simulation of Cyclotron Wave Growth in a Helical Slow Wave Structure," submitted to Phys. Fluids.

6. R. M. Bevensee, Electromagnetic Slow Wave Systems, (John Wiley and Sons, New York, 1964).

7. W. E. Drummond et. al., "Quarterly Status Report for Period 1 March 1977-31 May 1977," Austin Research Associates Report I-ARA-77-U-47, (June 1977).

8. B. B. Godfrey, "Linear Theory of Radially Inhomogeneous Unneutralized Relativistic Electron Beams," submitted to IEEE Trans. Plasma Sci.

9. B. B. Godfrey, "Numerical Simulation of Autoresonant Acceleration," IEEE Trans. Plasma Sci. 5, 223 (1977).

APPENDIX E

COMPARISON OF AUSTIN RESEARCH ASSOCIATES AND LOS ALAMOS SCIENTIFIC LABORATORY LOOP-DRIVE BOUNDARY CONDITIONS

Los Alamos Scientific Laboratory report LA-7599-MS
February 1979

COMPARISON OF AUSTIN RESEARCH ASSOCIATES AND LOS ALAMOS SCIENTIFIC LABORATORY LOOP-DRIVE BOUNDARY CONDITIONS

by

William R. Shanahan

ABSTRACT

A comparison of two different models for boundary conditions appropriate to the resonant-loop-drive slow-wave structure is presented. The first model is based on a low frequency approximation in which a capacitive field-current relationship is invoked. The second model is essentially a rigorous field theory approach in which no such low-frequency assumption is made. Significantly lower growth rates are obtained from the latter approach than from the former. Reasons for this difference are sought in an examination of the radial eigenfunctions of the azimuthal electric field.

Interaction of a relativistic electron beam with the resonant-loop-drive slow-wave structure has been proposed by Austin Research Associates (ARA) as a method of achieving slow cyclotron wave growth alternative to that provided by use of a helical structure.[1] At the time that this proposal was made, an accompanying analytic study seemed to indicate that growth rates and lengths comparable to those achievable by the use of a helix were to be expected. During the past few months, we at LASL have conducted an independent study of this proposed method of wave growth.[2] Early in the course of this study, it became apparent that the validity of several of the assumptions in the ARA analysis was not altogether self-evident. Since these assumptions, particularly those pertaining to boundary conditions, were made in the interests of obtaining an analytically tractable model of the loop-drive, we embarked upon a purely numerical investigation with what were deemed to be a more realistic set of boundary conditions. Growth rates lower than an order of magnitude of those predicted by ARA have

been obtained. The purpose of this report is to delineate the differences between ARA and Los Alamos Scientific Laboratory (LASL) boundary conditions and to present numerical evidence for the importance of these differences.

The resonant-loop-drive slow-wave structure, proposed by ARA, consists of a z-slotted waveguide about which are placed conducting straps, which are interrupted periodically, both axially and azimuthally, by capacitive gaps. The periodicity introduced into configuration space by the presence of the gaps is mirrored, via Floquet's theorem, by the ω-k space structure of the positive-energy vacuum mode, thereby intersecting the less affected negative-energy cyclotron mode. A resonant transfer of energy from the latter to the former is thus effected, giving rise to growth of the desired cyclotron mode. Physically, the radial modulations requisite to cyclotron mode growth may be viewed as arising from interaction between the first-order azimuthal velocity perturbation and the zero-order axial magnetic field. The first-order velocity perturbations are driven by azimuthal electric fields generated inductively by the time-dependent first-order axial magnetic field which is produced by the azimuthal currents flowing in the conducting straps. These currents are driven by the azimuthal electric fields, thus completing the feedback loop necessary for any instability.

The ARA analysis of the growth mechanism described above proceeded on the basis of a number of assumptions.[1] Firstly, although the azimuthal capacitive gaps are in reality situated at discrete points about the circumference, it was assumed that these are sufficiently numerous that the capacitance may be assumed to be uniformly distributed. In the spirit of low-frequency lumped-element circuit theory, it was asserted that from this it followed that the current in the inductive strap and the azimuthal electric field were related by the capacitive relation:

$$I_\theta = C \frac{1}{d} \int_0^d \dot{E}_\theta(z)\, dz \quad , \tag{1}$$

where an average of the electric field has been effected over the axial length of the strap. This equation was then combined with well-known jump conditions on the tangential magnetic field to give

$$\Delta B_z(z) = \frac{4\pi C}{d} \sum_{n=-\infty}^{\infty} \mathrm{Str}(z) \int_{nL}^{d+nL} \dot{E}_\theta(z')dz' \quad , \tag{2}$$

where Str(z) is that combination of step functions specifying the position of the conducting straps. Using Eq. (2), supplemented by the corresponding conditions for the tangential electric field, matching was effected between interior and exterior solutions to yield the desired dispersion relation. Analysis of this dispersion relation yielded the significant growth rates referred to above.

Our principal reservations concerning this analysis center about an apparent conflict between the assumptions which underlie the capacitive relation, Eq. (1), and the basic jump condition leading to Eq. (2). Essentially, Eq. (1) implies an identification of the conduction with the displacement current, which is equivalent to assuming curl B = 0, whereas the jump condition Eq. (2) requires that this quantity be finite. Further, the preceding analysis assumes that the azimuthal electric field is finite at every point about the circumference of the loop, where in reality the electric field will vanish, to within a very good approximation, on the conducting straps. Since the azimuthal electric fields play a key role in the growth mechanism, it is not altogether clear that this assumption is not without significant consequences. Of course, it was also recognized that the assumption of continuously distributed capacitance precluded the possibility of examining the coupling among azimuthal modes induced by the azimuthal gaps.

Despite these objections, it might be thought that the ARA analysis would nevertheless yield qualitatively correct results and that the points just alluded to would yield only refinements of these results. Such basically low frequency arguments are frequently used in microwave engineering and often lead to quite satisfactory results. To resolve these issues, we have conducted a numerical investigation of the resonant-loop-drive employing a more realistic set of boundary conditions. These boundary conditions are simply that the azimuthal electric fields vanish everywhere on the conducting straps and possess continuous radial derivatives in the gaps. The z-slotted waveguide assures that $E_z = 0$ at the loop radius. These conditions may be summarized as

$$\left(\frac{\partial E_\theta^{(1)}(r)}{\partial r} - \frac{\partial E_\theta^{(2)}(r)}{\partial r} + \left\{ E_\theta^{(1)}(r) - \left[\frac{\partial E_\theta^{(1)}(r)}{\partial r} - \frac{\partial E_\theta^{(2)}(r)}{\partial r} \right] \right\} \times \mathrm{Str}(z,\theta) \right)_{r=a} = 0 \quad , \tag{3}$$

where a designates the radius of the slow-wave structure and $\mathrm{Str}(z,\theta)$ is that combination of step functions specifying both the axial and azimuthal positions of the conducting straps. The superscripts (1) and (2) refer respectively to the regions interior and exterior to the loop drive. Further, the entire beam slow-wave structure system was assumed to be surrounded by an outer conducting wall at which the usual metallic boundary conditions apply.

These boundary conditions have been incorporated into a numerical code, GRADR, designed previously by B. Godfrey[3] to investigate nonperiodic geometries. GRADR performs normal mode analyses of linear perturbations made about self-consistently generated equilibria. GRADR produces not only the proper eigenfrequency, but also plots of the corresponding radial eigenfunction. For purposes of comparison, two different versions of ARA boundary conditions were also implemented in the code. One version was identical to that used by ARA, whereas the other dispensed with the z-averaging present in Eq. (1). Because GRADR deals with normal modes of given axial wave number and azimuthal quantum number, the above equations must be subjected to several manipulations before they are programmed. Details appear elsewhere.[2] Here we summarize the results.

Our results are presented in three sets of two graphs each. The first graph in each set exhibits the growth rate plotted as a function of axial wave number. The second exhibits the nature of the azimuthal electric field as a function of the radial coordinate for an eigenfunction corresponding to a point near the maximum of the first graph. These graphs have been selected from a more complete set of radial eigenfunction graphs generated by GRADR. As will be noted further below, the azimuthal electric field plot selected for display here is the most revealing of these graphs.

The parameters used to generate these graphs were chosen to model the proof-of-principle experiment. These were radius of beam = 2.65 c/ω_b, loop radius = 3.8 c/ω_b, and $\omega_c/\omega_b = 2$, where ω_c is the zero-order cyclotron frequency and ω_b is the beam plasma frequency. In addition, the outer wall has a radius

fifteen times that of the loop which, for these purposes, is essentially infinite. Further, while the tuning of the slow-wave structure may be simply achieved in the case of ARA boundary conditions by the adjustment of a free parameter, for the LASL boundary conditions this must be accomplished by appropriate selection of the various geometric factors involved. For the cases presented here, we have chosen d/L and $\theta_s/\theta_0 = 0.5$, where L is the axial periodicity length, d is the axial length of the strap, and θ_0 and θ_s are the corresponding azimuthal quantities. Further, $2\pi/L = 1$ and two azimuthal gaps have been employed. It was found that adjustment of these parameters alone would not yield the desired low resonant frequency. Further reduction was obtained by filling the space between the slow-wave structure and the outer conducting wall with a material of constant dielectric constant. Here we have chosen this constant to be 30. The unit of length is here c/ω_b, which, for projected ARA parameters, is approximately equal to a centimeter.

Figure 1 corresponds to runs made with LASL boundary conditions, Fig. 2 to those made with ARA boundary conditions, while Fig. 3 is identical to Fig. 2 except that the z-averaging of the azimuthal electric field has been removed. The most striking aspect of these graphs is, of course, that the LASL boundary conditions yield much reduced growth rates compared to those obtained with ARA boundary conditions. Consistently, the range of unstable axial wave numbers is also rather narrower. Removing the z-averaging slightly increases the growth rates obtained with ARA boundary conditions and broadens the range of instability. The group velocity observed in the region of instability for all three cases was approximately 0.5. Thus, these temporal growth rates are relevant to the question of growth length.

It is difficult to come to a definitive conclusion regarding the qualitative source of the quantitative differences in the growth rate exhibited here. Examination of the radial eigenfunctions of three cases considered generally fails to reveal any striking differences. However, a comparison of the azimuthal electric field plots reveals an exception to this statement. For all three cases the real parts of this component are approximately equal, whereas for ARA boundary conditions, both averaged and unaveraged, significantly larger values of the imaginary components at the position of the loop are observed. The absolute values of the azimuthal electric field at the loop for the ARA boundary conditions are approximately three times greater than those obtained with LASL boundary conditions. This observation leads us to speculate that the

conducting nature of the inductive straps, which is contained implicitly in the LASL boundary conditions but is absent from the ARA formulation, is a principal source of the differences in growth rate.

Originally, we had intended an extensive study of the resonant-loop-drive in a variety of parameter regimes, including the study of the variation of growth rate with beam energy and magnetic field strength. The observation of such small growth rates, however, seems to render such studies of purely academic interest.

REFERENCES

1. W. E. Drummond et al., "Quarterly Status Report for Period 1 March 1977-31 May 1977," Austin Research Associates, Inc. report (1977).

2. William R. Shanahan, Brendan B. Godfrey, and Rickey J. Faehl, "Slow Cyclotron Wave Growth by Periodic Inductive Structures," to be published in the Proceedings of the Third International Conference on Collective Methods of Acceleration, Laguna Beach, California, May 22-25, 1978.

3. B. B. Godfrey, "Linear Theory of Radially Inhomogeneous Unneutralized Relativistic Electron Beams," to be published in IEEE Trans. on Plas. Sci.

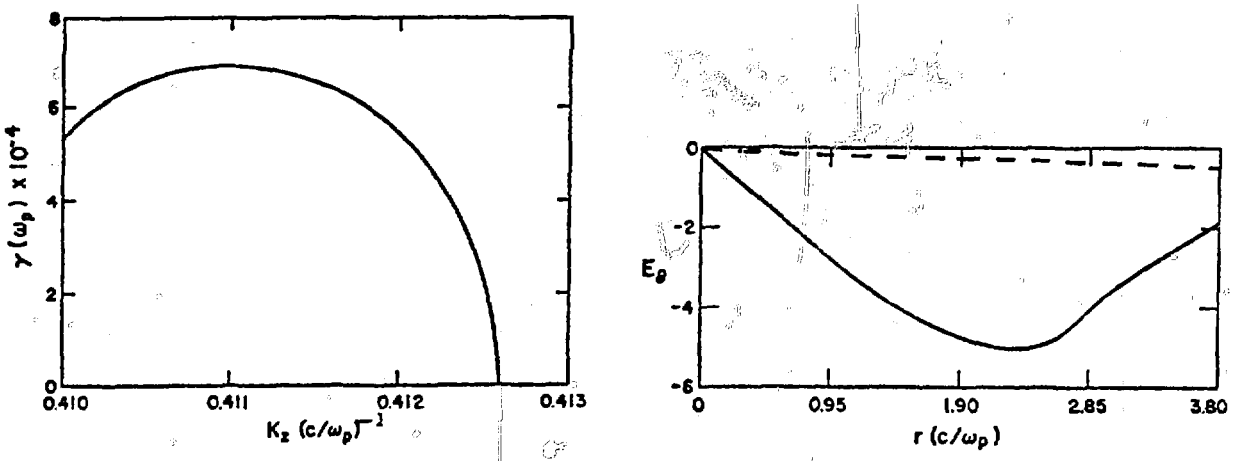

Fig. 1. LASL boundary conditions.

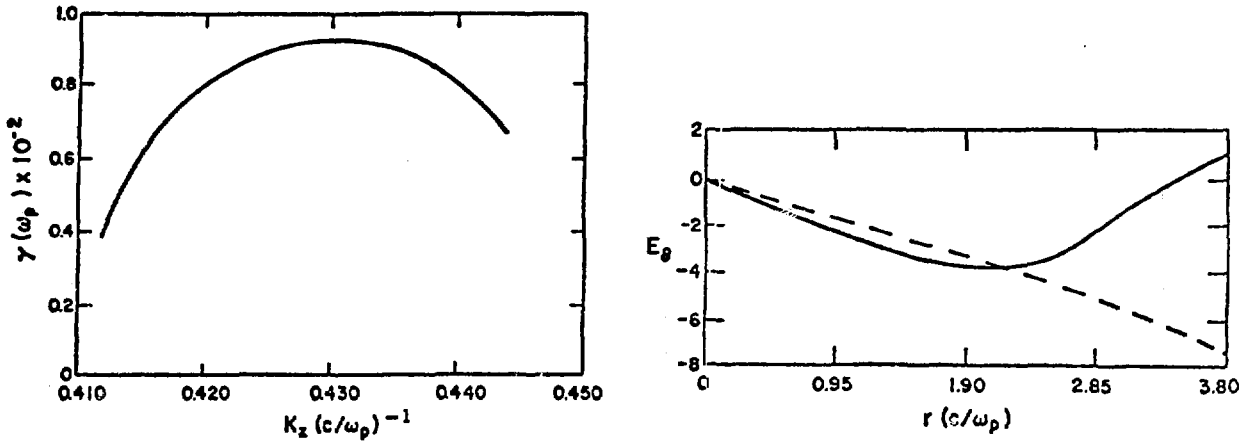

Fig. 2. ARA boundary conditions with z-averaging.

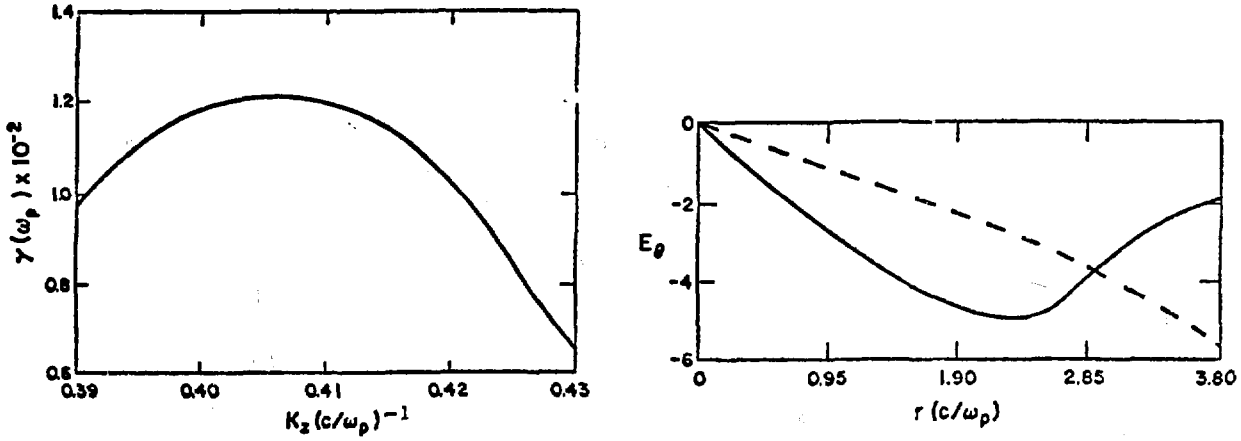

Fig. 3. ARA boundary conditions without z-averaging.

APPENDIX F

SELF-DRIVEN ANTENNA

SELF-DRIVEN ANTENNA

by

Rickey J. Faehl

ABSTRACT

Various waveguide configurations are studied numerically for the purpose of exciting traveling cyclotron waves by the beam self-fields. Efficient excitation is found in at least one configuration, but it is accompanied by large zero-frequency growth.

State-of-the-art rf power supplies are limited in their ability to excite large-amplitude beam cyclotron waves. To reach levels of 1-2 $\times$ 10^5 V/cm necessary for proof-of-principle experiments, the wave must be amplified in the waveguide. This has lead to research at LASL and ARA on helical and inductive loop-type beam wave amplifiers. It has been observed, however, that the self-fields of these high-current, unneutralized electron beams are quite large already. In fact, field-induced breakdown of waveguide surfaces may be a continuing problem. Unfortunately, the self-fields are static while traveling fields are needed to accelerate the ions. The feasibility of driving a resonant antenna or cavity with the static fields has, therefore, been investigated by us using self-consistent particle simulations.

Several possible self-driven antenna configurations have been simulated by us. These studies have been very preliminary. No attempt was made to conduct parametric investigation or detailed analysis. The latter would require a full nonlinear analysis, for we are interested in the efficiency of the coupling, not the field structure in a complicated cavity.

Our work was directly inspired by a suggestion from T. Starke of ARA. He suggested that a quarter-wave helical antenna could be made to ring at the

desired frequency by opening the ground to the antenna after the beam had induced a small amount of current in it. We have not been able to simulate the configuration yet, due to difficulties in changing the antenna from grounded to floating. In the meantime, however, several interesting results have been deduced from the calculations.

Three configurations yielded promising results. These were (1) an iris-loading of the waveguide, with a pair of irises, (2) a cylindrical cavity, and (3) a cylindrical cavity connected to an improperly terminated helix.

A cylindrical beam with uniform density n_0 and radius R_B, inside a guide with walls at R_W, generates large static E_r and B_θ fields,

$$E_r = 2\pi e n_0 R_B^2/r \quad , \qquad R_B \leq r \leq R_W \quad . \tag{1}$$

With the transformation $\tilde{\phi} = e\phi/mc^2$, $\omega_p = (4\pi n_0 e^2/m)^{1/2}$, Eq. (1) then becomes

$$\tilde{E}_r = \frac{1}{2}[\omega_p^2 R_B^2/c^2]/r \quad , \tag{2}$$

where $\frac{1}{4}\ \omega_p^2 R_B^2/c^2 = 17$ kA. Thus for a 35-kA beam and r = 1-10 cm, the vacuum field is between 7×10^3 and 7×10^4 V/cm. These fields are thus larger than can be supplied to that region by conventional power supplies.

(1) With an iris structure, our intention is to disrupt these fields locally. This is in contrast to conventional accelerators, where they are formed into a periodic slow-wave structure. The iris disrupts the beam as follows: To achieve stable beam propagation in the presence of the large fields, a large external B_z field is needed. This induces an E × B drift in the θ-direction. The net V_θ rotation then couples with the B_z field to just cancel the radially outward[2] $E_r - V_z B_\theta$ force. The iris, however, must have $E_r = 0$ on its faces. The local disruption of E_r destroys the radial force balance and particles begin to pinch, searching for a new equilibrium position. As they propagate away from the iris, though, the field conditions revert to their previous state and the particles must return. The resulting overshoot of particles around their proper equilibrium leads to the commonly seen zero-frequency cyclotron wave with the particle trajectories given by

$$r(r_0,v_0,t_0) = |V_r(r_0,v_0,t_0)/(\omega - kv_0)| \quad , \tag{3}$$

where $\omega - kv_0 = \pm \Omega_0/\gamma_0$, $\omega = 0$. Any stationary discontinuity will generate the same behavior, but the iris is a particularly good example.

So far, we have only described how zero-frequency waves (undesirable) are created by the iris. To generate a finite frequency wave, we must employ an additional iris and the fact that the first had already disrupted the beam. Such a configuration is shown in Fig. 1.

When the iris responds to static fields, it excites a spectrum of evanescent and "propagating" disturbances, of which only the above-mentioned zero-frequency mode is seen far from the iris. These are all excited by a zero-frequency source, however, and so are likely to be zero-frequency themselves. During the rise time of the beam, transients are present. A finite frequency component of the rising beam current can then excite the iris at its frequency. With a single iris, these finite frequency components simply radiate away, and the beam excitation ceases when the "flat top" part of the pulse is reached. Addition of a second iris, however, allows the traveling wave excitations to feed back, or in other words, create a resonant cavity structure. The components which can resonate will continue to ring even after the steady current conditions are established.

To make these considerations more quantitative, consider a current form

$$I(t) = I_0[1 - \exp(-t^2/2\tau^2)] \quad . \tag{4a}$$

This pulse, therefore, has the frequency spectrum

$$I(\omega) = \sqrt{\pi/2}\ \tau I_0 e^{-\omega^2\tau^2/2} \quad , \tag{4b}$$

or it has a variance of $\Delta\omega = 1/\tau$. To maximize the component at a given frequency, ω_0, one needs a rise time of $\tau_0 = 1/\omega_0$. The problem is that for a desired frequency of, say, $\omega_0 = 0.10\ \omega_p$ in a beam with $n_0 = 10^{12}$ cm^{-3}, one finds $\tau = 0.15$ ηsec, which is an unreasonably fast rise time. While efficient excitation of such a resonant structure may thus prove difficult, it still should be possible to excite some time of traveling wave with paired irises.

These considerations were tested in a simulation with the following parameters $R_W = 5.7$, $R_B = 2.65$, $\gamma_0 = 7.0$, and irises extending from $R_I = 3.8$ to 5.7 at $z = 15.6$ and 19.3 with a rise time $\omega_p\tau = 25$. (These are similar to

parameters suggested by T. Starke for a quarter-wave helical antenna.) This simulation was similar to standard helical wave-growth runs, with the iris spacing being dictated by a minimum number of cells between irises for adequate wave resolution. If the wave excited was the lowest order cavity mode, one finds $\lambda_0 = 7.4$ or $k_0 = 0.85$. The space-charge depression was so large that the γ-spread in the beam ranged from $\gamma_{min} = 2$ to $\gamma_{max} = 4$. There is thus uncertainty about the value to be used to evaluate the cyclotron dispersion

$$\omega_\Omega = kv_0 - \Omega_0/\gamma \quad . \tag{5}$$

Probes measuring E_θ outside the beams did show a signal at $\omega = 0.29\ \omega_p$, however. This is consistent with Eq. (5) if the effective beam energy was $\bar{\gamma} = 3.6$, which is not unreasonable. The signal, however, was only an order of magnitude above the noise. This was completely dominated by the zero-frequency modulation, for which $\Delta R/R_B \gtrsim 20\%$. Furthermore, computer-generated movies showed only the zero-frequency mode.

The iris-driven beam did not indicate strong traveling cyclotron wave excitation, but very efficient coupling to the zero-frequency wave. The latter level of excitation is quite unsatisfactory and rather mitigates against this configuration. Nevertheless, Eq. (4b) indicates that the current component at $\omega = 0.29\ \omega_p$ was down by a factor of 10^{-12} from the steady current.[1] Excitation of a traveling wave to an order of magnitude above noise with this driving level indicates that the iris driver may yet prove interesting. The excitation may possibly be enhanced by reducing the outer wall radius, increasing the magnetic field or changing the iris separation. Analyzing the excitation seems beyond simple methods, however, so further study will entail more simulation.

(2) The second configuration, a cylindrical cavity, is depicted schematically in Fig. 2. The outer wall was again $R_W = 5.7$, the inner flange radius $R_F = 3.8$, and the beam $R_B = 2.65$. The magnetic field was such that $\Omega_0 = 2.0\ \omega_p$ and $\gamma_0 = 7$. Space-charge effects were much smaller in this configuration, although the beam energy still spanned almost an MeV, i.e., $\gamma_{min} = 4.0$ and $\gamma_{max} = 5.8$. The cavity walls were at $z = 15.6$ and 19.3. This geometry was thus similar in many ways to the iris structure.

Simulation results in this geometry were poor. One reason was the larger effective γ. Although cavity dimensions were virtually the same as the iris, the mean energy was much higher, $\bar{\gamma} \cong 5.5$. Thus, with $k_0 \cong 0.85$, Eq. (5)

predicts $\omega_0 \sim 0.5\ \omega_p$. Beam components at this frequency are reduced from the iris case by a factor of 5-10. Further, the zero-frequency modulation is only $\Delta R/R_B = 6\%$, so the cavity apparently does not couple with the beam efficiently. More detailed analysis may yet show a propitious regime for this cavity, but at present, results are not promising.

(3) The above configurations employed stationary structures. Traveling wave excitation required a temporal variation of the beam, as in the above cases, the rise time. The large self-fields which we hoped to tap were thus unavailable for excitation. If a traveling discontinuity could be induced, however, the static fields might be directly usable. Fortunately, we have already encountered such a disturbance in our helical growth investigation.

The helix is grounded to a perfect conductor, the outer wall flange, and initially uncharged. When the beam is injected, though, a large self-field E_r is induced at the helix radius. This induces a large current along the helix which attempts to maintain ground. Since the beam propagates at $v_0 = c\sqrt{1 - \gamma_0^{-2}}$, while charge can only advance at $v_{ph} \cong c \sin \psi$, ψ the pitch angle, the beam fields quickly outdistance the grounding current. The outer wall is much greater than the helix, so a large discontinuity appears in the self-fields. If this were stationary it would simply generate the familar zero-frequency wave. However, it is moving at v_{ph}, so the excitation is Doppler-shifted to finite frequency. Furthermore, we know this traveling field is resonant with the slow cyclotron mode, so it is actually amplified.

In early simulations with terminated helixes, we inadvertently excited this mode by employing too rapid a beam rise time. The beam cyclotron mode, generated at the front of the grounding pulse, grew so large it completely trapped the beam. By this we mean that no current could pass through the nonlinear cyclotron trapping region. These fields were significantly larger than even virtual cathode fields for similar currents. We have little doubt that large cyclotron waves can be self-excited in this fashion, but it was not clear that steady generation could be achieved.

The simulation configuration used is shown in Fig. 3. Parameters were similar to the simple cavity configuration except that the walls were at $z = 15.6$ and 22.4, and a sheath helix with $\psi = -15°$ was attached along the mouth of the cavity. The nominal wavelength for this cavity was $\lambda_0 = 13.6$, or $k_0 = 0.462$. Terminations on the helix were intentionally mismatched so the helix current would ring for a long period. When the beam was injected, a

large zero-frequency wave again appeared ($\Delta R/R_B \cong 10\%$) but a large, narrow bandwidth cyclotron traveling wave was also excited. Figure 4 shows an E_z probe on axis, at a location z = 130. While the excited frequency is two orders of magnitude above noise, the only reason it was detected was that the location happened to be at a null of the zero-frequency wave. Otherwise, this strong signal is masked. Nevertheless, since B_θ probes just outside the beams show the same signal with little attenuation away from the cavity, it is clear that the traveling wave is excited. The E_z magnitude on axis is 0.05 in units of $(4\pi n_0 mc^2)^{-1/2}$. For $n_0 = 10^{12}$ cm^{-3}, this corresponds to $E_z \cong 50$ kV/a. Although this configuration is successful at exciting the desired traveling wave, suppression of the accompanying zero-frequency mode must be accomplished before it can be regarded as completely satisfactory.

To briefly summarize the results, various waveguide configurations were simulated to study self-excitation traveling cyclotron waves. Although none were completely satisfactory, enough positive data was obtained to indicate that self-excitation may be feasible, however. The primary difficulty encountered was the concomitant excitation of undesirable zero-frequency waves. Until a simple method is found for preferentially suppressing these later, it does not appear that self-driven antennas will be of use in proof-of-principle experiments.

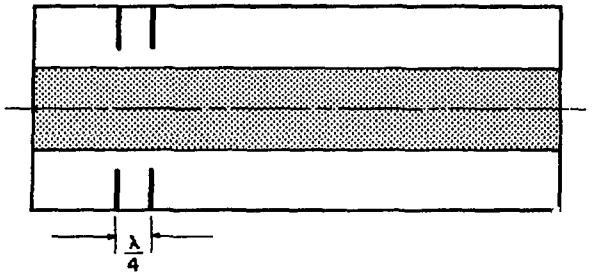

Fig. 1

Iris-driven antenna configuration with quarter-wave (λ/4) separation. Beam is shown as shaded region.

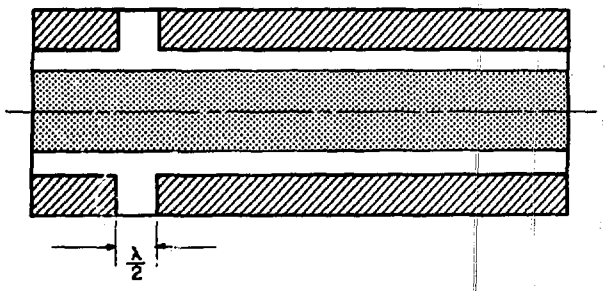

Fig. 2

Simple cavity configuration with half-wave (λ/2) width. Flange is indicated by slanted region.

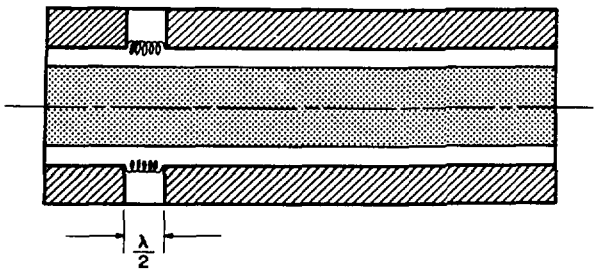

Fig. 3

Cavity plus helix configuration.

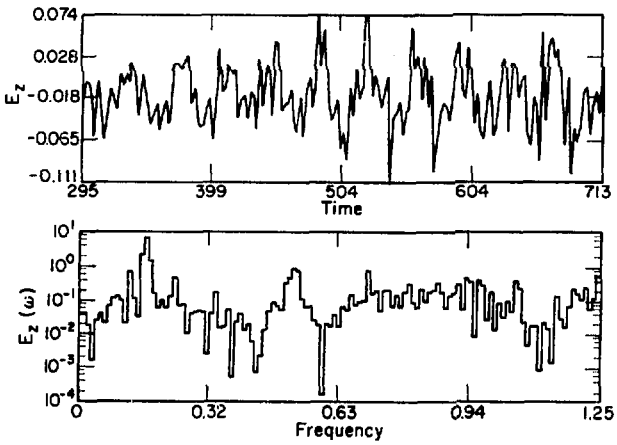

Fig. 4

E_z probe on axis for configuration in Fig. 3; (a) E_z as a function of time, (b) E_z as a function of frequency. Desired frequency is $\omega = 0.16\ \omega_p$.

APPENDIX G

BEAM VOLTAGE AND CURRENT PARAMETER STUDY FOR THE AUTORESONANT ACCELERATION PROOF-OF-PRINCIPLE EXPERIMENT

Published as a Los Alamos Scientific Laboratory report,
LA-7568-MS, November 1978

BEAM VOLTAGE AND CURRENT PARAMETER STUDY FOR THE AUTORESONANT ACCELERATION PROOF-OF-PRINCIPLE EXPERIMENT

by

Brendan B. Godfrey and Rickey J. Faehl

ABSTRACT

Due to flashover problems, Austin Research Associates, Inc. may be forced to perform its proof-of-principle autoresonant collective ion acceleration experiment at electron beam parameters of 2.25 MeV and 15 kA rather than the intended 3.0 MeV and 30 kA. We show that the original experimental goals still can be achieved provided the beam radius is reduced by a factor of two and a thinner anode foil is employed. More generally, our parameter study suggests that operating with beams of smaller radii improves cyclotron wave behavior during beam adiabatic compression or expansion.

I. INTRODUCTION

The autoresonant collective ion acceleration proof-of-principle experiment, as proposed,[1] was to accelerate protons to 30 MeV using a 3 MeV, 30 kA electron beam. The acceleration process was to be controlled by varying the beam guide magnetic field from 25 kg to 2 kg over several meters. Radius of the beam at maximum magnetic field strength was to be 1 cm. However, the electron beam generator has suffered persistent electrical breakdown problems for several months. To ameliorate these difficulties, initial experiments probably will be performed in the 2.25 MeV, 10-20 kA range.[2]

Previously we have made estimates of beam scatter by the anode foil,[3] cyclotron wave growth in a helix slow-wave amplifier,[4,5] and wave behavior during ion acceleration.[6-8] The computations assumed a 3 MeV, 30 kA beam. Here, we repeat the analyses for several combinations of reduced beam energy, current, and radius. We find that increased scatter due to decreased beam

voltage can be offset by use of thinner or less dense commercially available anode foils. Within reasonable limits, slow cyclotron wave growth in a helix amplifier is not strongly affected by electron energy and current. For the same beam radius and range of magnetic field strengths, the reduced current and voltage disasterously increase the ion acceleration length by a factor of 2.5, on the other hand. Fortunately, it is necessary only to reduce the beam (and waveguide) radius by one-half in order to return the acceleration length to manageable proportions.

Sec. II treats foil scattering, Sec. III wave growth, and Sec. IV ion acceleration. Few theoretical details are provided, since they are readily available in the aforementioned references. Some concluding observations are offered in Sec. V.

II. ANODE FOIL SCATTER

Excessive angular scatter in the beam electron trajectories leads to rapid damping of cyclotron waves. This scatter varies adiabatically with guide magnetic field strength. If the scatter is to be limited to 20° at the front of the acceleration section, where B_z^0 = 25 kg, then the beam must leave the diode, where B_z^0 = 2.5 kg, with a scatter no greater than 6°. Anode foil induced scatter depends on the material and thickness of the anode foil and on the electron energy approximately as

$$\theta = F^{1/2}/\beta^2\gamma \quad , \tag{1}$$

where F is obtained from Table I. The table of scattering coefficients was developed by L. E. Thode from Monte Carlo calculations.[3]

Original experimental plans called for a 1 mill. (25.4 μm) titanium foil, which for 3 MeV gives 5.4°. For 2.25 MeV, the value rises to 6.9°. Evidently, a different foil is needed for the lower voltage. One possibility is 1/2 mill. titanium, which gives 4.5° at the lower energy. More generally, any foil with F less than about 0.3 on Table I is acceptable with respect to the 6° scatter limit. Engineering considerations will bear heavily on the final choice.

III. CYCLOTRON WAVE GROWTH

Cyclotron waves required for autoresonant ion acceleration are to be first excited by an RF antenna and then amplified by a slow-wave structure. The helix

amplifier has been thoroughly investigated for the original beam parameters and appears to be a good choice. The need for initially low phase velocities sets the helix pitch angle at 8° for a 3.4 kg magnetic guide field. The ratio of helix radius $\underline{R}$ to beam radius $\underline{a}$ is optimal at about 1.5. With these helix parameters and the original beam parameters of 3.0 MeV, 30 ka, and 2.65 cm radius, the wave e-folding distance is 34.4 cm. Amplification by a factor of twenty can be achieved in a 1 m helix.

We have repeated these GRADR numerical calculations[4-6] for a 2.25 MeV beam of current 10, 15, or 20 kA and a radius of 2.65 or 1.32 cm. Table II gives wave frequency $\underline{\omega}$, wavenumber $\underline{k}$, and growth length $\underline{L}$ for various beam energies, currents, and radii. The e-folding length is seen to be relatively insensitive to beam parameters and in no case cited exceeds by 50% the 3 MeV value. Wave growth appears to be no problem.

IV. ION ACCELERATION

The variation of wave properties and the corresponding increase in ion energy in the acceleration section is determined from conservation of wave energy flux and from the ion equations of motion. Figure 1 shows the change with position of the wave phase and group velocities, and accelerating electric field, the beam envelope modulation, the ion energy, the wave potential well depth, and the guide magnetic field. The magnetic field decreases from 25.5 to 1.7 kg. Potential depth and ion energy are in MV, the electric field in MV/cm, and the axial distance in cm. The data is essentially that of Ref. 7, but reformated. The amplitude of the cyclotron wave at the entrance to the acceleration region is set by $\delta a = a/2$. Larger values of the beam envelope modulation are impractical. Ion energy reaches the desired 30 MeV at 8.5 m.

Figure 2 provides the same information for a 2.25 MeV, 15 kA electron beam, case 3 of Table II. Ions reach 30 MeV at 21.5 m, 2.5 times the Fig. 1 distance. A factor of two comes simply from cutting the total current in half. The remaining length increase is accounted for by the 20% increase in wave number at large B_z^0 for Fig. 2 relative to Fig. 1. Specifically, ka/2 is 1.56 as opposed to 1.31 at $B_z^0 = 25.5$ kg. Other things being equal, ka > 2 reduces the acceleration field sharply.

Results for the same 2.25 MeV, 15 kA beam but with beam and waveguide radius reduced by 1/2, case 6 of Table II, are given in Fig. 3. The distance needed to achieve 30 MeV ions drops dramatically to 6.0 m. The reduction

TABLE I

FOIL SCATTERING FUNCTION $\theta^2 = F/\beta^4\gamma^2$

X(μm)	127.0	254.0	508.0	762.0	1270.0	2540.0
Deuterium Tritium 50/50	0.00447	0.0114	0.0276	0.0455	0.0843	0.191

X(μm)	12.7	25.4	50.8	76.2	127.0	254.0
Mylar	0.0111	0.0292	0.0716	0.119	0.221	0.504
Kapton	0.0115	0.0300	0.0735	0.122	0.227	0.517
Beryllium	0.00944	0.0245	0.0597	0.0987	0.183	0.417
Graphite	0.0211	0.0526	0.125	0.205	0.378	0.852
Aluminum	0.0541	0.132	0.310	0.505	0.924	2.07
Titanium	0.168	0.397	0.913	1.47	2.67	5.91

TABLE II

SLOW CYCLOTRON WAVE GROWTH IN AN 8° HELIX WITH
B_z = 3.4 kg and R/a = 1.5

V(MeV)	I (kA)	a (cm)	ω_0 (3.10^{10}sec^{-1})	k (cm^{-1})	L (cm)
3.0	30	2.65	0.060	0.40	34.4
2.25	20	2.65	0.077	0.52	32.7
2.25	15	2.65	0.075	0.50	38.9
2.25	10	2.65	0.072	0.48	49.3
2.25	20	1.32	0.079	0.48	30.8
2.25	15	1.32	0.077	0.47	34.5
2.25	10	1.32	0.076	0.47	42.8

appears due solely to the smaller value of ka/2 at z = 0, namely 0.76. Also significant, the well depth at the start of acceleration is much greater, facilitating initial ion trapping. We conclude, therefore, that decreasing the beam radius to about one-half the originally planned value is both necessary and sufficient for achieving the projected 30 MeV ion energies at reduced beam energy and current.

As an interesting sidelight, we note that the ion energy corresponding to $B_z^0 = 1.7$ kg is 20% greater in Fig. 3 than in Fig. 2. The difference is explained in terms of the approximate dispersion relation for slow cyclotron waves,[6]

$$\omega_0 = kv - [\omega_c^2/\gamma^2 - \omega_p^2/\gamma^3]^{1/2} \quad . \tag{2}$$

Roughly, the corresponding phase velocity squared is

$$v_\phi^2 = (\omega_0 \gamma v/\omega_c)^2/(1 - \omega_p^2/\gamma\omega_c^2) \quad . \tag{3}$$

Decreasing the beam radius from Fig. 2 to Fig. 3 changes the denominator of (3) from about 0.95 to 0.80. Thus, operating nearer the beam equilibrium limit enhances the variation of ion energy with magnetic field. It is, unfortunately, not clear that this observation has practical value.

V. SUMMARY

We have seen that electron beam reduced energy and current, due to generator problems, should have no significant impact on the proof-of-principle experiment provided beam radius is sufficiently reduced. Indeed, a 2.25 MeV, 15 kA beam injected into the acceleration region with 0.5 cm radius gives a shorter ion acceleration length than does the original 3.0 MeV, 30 kA beam injected with a 1.0 cm radius.

These specific numerical examples emphasize the general rule that ka/2 be less than unity to maximize acceleration rates. Even with the originally proposed experimental parameters, reduced beam radius would give better results. Admittedly, there are experimental problems associated with obtaining small diameter beams. Our numerical analyses nonetheless indicates that efforts in this direction should be made.

This research was performed under the auspices of the U.S. Department of Energy.

REFERENCES

1. W. E. Drummond, G. I. Bourianoff, D. F. Brower, D. E. Hasti, W. W. Rienstra, M. L. Sloan, J. R. Thompson, J. R. Uglum, and H. V. Wong, "Proof of Principle Experiment for the Auto-Resonant Accelerator," I-ARA-76-U-100, Austin Research Associates, 1976.

2. M. L. Sloan, private communication, 1978.

3. L. E. Thode, unpublished.

4. B. B. Godfrey, R. J. Faehl, B. S. Newberger, W. R. Shanahan, and L. E. Thode, "Relativistic Electron Beam Cyclotron Wave Growth in Helical Slow Wave Structures," in Proc. Second International Topical Conference on High Power Electron and Ion Beam Research and Technology (Cornell Univ., Ithica, 1977), Vol. II, p. 541.

5. R. J. Faehl, B. S. Newberger, and B. B. Godfrey, "Simulation of Cyclotron Wave Growth in a Helical Slow Wave Structure," Phys. Fluids, to be published.

6. B. B. Godfrey, "Linear Theory of Radially Inhomogeneous Unneutralized Relativistic Electron Beams," submitted to IEEE Trans. on Plas. Sci.

7. B. B. Godfrey and B. S. Newberger, "Wave Amplitude Variation and Energy Flow in Autoresonant Collective Ion Acceleration," J. Appl. Phys., to be published.

8. R. J. Faehl, W. R. Shanahan, and B. B. Godfrey, "Nonlinear Characteristics of Cyclotron Waves in an ARA Configuration," in Proc. Third International Conference on Collective Methods of Acceleration (Univ. California, Irvine, 1978), to be published.

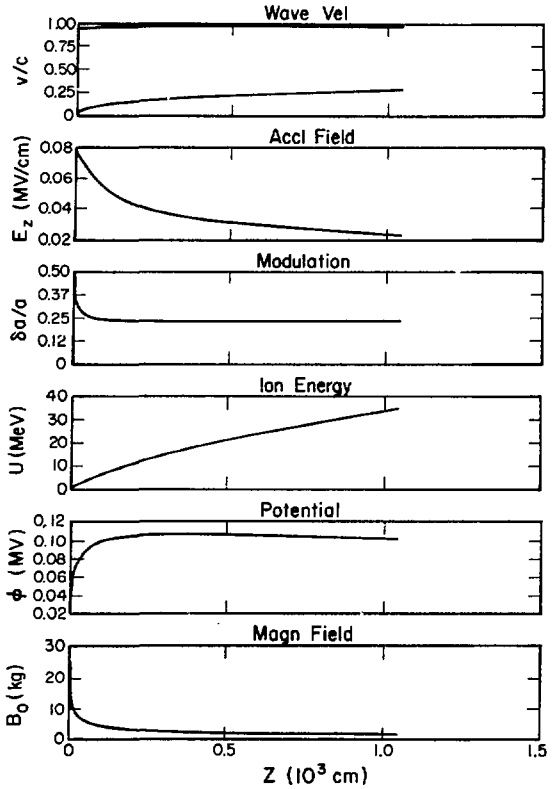

Fig. 1. Variation of wave parameters and beam energy in the acceleration section of the proof-of-principle autoresonant acceleration experiment for a 3 MeV, 30 kA electron beam injected at the left with a 1.0 cm radius. Wave frequency is $\omega_0 = 1.80\ 10^9\ \text{sec}^{-1}$.

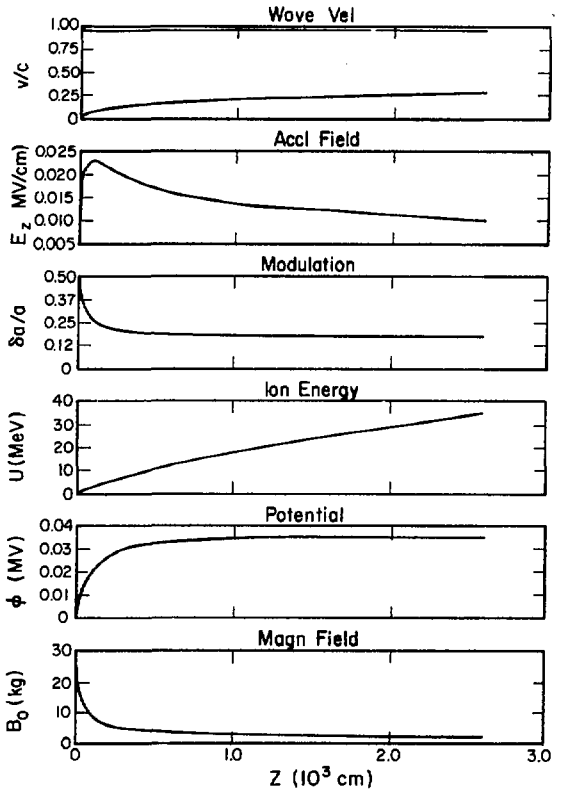

Fig. 2. Variation of wave parameters and beam energy in the acceleration section of the proof-of-principle autoresonant acceleration experiment for a 2.25 MeV, 15 kA electron beam injected at the left with a 1.0 cm radius. Wave frequency is $2.25\ 10^9\ \text{sec}^{-1}$.

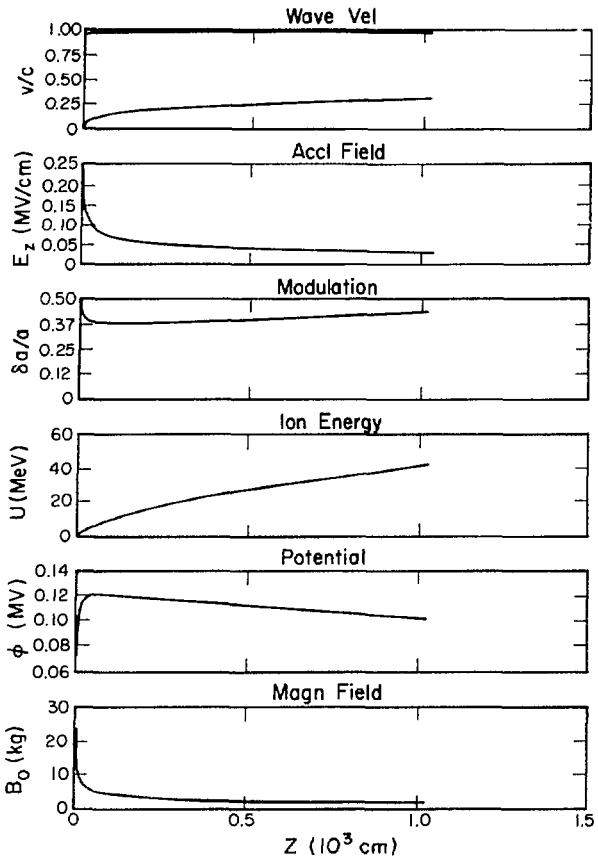

Fig. 3. Variation of wave parameter and beam energy in the acceleration section of the proof-of-principle auto-resonant acceleration experiment for a 2.25 MeV, 15 kA electron beam injected at the left with a 0.5 cm radius. Wave frequency is $2.31\ 10^9\ sec^{-1}$.

APPENDIX H

VIRTUAL CATHODE ION ACCELERATION IN VACUUM ("LUCE GEOMETRY")

VIRTUAL CATHODE ION ACCELERATION IN VACUUM ("LUCE GEOMETRY")

by

R. J. Faehl

ABSTRACT

Simulations have been performed to study collective ion acceleration from a dense plasma slab by a relativistic virtual cathode. Deep potentials are not observed. Bulk acceleration to 2-3 $mc^2(\gamma_0 - 1)$ is nevertheless measured. An inductive acceleration mechanism is proposed, which depends on force neutralized beam propagation.

I. INTRODUCTION

Proposals for utilizing the collective fields of intense relativistic electron beams to accelerate ions have now been extant for over a decade. Though many ingenious and imaginative schemes have been advanced, the most conspicuous success in the laboratory has occurred when virtual cathodes have been formed in either vacuum or a low-pressure gas fill. Ions have been accelerated to over ten times the electron beam energy[1-4] and total ion pulses in excess of 10^{12} ions have been routinely measured. These experiments have been repeated in many different laboratories. With repetition, the data base has gradually increased and uncertainties diminished. Unfortunately, while many groups have undertaken the experiment, no one has yet suggested a quantitative explanation for the acceleration. With this theoretical/experimental disparity in mind, we undertook a numerical study of this problem using two-dimensional relativistic particle simulations. It was hoped that analysis of the simulations would shed light on the responsible acceleration mechanism. These indeed have yielded new insights into the complex ion/virtual cathode dynamics, but the very high energy ion tail [$\varepsilon_{ion} \gtrsim 10\ mc^2\ (\gamma_0 - 1)$] has not been observed

to date. The results nevertheless should lead to a radical reevaluation of basic ion acceleration experiments. Before proceeding to the simulation results, however, it is instructive to review the consensus understanding of virtual cathodes.

II. VIRTUAL CATHODE FOLKLORE

Theoretical understanding of relativistic virtual cathodes, with one exception,[5] is due to a series of one-dimensional analyses.[6,7] The virtual cathode is presumed to form if a current larger than the critical one is injected into a waveguide. A number of analyses have been conducted to determine this space-charge limiting current.[8-11] Numerical investigations have also been performed.[11,12] The analytic virtual cathode studies, however, do not directly incorporate this information. They furthermore become very questionable near the actual particle turning point. One of the first papers to address the question of reflection and the electrostatic potential magnitude of a virtual cathode was by Poukey and Rostoker.[7] Poukey and Olson[13] later extended that analysis to two dimensions and performed two-dimensional electrostatic simulations to test the analysis. Many of the present widespread conceptions about virtual cathodes are derived from these pioneering papers.

An important result derived from the Poukey and Olson analysis was that a deep, stationary potential well could form at the virtual cathode. Under certain conditions, in fact, ultrarelativistic beams could yield maximum potential of $|e\phi_{max}| \cong 2\text{-}3\ mc^2(\gamma_0 - 1)$. Technically, these were limited to the time of first particle reflection; but when supplemented by electrostatic simulations, the results seemed to have broader validity.

The "deep" potential well had clear implications to collective ion acceleration. If any ions happened to become trapped in it (through diffusion, ionization, etc.), they could be accelerated electrostatically to $\varepsilon_{ion} \cong 2\text{-}3\ mc^2(\gamma_0 - 1)$. Since the well, moreover, was stationary, conservation of energy arguments implied that the ion energy should scale as the charge state, i.e., $\varepsilon_{ion} \lesssim Ze\phi_{max}$ Because the well was stationary, of course, no net acceleration would occur as long as it persisted, for the ions remained trapped. When ionization was occurring, this presented no problem. As soon as the monotonically increasing ionization density equals the electron beam density, the well will disappear in a nonadiabatic fashion and ions can propagate freely. These points represent only a narrow abstraction from the Olson-Poukey model.

They are discussed only because these were just the salient features observed in a series of careful experiments.[14-17] Ion acceleration in a neutral gas fill yielded peak energies of just less than three times the beam kinetic energy, with the peak in the ion spectrum centered near $3/2\ mc^2(\gamma_0 - 1)$.

It is natural to identify the experimental ion acceleration data with a "deep well" because they are entirely consistent with theoretical predictions. Both the peak ion energy and spectrum, plus a later observed scaling of ion energies proportional to $Z\phi_{eff}$, where Z is the ionic charge state and ϕ_{eff} an effective electrostatic potential, indicated that the mechanism was purely electrostatic, an intrinsic feature of virtual cathodes. Nevertheless, as we will discuss in the next section, fully electromagnetic simulations of virtual cathode formation and evolution show no such "deep" well when realistic parameters are employed. This apparent paradox can be traced to a number of assumptions, which are not self-consistent.

Before describing the simulation results, we should point out one obvious inconsistency with the electrostatic model of ion acceleration. The cold fluid energy equation for the electron beam is

$$\frac{d\gamma}{dt} = -e\bar{v} \cdot \bar{E}/mc^2 \quad .$$

In steady state, $(mc^2\gamma - e\phi)$ is a constant of the motion, so one can apply simple trapping arguments to arrive at ion energies on the order of $\varepsilon_{ion} \leqq |e\phi|_{max}$. However, $|e\phi|_{max}$ is then limited to the initial beam energy, i.e., $|e\phi|_{max} \lesssim mc^2(\gamma_0 - 1)$. There is an obvious way around this, namely that the state is not steady. Then, a fully self-consistent model may yield potentials greater than the beam kinetic energy. Simple trapping arguments, however, can no longer be applied to calculate ion energy. The objection might be raised that an anomalously deep well could be established through transient dynamics of the initial well formation and then remain steady thereafter. Again, however, if the configuration is steady, the injected electrons would exhibit conservation of energy and be reflected at significant distances from the bottom of the well. Without replenishment from the cold, injected beam, it is difficult to imagine how an unneutralized structure like a virtual cathode could remain intact. While these are only heuristic arguments, they indicate that

ion acceleration in the potential of a virtual cathode may not be as simple as it seems.

III. SIMULATION OF VIRTUAL CATHODES

Previous 1- and 2-D electrostatic particle simulations have been conducted to study beam propagation and virtual cathode formation.[7,13,18] While the qualitative virtual cathode features may be expected to be correctly treated, questions of initial formation and subsequent oscillation of the structure raise doubts as to the role of time-varying fields. We have, therefore, employed a fully electromagnetic, relativistic simulation code, CCUBE, to follow the virtual cathode evolution. This code has been previously used for studies of collective ion acceleration,[19-21] plasma heating by beams, and vacuum beam propagation.[12] For this last, critical currents obtained in the simulation were compared with simple expressions and experiments. Good agreement there served to validate our confidence in the code for conducting these calculations. This study involved two distinct types of calculations, those with beam injection into a vacuum waveguide and those injected through a dense slab of plasma. Since the former provides more direct information about intrinsic virtual cathode bahavior, we will discuss them first.

A. Vacuum Injection Through a Metallic Foil

Solid relativistic electron beams were injected through a "metallic" ground plane in this type simulation into an evacuated cylindrical waveguide. With all units scaled to c/ω_p, $\omega_p = (4\pi e^2 n_p/m_e)^{1/2}$, the radius of the guide was much less than its length. Typical normalized radii were R = 4.7 - 14.5, with a length of Z = 50. (We are considering intense electron beams, so a reasonable beam density is $n_p = 10^{12}$ cm^{-3}. With this density, $c/\omega_p = 0.5$ cm.) The beam current, which was injected smoothly with a gaussian risetime,

$$I(t) = I_0[1 - \exp(-t^2/2\tau^2)] \quad ,$$

scaled with radius squared according to Budker's parameter, $I_0 \cong (\omega_p R_B/c)^2$. For these calculations the time step was typically $\Delta t = 0.04$, and the cell sizes $\Delta z = 0.5$, and $\Delta r = 0.2$. The injection boundary (anode) was a perfect conductor, that is radial and azimuthal electric fields were zero on its surface.

When a relativistic electron beam is injected through the anode, there are initially no space-charge fields. These are established within a few c/ω_p of the surface. If total current is below the waveguide critical current, propagation is permitted and the beam goes freely down the tube. (Several recent studies have confirmed improved expressions for this critical current[10,11] over widely used interpolation formulas.[8,9]) Current in excess of the critical one, however, leads to a discontinuous potential jump in the axial direction, disruption of propagation, and formation of a "virtual cathode." The waveguide can support currents only as large as the critical one, so any excess must be reflected, radially ejected, or "absorbed." By absorbed, we mean here that electrons stop at the virtual cathode and spend long periods of time in that region.

Previous models of the virtual cathode infer the peak potential by following a single particle to the point of first reflection.[7,13] This initial peak is seen in our simulations as a distinct formation feature. Because the potential continues to evolve, we distinguish this feature from the late time maximum and the average peak potential by denoting it as the "beam front potential." This is plotted in Fig. 1 as a function of injection current, in units of ν, where $\nu = 1$ corresponds to 17 kA. The lowest point is associated with a subcritical current, and the highest with a current of over 880 kA. Clearly the latter ($\nu = 52$) is much higher current than used to date in collective ion acceleration experiments. With a risetime of $\tau = 20\ \omega_p^{-1}$, however, the maximum beam front potential $|e\phi_{bf}/mc^2|$, exceeds $\gamma_0 - 1$ by only a factor of about 50%. For typical beam density, this is only a 1.2-nsec risetime. Moreover, Fig. 2 shows that the beam front potential decreases with increasing risetime.

The beam front potential that appears in Figs. 1 and 2 is the appropriate characteristic to compare with previous analytic models, but it is neither steady nor the characteristic potential of a virtual cathode, as can be seen in a typical time plot of $|\phi_{max}|$, shown in Fig. 3. The peak associated with formation is only a transient overshoot. It is not a steady-state condition. It is, however, in qualitative agreement with at least one aspect of earlier analytic models, scaling of potential magnitude with displacement from the anode. The large potential is associated with large displacement; but as the potential relaxes, it moves back toward the anode. It tends to remain at the minimum displacement in the absence of reflected current.

Beam front potential has been discussed first because it provides easy comparison between our simulations and results of previous studies. Potentials greater than the beam kinetic energy have been observed, but not in a steady potential distribution. Simple conservation arguments thus are not violated since the state is clearly time dependent. This does not directly aid in understanding either the initial or subsequent potential magnitudes, however. To understand this more clearly, we will therefore consider formation dynamics in more detail.

When an electron beam current greater than the space-charge limit is injected into a waveguide, a virtual cathode is expected to form. In fact, however, this does not happen instantaneously. Analysis of thin, annular beams shows that there is still a residual kinetic energy at the space-charge limiting currents, i.e., $mc^2(\gamma - 1) \cong mc^2(\gamma_0^{1/3} - 1)$. Solid beams, which we employed in the simulations, are not so susceptible to analysis,[10] but the simulations themselves do exhibit this qualitative behavior. The minimum kinetic energy though is not proportional to $(\gamma_0^{1/3} - 1)$. Thus, we see that initially, the electron beam continues to flow at all radii, with the velocity on axis reduced to between v = 0.5-0.75 c. This state is not stable, however.

We have numerically studied the linear dispersion of beams very close to the space-charge limit. None of the cold beam modes are found to be unstable, but the velocity of slow space-charge waves (both phase and group velocity) is found to decrease toward zero. This property has been observed before, leading to the supposition by Breitzman and Ryutov[9] that accumulation of potential from these waves is the mechanism for beam stoppage. If the sign of the potential were reversed, this would simply be a trapping argument, i.e., the wave potential must be at least large enough so that

$$|e\phi_{wave}| \gtrsim \frac{1}{2} m(v_e^2 - v_{ph}^2) \quad ,$$

where $v_{ph} = \omega/k$, the wave velocity, and v_e is an electron velocity. For a hollow beam, the criterion can be expressed relativistically

$$|e\phi_w| \gtrsim mc^2(\gamma_0^{1/3} - 1) \quad .$$

In fact, this only expresses the fact that the potential can interact directly with particles. Reflection is just the consequence when negative particles are in a negative potential. Since the beam configuration does not induce exponential growth of any waves (apparently!), where does this wave energy come from? There are several possibilities. After particle reflection commences, the reflected current is two-stream unstable with the original beam. Near the anode, velocity, density, energy, and rotation are all axially inhomogeneous, however, so even a convective analysis of the instability evolution is nontrivial. This is being pursued, but no estimates are yet available. In any case, it is irrelevant to the initial potential buildup. The thermal fluctuation level on the beam is another source of potential. In our simulations, we injected a cold beam, so the primary source of fluctuations was probably numerical. In an experiment, the source would be due to diode noise, foil scatter, etc. While the magnitude of potential fluctuations will effect the rate of potential buildup and possibly the location of particle reflection, it does not alter the eventual state, i.e., reflection of part of the current. There are reasons to believe that gradients near the anode may enhance the buildup process but this will require more analysis to evaluate.

Whatever the source of potential, once it reaches reflection levels, a new factor must be included in the virtual cathode dynamics, momentum transfer. This has not been taken into account in previous models. Nevertheless, if a particle with an initial momentum, $p_0 = \gamma_0 mc$, is reflected and re-enters the anode with $p_f = -\gamma_0 mc$, which is commonly observed in simulations, the momentum imparted to the reflecting object is not insignificant. Furthermore, for the high current beams in which we are interested, the momentum flux or pressure at the reflection plane can be very large.

Three things can occur when an electron approaches a cylindrical virtual cathode. If its radial coordinate is large enough so that

$$mc^2[\gamma(r) - 1] - e\phi(r)/mc^2 > 0 \quad ,$$

the particle retains a finite kinetic energy and simply propagates through the virtual cathode. This transmission should not be considered as an "emission"; it is simply in a part of phase/coordinate space that possesses adiabatic trajectories. The particle radius is such that $mc^2(\gamma - 1) - e\phi(r)/mc^2 << 0$, reflection occurs, along with a momentum transfer of $\Delta p \cong 2\gamma_0 mc$. Finally, if

$mc^2(\gamma - 1) - e\phi(r)/mc^2 \cong 0$, the electron can spend long periods of time near the reflection point, i.e., be "absorbed," while giving up $\Delta p \cong \gamma_0 mc$. This situation can occur on-axis during the initial formation and off-axis at any time. Once "absorbed," these electrons are only marginally relativistic, and so there are no relativistic mass corrections. When these particles are subjected to the large, reflection-induced pressures, they commence to move rapidly away from the anode. Since the potential fluctuations are embedded in this stratum, they are carried with the particles. Thus, the peak potential and plane of reflection are accelerated away from the anode. The minimum kinetic energy of the steady space-charge limited current for a solid beam is greater than zero but usually less than $mc^2(\gamma_0^{1/3} - 1)$. The flux of particles to the reflection point is thus drastically reduced. Little further acceleration occurs once the virtual cathode attains the electron velocity. While this propagation takes place, however, potential fluctuations are again building up near the anode. When they have reached a magnitude sufficient to reflect electrons, a new virtual cathode forms, further reducing the particle flux to the original reflecting structure. Clearly the rate at which this process repeats depends both on the magnitude of current in excess of the space-charge limit, that is the magnitude of reflection, and the spectrum of fluctuations on the beam.

Further analysis on the above model is required to make it quantitative, but it does clearly illustrate the repetitive, dynamic nature of a vacuum virtual cathode. This is essential for understanding the fields associated with it, which as applied to collective ion acceleration is the chief reason for examining it in such detail. The above picture is much less simple and, in a sense, less satisfying than a steady,"deep-well" model. A steady well, however, is energetically limited to a depth of $|e\phi/mc^2| \leqq \gamma_0 - 1$. Only by considering time-dependent behavior, initially the fluctuations but later the gross motion of the virtual cathode, can deeper wells be constructed. In fact, the macroscopic motion can be exploited to explain the potentials observed in simulations. A steady, repulsive well can not lead to net energy transfer to the electrons, that is $\langle E \cdot J \rangle = 0$. Transmitted particles are first decelerated, then accelerated back to their original energy; this is a basic feature of steady, electrostatic wells. In a sequence of moving wells, however, particles in proper regions of phase space can remain in synchronism with the virtual cathode fields for long periods of time. Other particles can experience

repulsive fields in alternating directions as a train of virtual cathodes passes and so be quasi-confined. Particles which remain in one region long enough approach a "thermalized" state. Such a situation is observed in simulation around the virtual cathode in the near-axis region. Associated with such an ensemble, there should be a potential energy,

$$\left\langle \frac{p^2}{2m} \right\rangle \cong \langle e\phi \rangle \quad .$$

Figure 4 shows the energy phase space (γ - z) of a virtual cathode after many oscillations (25). Figure 5 shows the associated distribution function. Only near the virtual cathode do particle energies drop below (γ - 1) = 0.5, so it is plausible to attribute the distribution around $mc^2(\gamma - 1) = 1.3$ with an rms mean energy. Although the distribution is not believed to be strictly Maxwellian, it is not unreasonably far from it. This also provides a convenient measure of the average energy.

Though interaction of beam electrons with the virtual cathode is admittedly complicated near the reflection point, certain correlations are still evident. Peak potential in the waveguide was monitored as a function of both position and time. Not surprisingly, it remained localized near the axis in the vicinity of the virtual cathode. This, therefore, gives us an indication of the local dynamic behavior. As Fig. 6b, a plot of axial position of the peak potential as a function of time shows, the "virtual cathode" exhibits periodic bounded motion. While the figure suggests oscillation, however, computer generated movies clearly indicate a train of monotonically moving virtual cathodes. The magnitude of peak potential is shown in Fig. 6a as a function of time, where $mc^2(\gamma_0 - 1) = 4$ for this calculation. Both average and fluctuating values are indeed above the initial beam kinetic energy, but only by a factor of 40%. In fact, the highest fluctuation we have observed to date corresponded to only $e\phi/mc^2|_{max} \cong 1.7(\gamma_0 - 1)$, and the current, I = 880 kA, was greater than the space-charge limit by a factor of 20. Figure 7 shows the results of series of simulations with $\gamma_0 = 5$, of both the peak average and fluctuating potentials as a function of normalized current ν. The measured virtual cathode period τ measured in our calculations is indicated in Fig. 8, also as a function of ν. The apparent similarity between Figs. 7 and 8 suggests that the potential scales with τ^{-1}, which is consistent with our correlation of large potentials

with time-dependent virtual cathode behavior. This hypothesis is difficult to quantify because the relation between ω_{osc} and ϕ_{max} is not functionally simple. Identification of the excessively large potential with regular periodic motion is misleading, however. Injection of a noisy beam leads to highly irregular fluctuations, but roughly the same potential as calculations involving quiet beams. Temporal virtual cathode dynamics in general are the key factor leading to $(e\phi/mc^2) > \gamma_0 - 1$.

This discussion of virtual cathode dynamics in vacuum has been fairly detailed because our fully electromagnetic simulation results are significantly different from previous analytic or numerical ones. The primary difference is absence of deep stationary electrostatic wells. Peak potentials were observed in excess of the beam kinetic energy, $mc^2(\gamma_0 - 1)$, but only by a factor of 1.7. That calculation furthermore corresponded to a beam current far greater than any used for collective acceleration experiments to date. It also had a current risetime on the order of $\tau_R \cong 1$ nsec, which is faster than used in most experiments. As Fig. 2 shows, peak potential decreased with increasing risetime. Our conclusion from these calculations is that potentials associated with virtual cathode experiments probably did not exceed the beam kinetic energy by a significant factor, such as 2. This leaves open the question then as to how a large number of ions were accelerated to between 2-3 times the beam kinetic energy. In the next section, we discuss simulation of beams injected through a dense plasma slab. Though identification of this configuration with any experiment is arguable, the model problem is nevertheless found to shed considerable insight into the acceleration mechanisms actually operative.

B. Injection Through a Dense Plasma Slab

Two-dimensional simulations performed to study collective ion acceleration by a virtual cathode from a dense neutralized plasma have yielded interesting and surprising results. The virtual cathode was formed by injecting a supercritical relativistic electron beam through a finite plasma slab. Formation occurred only after the beam had transited the slab. Ions were attracted to the resulting potential well and plasma electrons repelled. In this way, it was possible to follow the self-consistent interaction of ions with the beam fields in a model geometry which bore some semblance to those created experimentally. It must be emphasized that the initial calculations were performed more to gain understanding of key mechanisms than to duplicate any given experiment. Although the numerical results strongly suggest certain experimental ones, we feel

this was due more to insensitivity of the accelerating mechanism than to any bias in the calculations.

In a typical simulation, the background plasma was 35 more dense than the beam, i.e., $n_p = 35\ n_b$. This choice was predicated both by numerical constraints and debye screening arguments. The plasma slab was felt to be sufficiently dense to screen out beam fields and to provide realistic ion flux into the potential well, though this latter requires some explanation. Recent measurements of the anode plasma indicate a density, $n = 10^{17}$ cm^{-3}, and temperature, θ = 2-5 eV.[22] If ions could flow directly from the high-density region into the virtual cathode, the flux would be orders of magnitude greater than could be achieved in simulations. The plasma possesses an axial density profile, however. Virtual cathode formation cannot take place until the plasma density has dropped to significantly less than that of the beam, so an upper bound on density near the potential well is about 10^{12} cm^{-3}. After the well has formed it will exert a dc electric field on the plasma, which the latter in turn will attempt to screen. This screening length, the debye length, is roughly $\lambda_D \sim 10^{-3}$ cm at $n = 10^{12}$ but $\lambda_D \sim 5 \times 10^{-6}$ cm at $n = 10^{17}$ cm^{-3}. Therefore, the region directly influenced by virtual cathode fields is at moderately low density, with new particles diffusing into that region in a random, isotropic fashion. The situation is completely analogous to the amount of positive ion current drawn by a negatively biased probe, which saturates at fairly low voltage. The high-density plasma, therefore, plays only a minor role in determining ion flux into the potential well. In consequence of our use of reduced ion mass and high plasma temperature ($\theta \sim$ 0.3-3.0 keV), in fact, the ion flux in the simulations may be in excess of actual quantities. More sophisticated slab models are being contemplated at present to check the effect of the simple plasma model.

As with vacuum virtual cathode simulations, the electron beam was injected with a finite, gaussian risetime, with typical normalized time to full current of $\omega_p \tau = 60$. This corresponds to between 0.2-0.3 ηsec, which is exceedingly fast compared with experiments. Beam energy was usually $\varepsilon_b \cong 2$ MeV ($\gamma_0 = 5$) and current varied from I = 22-75 kA. The time step was $\omega_p \Delta t = 0.25$-0.50 (1-2 psec) and cell sizes were $\omega_p \Delta x/c = 0.8$ (0.10 cm) in both radial and axial directions. (Since all dimensions scale with density, the numbers in parenthesis should be interpreted as only representative physical dimensions.) The

radius of the waveguide ranged from $\omega_p R/c$ = 27-50 (2.7-5.0 cm) and the simulation length varied from $\omega_p L/c$ = 200-350 (20-35 cm).

A virtual cathode formed outside the plasma as soon as the current exceeded the space-charge limit. There was little delay from the time this current was attained until the reflection commenced. This suggests that the fluctuation level on the beam had been enhanced by propagation through the plasma. A similar phenomenon may be expected in experiments employing a dielectric insert in the anode, which will create a dense plasma with appreciable width. Potential well depth associated with the virtual cathode is only of order the beam kinetic energy, i.e.,

$$|e\phi|_{max} \cong mc^2(\gamma_0 - 1) \quad .$$

A sample profile of the potential along the axis immediately after virtual cathode formation is shown in Fig. 9a. It conforms qualitatively to previous expectations. Ions are immediately drawn into this well and accelerated to energies of ε_{ion} = 1-1.5 ε_b. It seems somewhat surprising that ions should receive more energy than there is potential until one notes that the accelerating field includes an electromagnetic as well as electrostatic component. The total field is $E_z = -\partial\phi/\partial z - (1/c)\partial A_z/\partial t$. Inductive forces have been previously neglected in virtual cathode analyses, but our simulations indicate they are highly significant.

Ions are accelerated to the above-mentioned energy in moderately short distances, such as $\Delta z \cong 10\ c/\omega_p$. As they propagate down the waveguide, they are not impeded in any sense by the potential "well." The apparent well shown in Fig. 9a only indicates that charge does not flow down the guide (there is no external field). Once ions propagate to the "uphill" side of this "well", they merely facilitate beam propagation farther down the tube. Late in time, the self-consistent ion/electron distribution results in a wide flat-bottomed "well," which still has roughly the same magnitude as it did initially. Such a potential distribution is shown in Fig. 9b, taken from the same calculations as Fig. 9a except at $\omega_p t$ = 900. Still later there is some indication that the depth of the well may decrease near the front edge, but in no case does charge neutralization play a significant role in the ion acceleration. The additional beam propagation is facilitated through force neutralization, which can occur

for ion densities as low as $n_i = n_b/\gamma^2$. We do not observe significant motion of the backedge of the potential.

How does this correlate with ion acceleration? First, magnitude of the virtual cathode potential is, on the average, no more than the beam kinetic energy, $|e\phi|_{max} \cong mc^2(\gamma_0 - 1)$. Second, ions are rapidly accelerated from the neutral plasma slab to energies in excess of the potential magnitude. Third, propagation of the ions permits more beam propagation but no "well" collapse, because the potential "well" does not exist in the sense that it can produce closed, bound ion trajectories. While these three features are not inconsistent with an electrostatic, albeit time-dependent, mechanism for ion acceleration, the argument is greatly weakened by the observation of continued, slower acceleration in the absence of any potential increase or synchronism.

Figure 10 shows a typical time history of maximum potential, $|e\phi_{max}/mc^2|$, while Fig. 11 depicts the maximum ion energy as a function time for two different ion species; M_i/m_e = 500, 1836. (Figure 10 corresponds to the calculation with M_i/m_e = 500.) Ion acceleration is qualitatively similar for both charge-to-mass ratios, with rapid acceleration followed by a more gradual one. The final energy reached in both calculations moreover is ε_i = 2-3 ε_b. Even more suggestive is a plot of maximum ion energy as a function of distance, Fig. 12. The heavier ions clearly do not travel as far in the same period of time, but they do attain the same energy at a comparable position down the drift tube. Since our simulations were only run for relatively short physical distances, i.e., L = 20-35 cm, there is some question whether we observed the maximum saturated ion energies. Energies of 2-3 times the beam kinetic energy nevertheless are consistent with bulk ion acceleration measured in many experiments. The ion spectrum, furthermore, is peaked at $\varepsilon_i \cong 1.5\ mc^2(\gamma_0 - 1)$.

There are at least two possible candidates for the acceleration mechanism. No deep potential well is observed, so that is not one of them. First, the additional beam current made possible by the ion pulse provides an inductive mechanism. There is fairly strong indirect evidence for this, since ion acceleration is correlated with an increase in $A_z|_{max}$ with time. Second, the self-consistent interaction of ions with the beam electrons can lead to fluctuating space-charge fields. Evaluation of this mechanism, however, requires calculation of field-particle correlation functions. It is also a higher order mechanism. Let us, therefore, examine the inductive mechanism in more detail to at least test its plausibility.

The actual evolution of A_z in time is contained within the simulation but involves time-varying current profiles, which are difficult to quantify. However, a simpler model problem can be posed, which is qualitatively similar to the observed dynamics. Consider an ion current flowing within a waveguide of radius R. Let the ions be moving at constant velocity v_i with density n_i and radius a < R. These ions allow a beam current to flow. The beam electrons also are contained within a radius a but have velocity $v_e \cong c$ and density $n_e = \langle\gamma\rangle^2 n_i$. The effective $\langle\gamma\rangle$ of the electrons is reduced greatly from the initial energy since they are transmitted through a virtual cathode. Simulation values give $\langle\gamma\rangle^2 \cong 5$, for $\gamma_0 = 5$. The total current is therefore

$$j = -en_i(\langle\gamma\rangle^2 v_e - v_i) \cong -en_i\langle\gamma\rangle^2 v_e \quad , \tag{1}$$

but its envelope moves at only v_i. For concreteness, let

$$j = j_0\{1 - \exp[(z - v_i t)/L]\} \quad , \tag{2}$$

where $j_0 = -en_e v_e f(r)$ and f(r) is the radial distribution function. This form for the current is not completely general but does possess many of the qualitative features seen in the simulations. It also allows us to explicitly evaluate $A_z(z,r,t)$ to determine if it can explain the acceleration.

The equation for A_z is, in the Lorentz gauge,

$$\frac{1}{r}\frac{\partial}{\partial r} r \frac{\partial A_z}{\partial r} + \frac{\partial^2 A_z}{\partial z^2} - \frac{1}{c^2}\frac{\partial^2 A_z}{\partial t^2} = \frac{4\pi}{c} j_z \quad , \tag{3}$$

where

$$j_z = \begin{cases} 0 \quad , & z > v_i t \\ j_0\left[1 - e^{-(v_i t - z)/L}\right] \quad , & z \leq v_i t \quad . \end{cases} \tag{4}$$

Equations (3) and (4) can be solved in a variety of ways, but the form of j_z suggests a transformation to new variables,

$$\xi_1 = \gamma_i(v_i t - z) \tag{5a}$$

$$\xi_2 = t \quad . \tag{5b}$$

Thus, $\xi_1 = 0$ is the head of the current pulse. A more complete description of the solution to a formally similar problem can be found in the literature.[23] Since solution of Eqs. (3) and (4), subject to the condition that A_z vanish on the wall, $A_z(R) = 0$ is straightforward and not particularly illuminating, and details are left to the Appendix. The solution is

$$A_z(r,\xi) = \sum_n c_n e^{q_n \xi} J_0(q_n r)/[q_n^2(q_n L + 1)] \quad , \qquad \xi \leq 0 \tag{6a}$$

$$\sum_n c_n J_0(q_n r)\{2/q_n^2 - 2e^{-\xi/L}[L^2/(q_n^2 L^2 - 1)] + e^{-q_n \xi}/[q_n^2(q_n L - 1)]\} \quad , \qquad \xi \geq 0 \tag{6b}$$

where

$$c_n = (-2\pi e n_e v_i/c) \int_0^R rf(r)\, J_0(q_n r)dr/(q_n R)^2 J_1^2(q_n R) \quad .$$

The inductive electric field is therefore $E_z|_{ind} = (-1/c)\partial A_z/\partial t$, where

$$\left(\frac{\gamma_i v_i}{c}\right) \sum_n c_n e^{q_n \xi} / q_n (q_n L + 1) \quad , \qquad \xi < 0 \qquad (7a)$$

$$E_z(r,\xi)|_{ind} =$$

$$\frac{\gamma_i v_i}{c} \sum_n c_n \left\{ e^{-\xi/L} \left[2L / \left(q_n^2 L^2 - 1 \right) \right] \right.$$

$$\left. - e^{-q_n \xi} / \left[q_n \left(q_n L - 1 \right) \right] \right\} \quad , \qquad \xi > 0 \quad . \qquad (7b)$$

Note that there is a resonance in both Eqs. (6) and (7) if $q_n L = 1$. Equation (6) possesses a separate solution for these resonant terms,

$$\sum_n c_n e^{\xi/L} \left(\xi_0 + 3L/2 \right) \qquad \xi < 0 \qquad (8a)$$

$$A_z(r,\xi)|_{res} =$$

$$\sum_n c_n \left[2L - e^{-\xi/L} \left(\xi - \xi_0 + L/2 \right) \right] \qquad \xi \leq 0 \qquad (8b)$$

This resonance need not be considered in too much detail, since it arose from the particular form we employed for the current pulseshape, i.e., exponential. The current shape that would evolve physically is determined by self-consistent interaction of electron beam, virtual cathode, and dense plasma. It seems to be qualitatively similar to simulation profiles, but details such as resonance points are probably too model dependent.

A more general characteristic can be deduced, however, simply from the fact that there are resonances which can greatly enhance the inductive field. In other words, a suitable risetime to the current pulse can resonantly drive the cavity. As the analysis shows, only one Bessel expansion at a time can be resonant, and the magnitude is determined by both waveguide dimensions and current radial profile. For instance, if $J_z \propto J_0(q_1 r)$, $c_1 = -4\pi n_e v_i / c$, $c_n = 0$ for all $n \neq 1$, while a flat radial profile yields

$$c_n = -4\pi e n_e v_e q_n R_b J_1(q_n R_b)/[q_n R J_1(q_n R)]^2 \quad .$$

In the latter, the Bessel amplitudes are both smaller and oscillate in sign. The current distribution in the radial direction, therefore, is highly significant in determining strength of the inductive electric field. Moreover, since the axial scale length, L, interacts strongly with the radial scale length, it is important to note that the model described above is not self-consistent; the length must change in time. To illustrate this, consider that the electron current distribution was tied to the accelerated ion distribution. The ions were assumed to be moving at constant velocity v_i. However, if the electric field calculated in Eq. (7), were applied to an ensemble of particles with different initial positions, (ξ_i), one would find that the (ξ_i) do not remain constant in time, nor do they change velocity uniformly. Thus, the distribution must spread and the scale length must change in time.

Ion energy can be calculated with the use of Eq. (7),

$$\varepsilon_i(r,z,t,z_0) = \int_{z_0}^{z} d\tilde{z}\, E_z[r,\tilde{z}(t),t] \quad , \tag{9}$$

where $\tilde{z}(t)$ is derived from

$$\tilde{z}(t) = z_0 + v_i t \int_0^t dt'/\gamma_i(z',t') + q/M_1 \int_0^t dt'/\gamma_i(z',t') \int_0^{t'} dt''E_z(z',t'') . \tag{10}$$

Solution of Eq. (9) and (10), however, requires self-consistent reconstruction of j(z,t) from ion trajectories. Numerical solution of this set is being undertaken with a previously described code,[24] but data is not yet available.

Before discussion of these results in context of previous simulations, analyses, and experiments, it is interesting to observe the effect of a strong guide field on ion acceleration. The magnetic field strength corresponded to $\Omega_0 = \omega_p$, where $\Omega_0 = eB_0/mc$. For typical electron beam parameters, this yielded

an absolute field strength of B_0 = 10-20 kG. The plasma electrons were moderately magnetized and the beam strongly magnetized, but ions were only marginally affected. This strong field case incidentally most closely conformed to vacuum virtual cathode configuration, in which peak potentials greater than $mc^2(\gamma_0 - 1)$ were observed. Peak potential was a secondary consideration here, however. The primary effect of the field was that it permitted transmission of a large, albeit hollow, electron beam current through the virtual cathode without agency of any ions. Thus, the additional current facilitated by force neutralization comprised a relatively small fraction of the total current. In fact, the integrated axial current

$$\langle j_z \rangle = \int dv j_z / \int dv$$

saturated in this simulation, whereas it had increased linearly in time in simulations without an external field. The ion energy furthermore saturated in this case. Ions reached about $\varepsilon_i \leqq 2.2\ mc^2(\gamma_0 - 1)$ by $\omega_p t = 900$ and received no more energy until the end of the calculation at $\omega_p t = 1700$. During that time, they propagated from $\omega_p z/c = 150$ to $\omega_p z/c = 300$. Figure 12 shows that ions received a sizable energy increment over that distance in an unmagnetized waveguide. Therefore, the effect of a guide magnetic field was to degrade the maximum ion energy while not completely inhibiting collective ion acceleration.

IV. DISCUSSION OF SIMULATION RESULTS AND COMPARISON WITH PREVIOUS WORK

It has been observed in a variety of experimental configurations that injection of an intense relativistic electron beam with current above the space-charge limiting current will lead to acceleration of a large number of ions to between 2 and 3 times the beam kinetic energy. The ion energy was furthermore measured to be about the same regardless of the ion mass. Measurements with a Thomson parabola furthermore indicated that energy did scale with ion charge state, Ze. This is all consistent with a simple electrostatic model, provided that a potential $e\phi = \cong 2\text{-}3\ mc^2(\gamma_0 - 1)$ existed. That point seemed to be settled when two-dimensional electrostatic simulations were performed which showed agreement with earlier analytic models. Estimates of the effect of neglecting time-dependent electromagnetic fields indicated that these should be small. The overall success and simplicity of this model have led to its wide utilization in the field of collective ion acceleration. Unfortunately, more

sophisticated calculations and preliminary experiments conducted to study virtual cathode characteristics have failed to verify the central point, existence of a "deep," steady potential well. In fact, on the basis of calculations performed in this study, it seems likely that results may have been misinterpreted because the mechanism bore a clear signature of an electrostatic potential well.

The results of our program of numerical simulation indicate the following:

(1) Potentials greater than the beam kinetic energy, $mc^2(\gamma_0 - 1)$, can form in a virtual cathode, but they are not steady and scale with magnitude of injected beam current. Highest potentials seen were $|e\phi| \cong 1.7\ mc^2(\gamma_0 - 1)$ at a current, I = 880 kA, much higher than any used in collective ion experiments.

(2) Injection of an electron beam through a dense plasma slab results in bulk acceleration of ions to between 2 and 3 times the initial beam energy. The spectrum is peaked at $\varepsilon_i = 1.5\ mc^2(\gamma_0 - 1)$. A large component of the energy is gained after leaving the steep potential gradient, at distances of 1-10 cm from the dense plasma. Magnitude of the potential well was $|e\phi| = (1 \pm 0.20)mc^2(\gamma_0 - 1)$.

(3) Presence of a moderately strong magnetic field degrades collective ions acceleration but does not destroy it.

(4) In geometries examined to date, no high-energy ion tail, i.e. $\varepsilon_i \cong 10\ mc^2(\gamma_0 - 1)$, has been seen in the simulations.

Some of these results are consistent with experiments. For instance, we found that ions with different charge-to-mass ratios were accelerated along similar energy trajectories. In numerical simulations, only the ratio q/M appears. Thus, the just-mentioned result was predicated on ions with the same charge state but different mass. If it were interpreted as ions of the same mass but different charge, we recover the observed charge state scaling, since energy was calculated from measured velocity and assumed mass. The simulations do not distinguish between either interpretation. Since no large potentials were present, it seems likely that this electrostatic "characteristic" was due to self-consistent inductive forces. The accelerating fields apparently fall off after a relatively short distance from the virtual cathode due to evolution of

the ion/electron current profile. This latter point, however, requires further analysis, as do details of the observed charge and mass scalings.

There are several aspects about the simulations which require discussion. Earlier simulations showed deep potentials; the present ones do not. It is possible that the differences were due to neglect or inclusion of time-dependent electromagnetic fields. An important asset and liability of simulations is their self-consistency. Neglect of electromagnetic fields, for instance, does not make them less so, but it does alter particle trajectories and, hence, evolution of the n-particle system. For phenomena in which known analytic results exist, the validity of a simulation can be directly checked; otherwise, the numerical model can be at variance with reality without being obvious. Analytic models do exist for early time virtual cathode characteristics. These are not appropriate for describing late time dynamics, however, nor do they admit ready criterion for ascertaining their regimes of validity. In our fully electromagnetic calculations, potentials greater than the kinetic energy are observed; but the currents at which they occur are quite high. Though analytic estimates of potentials, $|e\phi| \cong (2\text{-}3)mc^2(\gamma_0 - 1)$, may occur physically, it seems that the injected current must be so excessively large as to have little practical applicability at present. It is, furthermore, possible that axial electric fields in our calculations may be similar to those earlier simulations, since the time derivative of A_z compensates to some extent for the reduced ϕ.

In any case, it is misleading to represent the present results as being definitive. While one needs the more general calculation to evaluate the applicability of simpler simulations, our calculations do not encompass all possible physics. Though fully relativistic and electromagnetic, there is no guarantee that important effects do not occur on shorter time or length scales. The debye length, for instance, is only marginally resolved in the dense plasma, although it probably is in the accelerating region. The time step, moreover, is only sufficient to resolve microwave radiation. Bremsstrahlung and synchrotron emission could conceivably lead to radiation damping near the virtual cathode. Rough estimates do not indicate this to be a strong effect, but a priori arguments can be misleading. An effect which may play a role in virtual cathodes is growth of nonaxisymmetric modes driven by velocity shear. Since the calculations are axisymmetric, such phenomena cannot be observed. Further study of these and other sources of error in the calculations is under way, but the

interaction of many effects suggests the desirability of conducting three-dimensional simulations. These, however, are not feasible at present.

Future study of virtual cathode-induced acceleration will be divided between numerical simulation in higher energy and current regimes and analytic investigation of the inductive acceleration mechanism. In particular, source of the high-energy tail will be pursued. Understanding the acceleration mechanism should permit identification of intrinsic limitations and means of optimizing the accelerated ion pulse. Utility of the virtual cathode mechanism as an injector for other collective accelerators seems to be its most reasonable application, although existing performance may be suitable for light-ion-driven inertial confinement fusion.

REFERENCES

1. J. S. Luce, "Neutrons and Radioisotopes Produced by Collective Effect Acceleration," Ann. N.Y. Acad. Sci. 251, 217 (1975).

2. W. W. Destler and H. Kim, "Linear Beam Collective Ion acceleration for Fusion Applications," Proc. 3rd Int. Conf. on Collective Methods of Acceleration, Laguna Beach, California, May 22-25, 1978, to be published.

3. J. A. Pasour, R. K. Parker, R. L. Guillickson, W. O. Daggett, and D. Pershing, " Collective Ion Acceleration and Intense Electron Beam Propagation within an Evacuated Waveguide," Proc. 3rd Int. Conf. on Collective Methods of Acceleration, to be published 1979.

4. R. F. Hoeberling, "Collective Ion Acceleration on the PR1590," Proc. 3rd Int. Conf. on Collective Methods of Acceleration, to be published 1979.

5. V. S. Voronin, Yu. T. Zozulya, and A. N. Lebedev, "Self-Consistent Stationary State of a Relativistic Electron Beam in a Drift Space," Sov. Phys.-Tech. Phys. 17, 432 (1972).

6. H. R. Jory and A. W. Trivelpiece, "Exact Relativistic Solution for the One-Dimensional Diode," J. Appl. Phys. 40, 3924 (1969).

7. J. W. Poukey and N. Rostoker, One-Dimensional Model of Relativistic Electron Beam Propagation," Plasma Phys. 13, 897 (1971).

8. L. S. Bogdankevich and A. A. Rukhadze, "Stability of Relativistic Electron Beams in a Plasma and the Problem of Critical Currents", Sov. Phys.-Usp. 14, 163 (1971).

9. B. N. Breitzman and D. D. Ryutov, "Powerful Relativistic Electron Beams in a Plasma and in a Vacuum (Theory)," Nuc. Fusion 14, 873 (1974).

10. J. R. Thompson and M. L. Sloan, "Limiting Currents for Injection of an Unneutralized Magnetized Relativistic Electron Beam into a Cylindrical Drift Tube," Phys. Fluids 21 2032 (1978).

11. D. J. Sullivan and N. F. Roderick, "Simulation of Space-Charge Limiting Current in Relativistic Electron Beams," Phys. Fluids 22 (to be published in April 1979).

12. L. E. Thode, B. B. Godfrey, and W. R. Shanahan, "Vacuum Propagation of Solid Relativistic Electron Beams: Correlations Among Experiments, Simulation, and Theory," Phys. Fluids 22 (to be published in 1979).

13. J. W. Poukey and C. L. Olson, "Computer Studies of Collective Ion Acceleration," Phys. Rev. A 11, 691 (1975).

14. D. C. Straw and R. B. Miller, "Dependence of Ion Acceleration on Limiting Current in Relativistic Electron Beams," Appl. Phys. Lett. 25, 379 (1974).

15. R. B. Miller and D. C. Straw, "Observations of Collective Ion Acceleration with Drifting Intense Relativistic Electron Beams," J. Appl. Phys. 47, 1897 (1976).

16. R. B. Miller and D. C. Straw, "Scaling Studies of Collective Ion Acceleration with Intense Relativistic Electron Beams," IEEE Trans. Nucl. Sci. 22, 1022 (1975).

17. D. C. Straw and R. B. Miller, "Effect of High v/γ Elctron Beams for Collective Ion Acceleration," J. Appl. Phys. 47, 4681 (1976).

18. A. A. Kolomenskii and M. A. Novitskii, "Two-Dimensional Model for the Propagation of a High-Current Electron Beam and Ion Acceleration from a Gas," Sov. Phys-Tech. Phys. 21, 23 (1978).

19. B. B. Godfrey, "The Localized Pinch Model as a High Energy Ion Acceleration Mechanism," IEEE Trans. Plasma Sci. 6, 256 (1978).

20. R. J. Faehl, B. B. Godfrey, B. S. Newberger, W. R. Shanahan, and L. E. Thode, "Computer Simulation of Collective Ion Acceleration by Discrete Cyclotron Modes," IEEE Trans. Nucl. Sci. 24, 1637 (1977).

21. R. B. Miller, R. J. Faehl, T. C. Genoni, and W. A. Proctor, "Collective Ion Acceleration in a Traveling Virtual Cathode," IEEE Trans. Nucl. Sci. 24, 1648 (1977).

22. J. Adamski, "FX 75 Experiments, Final Report," DASG60-77-C-55 (1978).

23. S. Putnam, "Theoretical Studies of Intense Relativistic Electron Beam-Plasma Interactions," DNA-2849F (1972).

24. R. J. Faehl and B. B. Godfrey, "Collective Ion Acceleration Through Temporal Modulation of Relativistic-Electron-Beam Energy," Phys. Rev. Lett. 40, 1137 (1978).

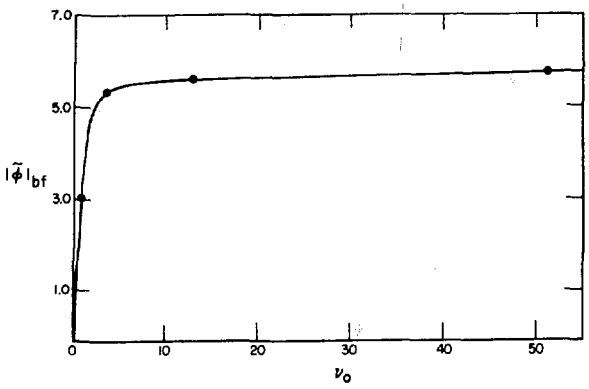

Fig. 1.

Peak beam front potential ϕ_{bf}, as a function of $\times/\gamma_0$; $\gamma_0 = 5.0$ (2.0 MeV), $\tau_R = 20.0\ \omega_p^{-1}$, $R_{wall}/R_{beam} = 2.0$, $\Omega = 8.0\ \omega_p$.

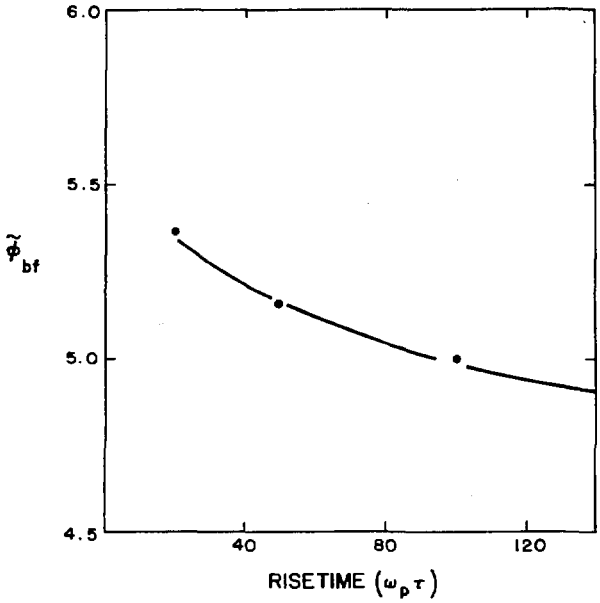

Fig. 2.

Peak beam front potential, ϕ_{bf}, as a function of risetime, τ_R, $\nu = 3.73$ (53 kA), other parameters same as in Fig. 1.

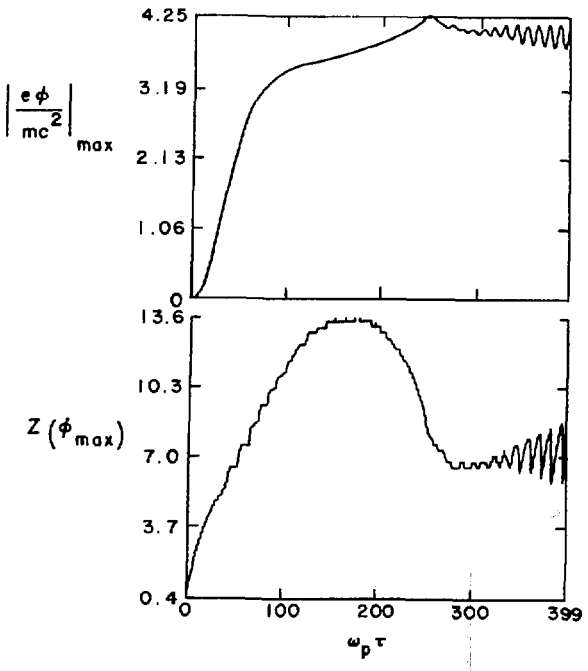

Fig. 3a.

Typical time history of $|\phi|_{max}$; $\gamma_0 = 5.0$, $\nu = 3.73$, $R_{wall}/R_{beam} = 2.0$, $\Omega = 8.0\ \omega_p$.

Fig. 3b.

Position of $|\phi|_{max}$ as function of time.

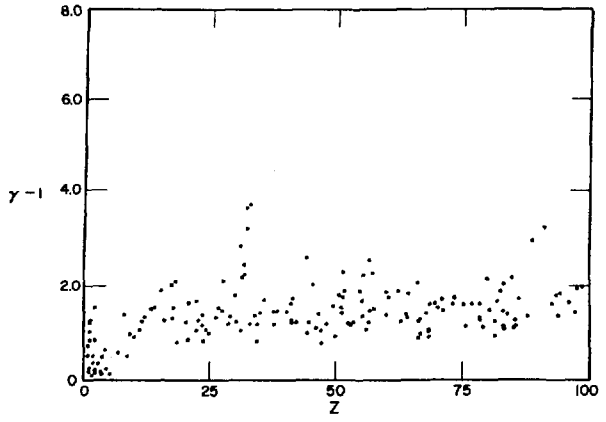

Fig. 4.

Energy phase space of a virtual cathode, $(\gamma - 1)$ vs z; $\gamma_0 = 5.0$, $\nu = 2.5$, $R_{wall}/R_{beam} = 2.0$, $\Omega = 4.0\ \omega_p$.

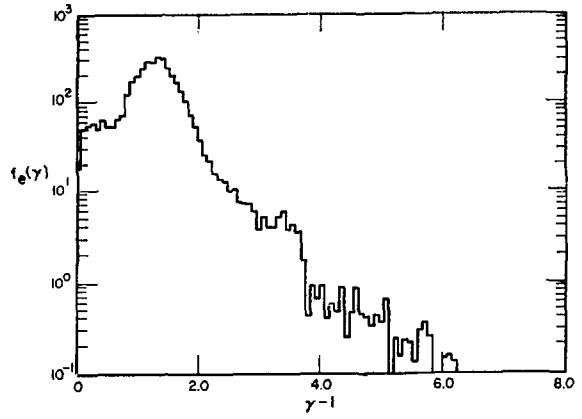

Fig. 5,

Spatially integrated energy distribution function, $f_E(\gamma)$ vs $(\gamma - 1)$, for same parameters shown in Fig. 4.

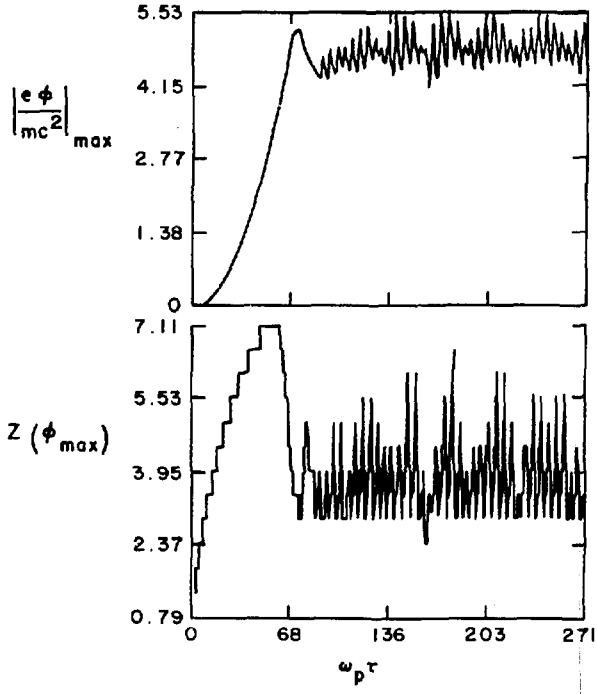

Fig. 6a.

Magnitude of peak potential as a function of time; $\gamma_0 = 5.0$, $\nu = 3.73$, $R_{wall}/R_{beam} = 2.0$, $\Omega = 8.0\ \omega_p$.

Fig. 6b.

Axial (z) position of peak potential as a function of time.

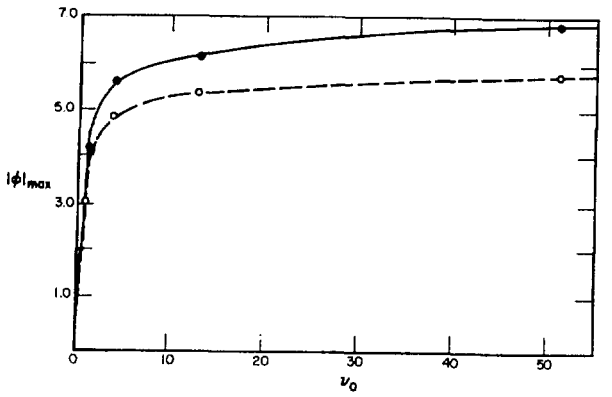

Fig. 7.

Peak potential as a function of normalized current, ν; $\gamma_0 = 5.0$, $R_{wall}/R_{beam} = 2.0$.

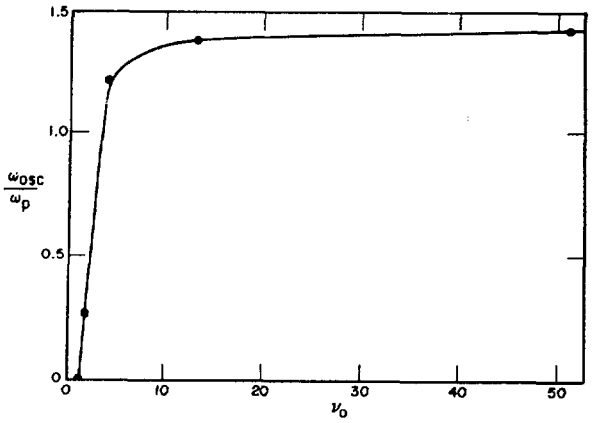

Fig. 8.

Frequency of virtual cathode oscillation, $\omega_{osc} = 2\pi/\tau$ as a function of current, ν, for same parameters as Fig. 7.

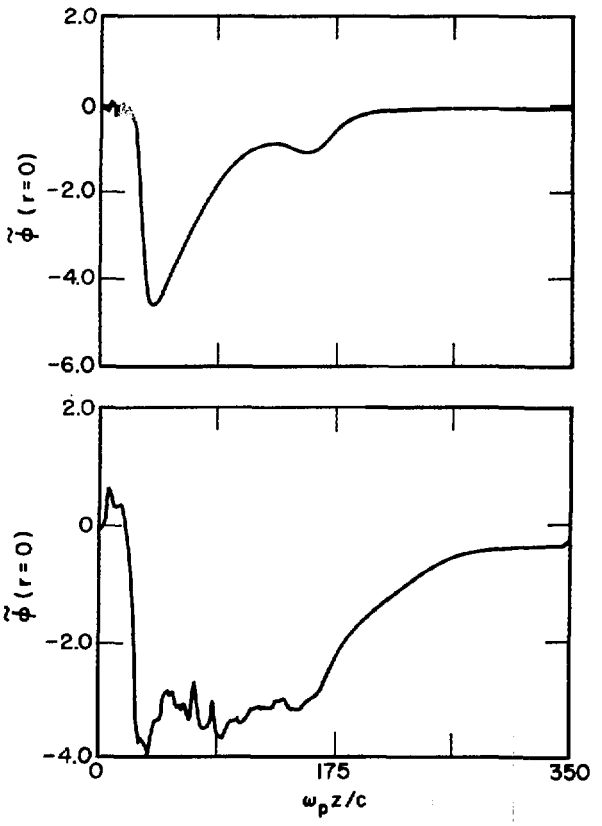

Fig. 9a.

Spatial profile of potential on axis at $\omega_p t = 180$, immediately after virtual cathode formation, $\gamma_0 = 5.0$, $\nu = 1.4$, $R_{wall}/R_{beam} = 2.0$, $\Omega = 0.0$.

Fig. 9b.

Spatial profile of potential on axis at $\omega_p t = 1000$.

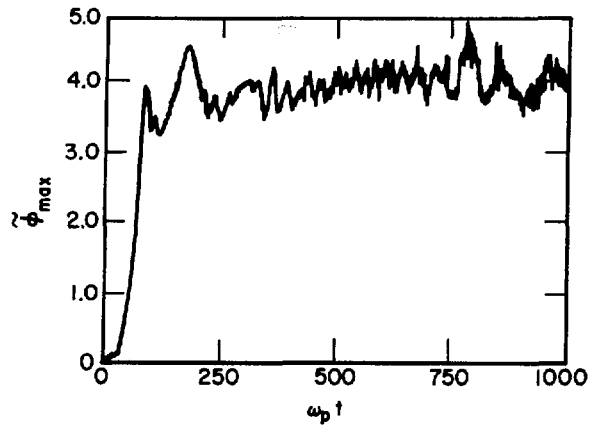

Fig. 10.
Magnitude of peak potential as a function of time, with ion acceleration occurring continuously, $\gamma_0 = 5$, $v = 1.4$, $R_{wall}/R_{beam} = 2.0$, $M_i/m_e = 500$.

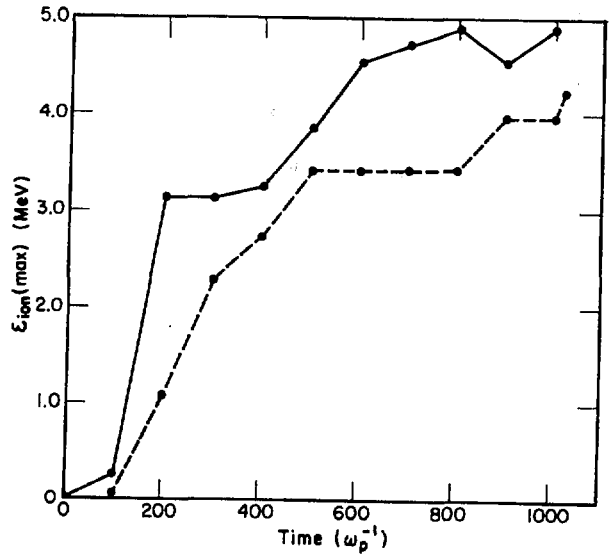

Fig. 11.
Maximum ion energy as a function of time, corresponding to time interval in Fig. 12.

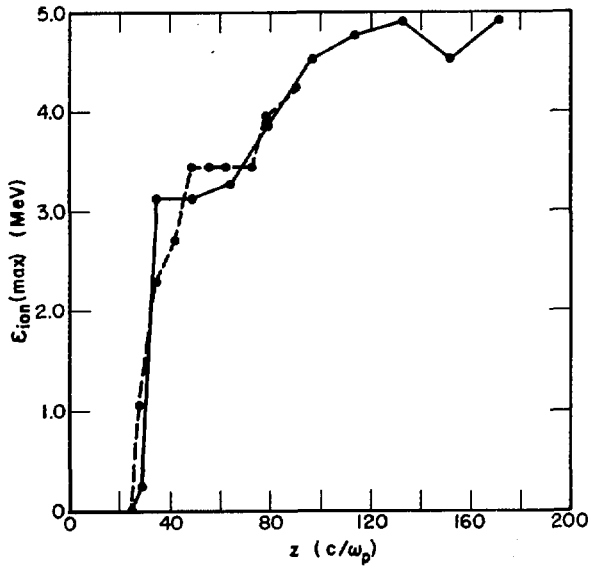

Fig. 12.
Maximum ion energy as a function of z, during the time interval in Fig. 11.

APPENDIX I

TRAVELING VIRTUAL CATHODE ACCELERATOR STUDIES

TRAVELING VIRTUAL CATHODE ACCELERATOR STUDIES

by

Rickey J. Faehl

ABSTRACT

Simulations of a traveling virtual cathode collective accelerator have been performed. Previous calculations had shown turbulent motion of the virtual cathode, but this is greatly improved when a linear current rise is applied. Ions with a mass-to-charge ratio of 1/50 are accelerated to $v_1 = 0.4$ c.

In the FY77 report, we presented numerical results on the traveling virtual cathode accelerator. This concept involves injection of an intense relativistic electron beam into an evacuated waveguide whose radius varies as a function of axial position.[1] The space-charge limiting current of a cylindrical beam, therefore, also depends on position. By varying the beam parameters in time, it was hoped that a virtual cathode could be formed far from the injection plane and moved in a controllable fashion to accelerate ions to high energy. A linearly diverging waveguide was employed in those calculations with no ions present. Constant current injection yielded virtual cathode formation far from either injection or extraction planes. Though fields of moderate magnitude ($E \sim 2 \times 10^5$ V/cm) were created, a build-up of fluctuations led to irregular motion of the virtual cathode, which seemed unsuitable for collective acceleration purposes. Since then it has been found that a somewhat smaller field can be moved smoothly toward the anode by injecting a linearly increasing beam current. Though this mitigates against positive ion acceleration, it may be possible to accelerate negative ions. The following study was, therefore, conducted to determine the suitability of the moving fields for negative ion acceleration.

A series of simulation calculations were performed with a hollow relativistic electron beam which had $\gamma_0 = 5$ (2 MeV). The waveguide had a linearly increasing radius section which, in units of c/ω_p, diverged from a radius of $R_1 = 5.44$ at $z = 170$ to $R_2 = 10.88$ at $z = 340$. The inner beam radius was $R_{bi} = 2.18$ and the outer radius $R_{bo} = 3.11$, yielding a normalized beam current $\nu = 1.24$ (21 kA). A solenoidal magnetic field was imposed of strength $\Omega_0 = 4.0\ \omega_p$, where $\omega_p = (4\pi e^2 n_b/m)^{1/2}$ and $\Omega_0 = eB_0/mc$. This beam is below the space-charge limit at the injection plane, but by $z = 340$, the limiting current is well below that of the beam. Thus, a virtual cathode should form in the interior. With risetime to full current of $\omega_p \tau_R = 75$, we expect steady propagation throughout a waveguide of length $L = 170$ by $\omega_p t = 250$. At $\omega_p t = 325$, we superimposed a linearly increasing component on the steady current, $I = I_0[1 + (t - 325)/500]$.

Two completely different versions of CCUBE were employed in this study. The first was employed for the previous traveling virtual cathode studies. It used potentials $(\bar{A},\phi)$ to move particles and canonical momentum for the particle quantities. For these purposes, it will be referred to as the "old code". The other version used ordinary relativistic momenta ($p_i = \gamma m v_i$) and electromagnetic fields $(\bar{E},\bar{B})$. This "new code", however, differed radically from the old one in its use of an arbitrary order Galerkin particle mover and a new area weighting scheme for current densities and fields. The new code is a bit faster, more flexible, preserves the continuity equation better, and gives more quiescent transverse fields. Longitudinal fields, however, can be significantly noisier. The trade-off between electrostatic and electromagnetic noise can be advantageous in some situations, deleterious in others. A priori evaluation of the relative effects, moreover, is difficult since it is not trivial to decouple longitudinal from transverse contributions to the time-dependent fields. It is safe to say, though, that noise properties in the two versions of CCUBE are different.

Steady conditions, exceeding the space-charge limit, were reached by $\omega_p t \cong 250$. Electric field fluctuations, however, accreted far more slowly in this geometry than are typically seen in simulations of virtual cathodes near the anode. Observable build-up did not occur until $\omega_p t \gtrsim 320$ and first reflection, not until $\omega_p t = 400$-420. These results were obtained with the new version. Using the older version, onset of reflection was delayed to $\omega_p t \cong 500$. The location of first reflection furthermore differed somewhat. In the new

code reflection commenced at roughly z = 255, while calculations with older versions indicate virtual cathode formation at between z = 275-305.

Despite the apparent discrepancy between the two code versions, it should be remembered that any given simulation is completely deterministic and reproducible. First-order phenomena must always be consistent for the simulation to be valid. Second- and higher-order interactions, however, can be affected by cell or time-step size, number of particles per cell, ordering of numerical operations, or particle weighting. Numerical fluctuations due to particle discreteness or finite cell size are able to couple directly with physical fluctuations. In fact, in a set of operations which are repeated many times, i.e., typically thousands, interchange of numerical operations which are algebraically commutative can lead to discrepancies in the second or third significant digit. If the results were susceptible to numerical details though, simulation of plasma phenomenon would have little general validity. Fortunately, it is characteristic of these fluctuations that they have a mean of zero; first-order trajectories and fields tend to be invariant when averaged over many fluctuation times, i.e., autocorrelation times. When considering higher order moments of the physical quantities, though, constant caution must be exercised to ensure that numerical fluctuation effects have been accounted for.

This discussion is motivated by differences in virtual cathode formation in two different versions of CCUBE. If the formation process were governed by first-order quantities such as total current, beam energy, or beam and waveguide dimensions, then there should be no discrepancy. If the local space-charge limiting current were exceeded, propagation would be disrupted and the virtual cathode would form. This does not explain the long interval between establishment of steady conditions and first electron deflection, however. (For typical beam parameters, this interval is on the order of 2 nsec!)

On the other hand, if virtual cathode formation is caused by fluctuation build-up due to space-charge modifications of Langmuir wave dispersion, the apparent discrepancies are plausible. The geometrical factor governing space-charge limiting current is approximately $f = [1 - (b/a)^2 + 2\ell n(R_w/a)]^{-1}$, where b is the inner beam radius, a the outer beam radius, and $R_w = R_0 z/L$ in our case, is the waveguide radius. Taking the two extremal formation positions, $z_{min} = 255$ and $z_{max} = 305$, one finds a relative difference,

$$2(f_{min} - f_{max})/(f_{min} + f_{max}) \cong 15\% ,$$

which is not unreasonable for a noise-induced process. Moreover, the fact that the more distant virtual cathode forms significantly later is consistent with accumulation of slowly propagating potential fluctuations.

An interesting aspect of virtual cathode formation is its similarity to classical phase transitions. The critical point is space-charge limiting current. The actual transition, however, is driven by build-up of fluctuations, which provide the necessary free energy. The new state, involving a phase space separatrix between reflected and transmitted electrons, is clearly higher energy, since reduction of the current will lead to convection of potential downstream and complete beam propagation again. The analogy with phase transitions probably can not be pushed too far, since, as was discussed in Appendix H, self-consistent inclusion of reflected electrons can lead to a time-dependent state. We are pursuing this interesting point, however.

In steady-current simulations, the virtual cathode was observed to undergo progressively more violent, irregular oscillations. This is consistent with the kind of oscillations observed in near-anode virtual cathodes, correlated with reflected electrons. Such behavior is not conducive to long ion/field synchronism. When a linearly increasing current component was superimposed on the steady current, however, the virtual cathode commenced to move smoothly toward the anode. This is the correct qualitative behavior predicted by simple space-charge limiting considerations. Fluctuations around the gross motion were very minor as Fig. 1, a plot of the reflection position as a function of time, shows. A small inflection near $\omega_p t = 470$ can be associated with reflection of electrons. In general, however, very little electron reflection was observed as the virtual cathode propagated from $z = 255$ to $z = 185$, and the "trajectory" was very smooth.

A new feature of the moving virtual cathode is the formation of new virtual cathodes behind the original as current is increased. These also propagated toward the anode. Figure 2 shows a typical energy phase space plot at $\omega_p t = 520$. The associated axial electric field is plotted in Fig. 3. These propagate with roughly constant spacing. The trajectories of three co-linear virtual cathodes are depicted in Fig. 4.

This multiple virtual cathode structure is seen in both new and old versions of CCUBE. As Fig. 5 shows, the trajectories are both displaced in time

and space. This was discussed above. If they are replotted, however, in terms of the approximate local current,

$$I' = I_0\left[1 + \left(\frac{t - t_0 - z/v_0}{\tau}\right)\right],$$

the agreement is satisfactory. Also plotted in Fig. 6 is the theoretical trajectory for our linearly increasing current; it clearly does not describe the trajectory quantitatively. Thus while virtual cathode motion is roughly derivable from simple space-charge arguments, reasonable agreement apparently requires a more sophisticated treatment. This latter will be needed to design an effective negative-ion accelerator. In the meantime, however, we can employ the observed motion heuristically to study collective ion acceleration.

The virtual cathode motion in Fig. 1 exhibits acceleration ranging from $|\tilde{a}| = 2.5 \times 10^{-4}$ to 6.5×10^{-3} in units of $\omega_p c$. For ion synchronism with this motion, we must keep $|q/M|E_z > |\tilde{a}|$. Since the observed peak field, in commensurate units, $(4\pi n_0 mc^2)^{1/2}$, is $E_z \lesssim 0.2$, we must choose a nonphysical charge-to-mass ratio, $|q/M| \geq 1/30$ ($q/M = -1$ for electron) to ensure ion acceleration. The ratio actually used was $|q/M| = 1/50$ for both positive and negative ions, so desynchronism is expected. The source for ions in our simulations was a plasma slug with length $L_p = 20\ c/\omega p$, mean radius $R_p = 1.0$, and density $n_p = 10^{-3}\ n_0$. Low density was employed so that the accelerated ion bunch would not significantly perturb the virtual cathode motion and also to minimize plasma shielding of the virtual cathode fields. In fact, it is possible that a high-density bunch, i.e., $n_p \cong n_0$, would lead to self-synchronism of fields with the negative ions in a constant current beam. This conjecture has not been tested yet, but it seems to merit further investigation.

Figure 7 shows phase and configuration space for both ion species at $\omega_p t = 420$, the time of initial virtual cathode formation. An analogous set of figures at $\omega_p t = 560$ (Fig. 8) shows that both species have been accelerated, albeit in opposite directions. As expected, the negative species have received the bulk of the energy, reaching velocity of $v_z = \sim 0.4$ c, while the positive ions are accelerated only to $v_z = \sim 0.2$ c. With this charge-to-mass ratio, almost complete "snowplowing" of the negative ions is observed. Compression of the negative bunch has resulted in a density enhancement of roughly a factor

of 3 over initial density, but this is still a small perturbation on the beam density.

The results of these calculations can be briefly summarized. Injection of time-dependent current has caused a vacuum virtual cathode to move, in agreement with theoretical expectations. Irregular, turbulent motion seen in simulations of virtual cathodes formed in diverging waveguides, when constant current was injected, is found to be highly attenuated in the present case. Negative-ion acceleration is seen when a plasma slug is placed near the position of initial virtual cathode formation. Peak velocity of over $v_z = 0.4$ c is measured for a linear current risetime of 500 ω_p^{-1}.

There are still major issues unresolved about this collective ion acceleration. Constant current injection into a vacuum led to unsuitable virtual cathode characteristics; injection of a current form $I = I_0[1 + (t - t_0/\tau)]$, where $\omega_p\tau = 500$ yielded smooth virtual cathode acceleration back toward the anode, but at too high an acceleration to pick up realistic negative ions. A key question is whether there exists a parameter window in which smooth motion at a slow enough rate can be induced. This is not entirely academic, since it is plausible that the reason for laminar motion was because fluctuation flux into the virtual cathode was fast enough to prevent potential build-up large enough to induce significant reflection. Motion which is too slow may allow the large potential buildup and consequent high reflection flux. Better understanding of the noise level of electron beams would facilitate comparison with simulation results and permit more accurate evaluation of the viability of a traveling virtual cathode accelerator. Other questions, such as the effect of higher density plasmas and the rate at which these high fields induce negative ion stripping require further investigation. These will be pursued as time permits or until nonfeasibility is unambiguously demonstrated.

REFERENCE

1. R. B. Miller, R. J. Faehl, T. C. Genoni, and W. A. Proctor, IEEE Trans. on Nucl. Sci., NS-24, 1648 (June 1977).

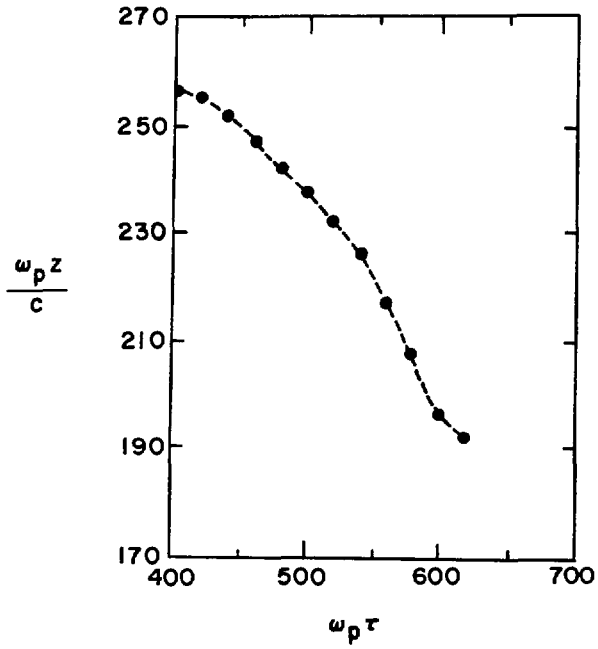

Fig. 1.

Position of electron reflection point ($\gamma = 1$) as a function time; $\Omega = 4\ \omega_p$, $\gamma_0 = 5$, $v_0 = 1.2$ V, $R_w = 5.44\ (z/170)$, $R_{bi} = 2.18$, $R_{bo} = 3.11$, $\nu = \nu_0[1 + (t - 325)/\tau]$, $\tau = 500$.

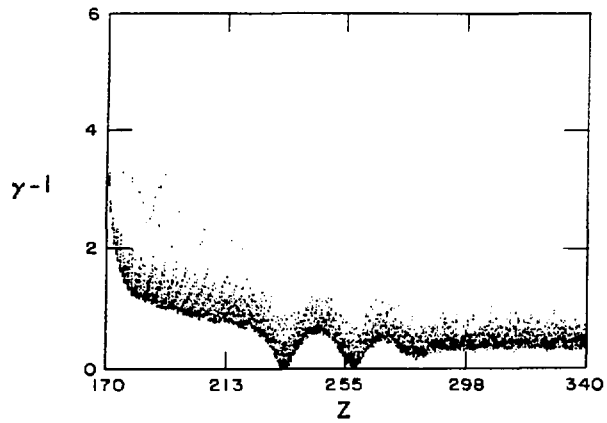

Fig. 2

Energy phase space at $\omega_p t = 520$, same parameters as in Fig. 1.

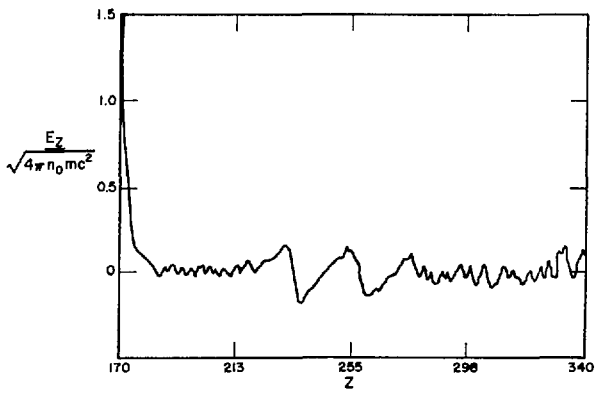

Fig. 3.

Axial electric field as a function of space for beam configuration shown in Fig. 2.

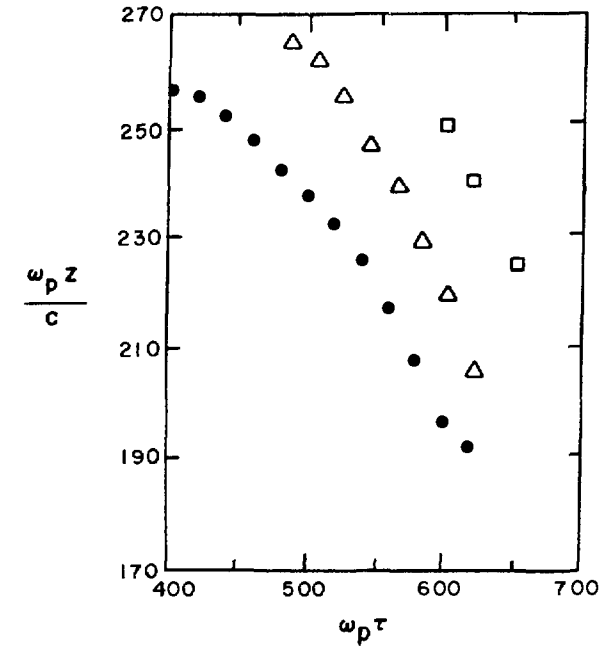

Fig. 4

Trajectories of multiple virtual cathodes such as in Fig. 2; primary, secondary, tertiary.

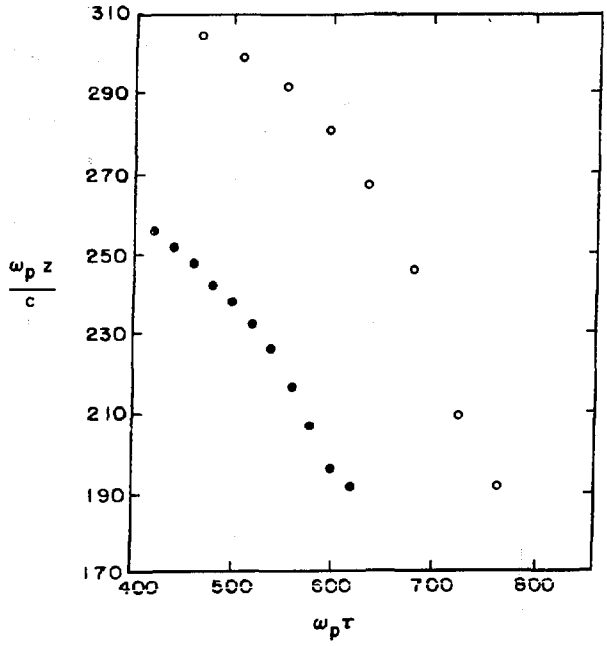

Fig. 5.

Trajectories of primary virtual cathodes calculated in old (·) and new (o) versions of simulation code.

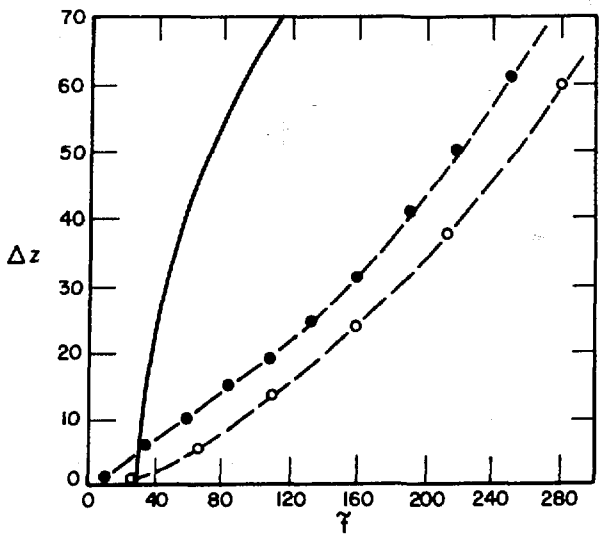

Fig. 6.

Trajectories shown in Fig. 5 plotted versus $\nu = \nu_0[1 + (t - t_0 - z/v_0)]$.

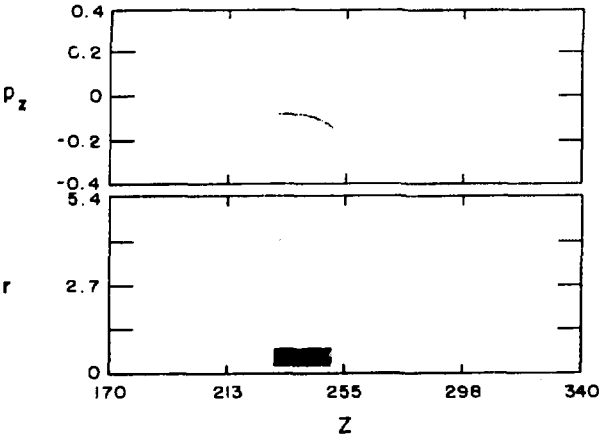

Fig. 7a.

Ion phase and configuration space plots at $\omega_p t = 420$, $|q/M_i| = 0.02$; negative ion p_z vs z and negative ion r vs z.

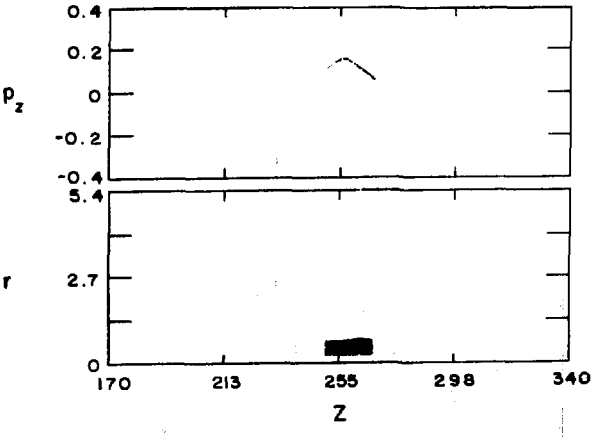

Fig. 7b.

Positive ion p_z vs z and positive ion r vs z.

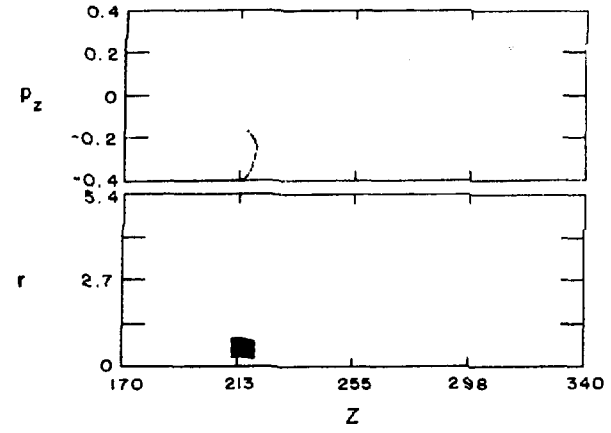

Fig. 8a.

Ion phase and configuration space plots at $\omega_p t = 560$, $|q/M_i| = 0.02$; *negative ion* p_z *vs* z *and negative* ion r vs z.

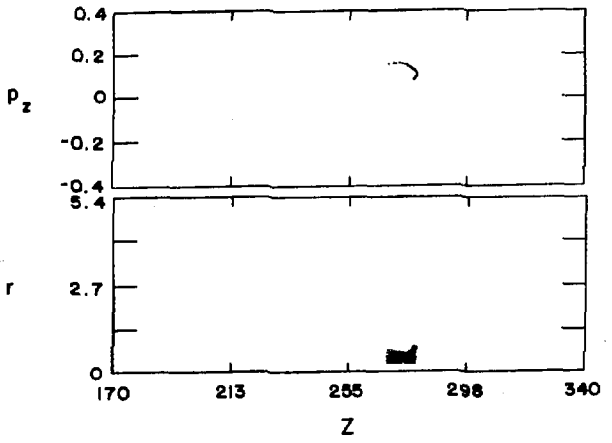

Fig. 8b.

Positive ion p_z vs z and positive ion r vs z.

APPENDIX J

A GALERKIN ALGORITHM FOR MULTIDIMENSIONAL PLASMA SIMULATION CODES

To be published as a Los Alamos Scientific Laboratory report.

A GALERKIN ALGORITHM FOR MULTIDIMENSIONAL PLASMA SIMULATION CODES

by

Brendan B. Godfrey

ABSTRACT

A Galerkin finite element differencing scheme has been developed for a computer simulation of plasmas. The new difference equations identically satisfy an equation of continuity. Thus, the usual current correction procedure, involving inversion of Poisson's equation, is unnecessary. The algorithm is free of many numerical Cherenkov instabilities. This differencing scheme has been implemented in CCUBE, an already existing relativistic, electromagnetic, two-dimensional PIC code in arbitrary separable, orthogonal coordinates. The separability constraint is eliminated by the new algorithm. The new version of CCUBE exhibits good stability and accuracy with reduced computer memory and time requirements. Details of the algorithm and its implementation are presented.

I. INTRODUCTION

Realistic computer simulation of intense relativistic beam phenomena typically is very demanding. Boundary conditions are complex and often have a dominant effect on the physics. Significant space and time scales usually are of disparate magnitudes. There is occasional need for exotic coordinate systems. In general, relativistic plasma PIC simulations are more prone to numerical instability than nonrelativistic plasma simulations. To cope better with these considerations, we have implemented a Galerkin finite element difference algorithm into an already existing two-dimensional plasma simulation code, CCUBE.

The Galerkin algorithm represents the electric and magnetic fields as sums of finite elements, in this case splines. Equations interrelating the

coefficients of the finite elements, effectively the field values at mesh points, are derived by inserting the expansion for the fields into the usual Lagrange variational integral and minimizing the integral with respect to the coefficients. This procedure not only gives a discretized set of Maxwell's equations but also specifies a consistant interpolation procedure between the fields and the simulation particles. Galerkin's method is employed successfully in many branches of computational physics and engineering. References 1 and 2 provide good overviews. Lewis has discussed the application of Galerkin's method in the spatial domain to plasma simulation,[3,4] while Godfrey has outlined the extension to space and time.[5,6]

In plasma simulation Galerkin algorithms conserve charge on the mesh, conserve momentum along cyclic coordinates, minimize energy errors, and ameliorate certain numerical instabilities.[7] It is the first of these features that we wish to emphasize. If the charge and current densities on the mesh satisfy a discretized equation of continuity, then Maxwell's equations may be advanced explicitly in time without inversion of Poisson's equation to obtain the electrostatic potential or to correct the longitudinal current. Dispensing with Poisson's equation greatly facilitates use of nonseparable coordinates and irregular boundaries.

Features of CCUBE, the two-dimensional plasma simulation code in which the algorithm has been implemented, can be summarized as follows. CCUBE was developed specifically for charged particle beams and, hence, is relativistic and fully electromagnetic. It runs in any orthogonal coordinate system, accommodates irregularly shaped boundaries and internal structures, and injects and absorbs particles at any of the boundaries. The code supports extensive diagnostics, generates movies, and is optimized for the CDC-7600 computer. More details are given in Ref. 8. CCUBE has been employed in a variety of applications, including electron beam heating of plasma, ion beam propagation, collective ion acceleration,[9,10] space-charge limited flow,[8] electron beam diodes, slow-wave structures,[11] and free electron lasers.

II. DESCRIPTION OF THE ALGORITHM

The heart of the Galerkin algorithm described here is the interpolation between particles and fields. The spatial interpolation procedure in two dimensions is

$E^{(3)}$, $J^{(3)}$, ρ	Linear in X_1 and X_2
$E^{(1)}$, $J^{(1)}$, $B^{(2)}$	NGP in X_1, linear in X_2
$E^{(2)}$, $J^{(2)}$, $B^{(1)}$	Linear in X_1, NGP in X_2
$B^{(3)}$	NGP in X_1 and X_2 .

NGP designates nearest grid point interpolation. The fields and currents are staggered on the spatial mesh in the groups just listed. See Fig. 1.

Further setting apart the algorithm is its requirement for temporal interpolation. As in conventional approaches, electric fields are applied to particles at discrete times. However, the magnetic field is applied throughout each time step, NGP interpolation in time. Moreover, during each time step the average current during the time step is computed, again NGP interpolation. The particle charge density is not needed except at initialization and for diagnostics. It is evaluated at discrete times. Actually performing these NGP temporal interpolations is, unfortunately, impractical. Therefore, we settle for an N point quadrature as an approximation. The magnetic field is applied to the particles at N uniformly spaced points in time during each time step. The instantaneous current is evaluated at each time point and the N values averaged to provide input to the field solver. The particle equations are explicitly

$$dx/dt = \gamma^{-1} P$$

$$dP/dt = E^{m} \delta(t - m\Delta t) + N^{-1} \sum_{i=1}^{N} \gamma^{-1} P \times B^{m+\frac{1}{2}} \delta(t - m\Delta t - \alpha_i \Delta t) \tag{1}$$

$$J^{m+\frac{1}{2}} = N^{-1} \sum_{i=1}^{N} \gamma^{-1} P \, \delta(t - m\Delta t - \alpha_i \Delta t)$$

$$\alpha_i = (i - \tfrac{1}{2})/N \qquad i = 1,N$$

For simplicity the equations are given for rectangular coordinates only. Generalization to curvilinear systems is straightforward. Note that we have considered in some detail the locations of the temporal quadrature points. The uniform spacing indicated generally is optimal. Although the quadrature approaches true NGP interpolation only as the number of points becomes infinite, using just a few points typically gives good results. Figure 1 illustrates the temporal evolution of particles and fields for N = 2.

The field equations naturally consistant with the interpolation procedures described above involve nine-point differencing. However, we have found that five-point differencing gives nearly as good accuracy with reduced computation per time step and a slightly relaxed Courant condition. Only when greater accuracy for high-frequency light-wave phase velocities is required is the nine-point scheme noticably superior. With this choice the electric fields are initialized from Gauss' law, Eq. (2).

$$\left[E^{(1),0}_{n_1+\frac{1}{2},n_2} - E^{(1),0}_{n_1-\frac{1}{2},n_2}\right]\Big/\Delta x_1 + \left[E^{(2),0}_{n_1,n_2+\frac{1}{2}} - E^{(2),0}_{n_1,n_2-\frac{1}{2}}\right]\Big/\Delta x_2 = \rho^0_{n_1,n_2} \quad . \qquad (2)$$

A similar expression exists for the magnetic fields,

$$\left[B^{(1),\frac{1}{2}}_{n_1+1,n_2+\frac{1}{2}} - B^{(1),\frac{1}{2}}_{n_1,n_2+\frac{1}{2}}\right]\Big/\Delta x_1 + \left[B^{(2),\frac{1}{2}}_{n_1+\frac{1}{2},n_2+1} - B^{(2),\frac{1}{2}}_{n_1+\frac{1}{2},n_2}\right]\Big/\Delta x_2 = 0 \quad . \qquad (3)$$

How these equations are best solved depends on the details of the physical configuration being initialized. Sometimes it is necessary to solve Eqs. (2) and (3) simultaneously with force balance equations for the particle distribution. In any case it is critical to satisfy the field initialization equations very accurately, as errors introduced here persist throughout the simulation. The electric and magnetic fields, once initialized, are stepped forward in time according to Eqs. (4) and (5), using currents defined above.

$$\left[E^{(1),m+1}_{n_1+\frac{1}{2},n_2} - E^{(1),m}_{n_1+\frac{1}{2},n_2}\right]\Big/\Delta t = -\left[B^{(3),m+\frac{1}{2}}_{n_1+\frac{1}{2},n_2+\frac{1}{2}} - B^{(3),m+\frac{1}{2}}_{n_1+\frac{1}{2},n_2-\frac{1}{2}}\right]\Big/\Delta x_2$$

$$- J^{(1),m+\frac{1}{2}}_{n_1+\frac{1}{2},n_2}$$

$$\left[E^{(2),m+1}_{n_1,n_2+\frac{1}{2}} - E^{(2),m}_{n_1,n_2+\frac{1}{2}}\right]\Big/\Delta t = -\left[B^{(3),m+\frac{1}{2}}_{n_1+\frac{1}{2},n_2+\frac{1}{2}} - B^{(3),m+\frac{1}{2}}_{n_1-\frac{1}{2},n_2+\frac{1}{2}}\right]\Big/\Delta x_1 \qquad (4)$$

$$- J^{(2),m+\frac{1}{2}}_{n_1,n_2+\frac{1}{2}}$$

$$\left[E^{(3),m+1}_{n_1,n_2} - E^{(3),m}_{n_1,n_2}\right]\Big/\Delta t = \left[B^{(2),m+\frac{1}{2}}_{n_1+\frac{1}{2},n_2} - B^{(2),m+\frac{1}{2}}_{n_1-\frac{1}{2},n_2}\right]\Big/\Delta x_1$$

$$- \left[B^{(1),m+\frac{1}{2}}_{n_1,n_2+\frac{1}{2}} - B^{(1),m+\frac{1}{2}}_{n_1,n_2-\frac{1}{2}}\right]\Big/\Delta x_2 - J^{(3),m+\frac{1}{2}}_{n_1,n_2}$$

$$\left[B^{(1),m+\frac{1}{2}}_{n_1,n_2+\frac{1}{2}} - B^{(1),m-\frac{1}{2}}_{n_1,n_2+\frac{1}{2}}\right]\Big/\Delta t = -\left[E^{(3),m}_{n_1,n_2+1} - E^{(3),m}_{n_1,n_2}\right]\Big/\Delta x_2$$

$$\left[B^{(2),m+\frac{1}{2}}_{n_1+\frac{1}{2},n_2} - B^{(2),m-\frac{1}{2}}_{n_1+\frac{1}{2},n_2}\right]\Big/\Delta t = \left[E^{(3),m}_{n_1+1,n_2} - E^{(3),m}_{n_1,n_2}\right]\Big/\Delta x_1 \qquad (5)$$

$$\left[B^{(3),m+\frac{1}{2}}_{n_1+\frac{1}{2},n_2+\frac{1}{2}} - B^{(3),m-\frac{1}{2}}_{n_1+\frac{1}{2},n_2+\frac{1}{2}}\right]\Big/\Delta t = -\left[E^{(2),m}_{n_1+1,n_2+\frac{1}{2}} - E^{(2),m}_{n_1,n_2+\frac{1}{2}}\right]\Big/\Delta x_1$$

$$+ \left[E^{(1),m}_{n+\frac{1}{2},n+1} - E^{(1),m}_{n+\frac{1}{2},n}\right]\Big/\Delta x_2 \quad .$$

It is interesting that within the context of the Galerkin algorithm the magnetic field equations, Eqs. (3) and (5), *are free of truncation error.* Substitution of the finite element expansions of the electric and magnetic fields into Maxwell's equations give Eqs. (3) and (5) identically without approximation. That Eq. (5) is exact means that finite element differencing schemes

based on scaler and vector potentials can be constructed such that they yield numerical results identical to the present algorithm based directly on the fields. Moreover, those potential algorithms are related by a limited algebraic gauge invariance.[5] The field equations given in this report are to be preferred only because they are more convenient to implement.

Although Eqs. (3) and (5) are truncation error-free, Eqs. (2) and (4) are not. Nonetheless, an algebraic relation exists among them. Substituting Eq. (2) into Eq. (4) yields

$$\left[J^{(1),m+\frac{1}{2}}_{n_1+\frac{1}{2},n_2} - J^{(1),m+\frac{1}{2}}_{n_1-\frac{1}{2},n_2}\right]\Big/\Delta x_1 + \left[J^{(2),m+\frac{1}{2}}_{n_1,n_2+\frac{1}{2}} - J^{(2),m+\frac{1}{2}}_{n_1,n_2-\frac{1}{2}}\right]\Big/\Delta x_2$$

$$+ \left[\rho^{m+1}_{n_1,n_2} - \rho^{m}_{n_1,n_2}\right]\Big/\Delta t = 0 \quad . \tag{6}$$

This relation is recognizable as an equation of continuity for the interpolated charge and currents. Note, however, that it follows naturally from the discretized electric field equations and is not introduced in some ad hoc fashion. Alternatively, Eq. (6) can be viewed as a consistancy relationship. If it is true, then Eq. (2) satisfied at one time step is necessarily satisfied at all time steps. Unfortunately, Eq. (6) is exact only for a true Galerkin algorithm. The quadrature approximation introduced into the particle equations, Eq. (1), gives rise to small errors in Eq. (6). Determining their magnitude is one goal of the simulations outlined in the following section.

III. PRELIMINARY TEST RESULTS

As a test of the algorithm, we have performed a series of simulations of a nonneutral relativistic electron beam propagating along a guide magnetic field in a metallic waveguide. Simulations are doubly aperiodic in cylindrical coordinates with $\Delta z = 0.391$, $\Delta r = 0.185$, and $\Delta t = 0.165$. (Units are chosen such that $c = \omega_p = 1$.) There are approximately four electrons per occupied cell. Standard smoothing is applied to the shortest wavelengths of the interpolated current. Beam parameters are $v = 1.75$, $\gamma = 7.0$, and $\omega_c = 2.0$. The beam enters through a ground plane and, therefore, bounces radially as it propagates. Such configurations are characteristic of some collective ion acceleration studies.[9] Figure 2 is a movie frame taken from one simulation. The beam enters from the

left and exits at the right, although some electrons strike the waveguide at r = 3.8 and are absorbed.

These accuracy tests were intended to be as realistic as possible. Thus, the results are presented even though the simulations were subsequently found to be weakly numerically unstable. The instability, which typically is absolute, occurs at large perpendicular wave numbers and arises from the interaction of high-frequency light waves and aliases of the Doppler-shifted beam modes. In other tests in which this instability is suppressed, accuracy is much improved. The present results, shown in Figs. 3 and 4, are nonetheless satisfactory.

In each figure we compare results for N = 1-, 2-, and 3-point quadratures. These results are contrasted with those of a "control" case, the canonical momentum algorithm discussed in Ref. 12 and implemented in an earlier version of CCUBE.

CCUBE is almost entirely vectorized, and for optimized running on the CDC-7600 employs the vector arithmetic package STACKLIB[13] and a few specially written vector routines.[14] Perhaps, a 25% increase in speed could be achieved by hand-coding key subroutines in assembly language but at the cost of considerable effort and a loss of flexibility. Figure 3a gives total central processor running time per particle per time step for our tests. Production runs for the same physical parameters would be nearly 10% faster due to a reduced need for diagnostics. The new algorithm actually is faster for one- and two-point quadratures and is equal in speed to the control algorithm for three points. The savings result principally from eliminating the Poisson equation solver, which is quite slow in curvilinear coordinates.

Continuity errors, a significant factor in evaluating the quadrature approximation to our Galerkin algorithm, are determined by evaluating the errors in Eq. (2) at late times. Figure 3b shows the relative RMS accumulated error at t = 200. For the control case, the usual current correction routine is bypassed. We see systematic improvement in the error as the number of quadrature points is increased. Recall that all these test simulations were mildly numerically unstable. Further simulations with that instability suppressed show a marked decrease in the continuity errors. We shall report on those results at a later date.

Both algorithms are of the "energy conserving" type[3,4] and exhibit very good total energy conservation over long periods of time as illustrated in

Fig. 4a. The accuracy is particularly impressive in view of the large energy fluxes through the boundaries. The linear decrease in energy error with increasing number of quadrature points results principally from the improved integration of cyclotron orbits about the magnetic guide field.

Relative noise levels given in Fig. 4b were obtained by comparing the peak amplitudes of high-frequency electric field fluctuations with the average amplitudes of the low-frequency electric fields. Relative energy densities were, of course, much lower and rarely exceeded one percent. Although some of this noise is physical, most of it is caused by particle discreteness effects near the boundaries and by the weak numerical instability already mentioned. Increasing the number of quadrature points decreases the former effect. It is straightforward to reduce further the noise levels by judicious smoothing, if desired.

IV. CONCLUSIONS

A proper evaluation of the Galerkin space-time-symmetric algorithm clearly requires additional practical experience. We offer as a tentative judgment that the Galerkin algorithm in CCUBE generally is competitive with more conventional finite difference algorithms and yields significant advantages in cases when solution of Poisson's equation is burdensome. Clearly, it is at its best in multidimensional curvilinear systems. In closing, we make some more specific observations.

The Galerkin algorithm facilitates simulations in complex geometries. Particle motion in large magnetic fields is treated well. Energy is very well conserved. Noise levels are adequately low, although current smoothing is sometimes required. Residual continuity errors accumulate slowly and, if desired, can be eliminated by occasional reinitialization of the electrostatic fields. Numerical Cherenkov instabilities[7,12] are to some extent suppressed. Computer requirements are not excessive.

ACKNOWLEDGMENTS

This project has profited from the contributions of far more people than can be acknowledged individually here. Their assistance is no less appreciated. This research was performed under the auspices of the U. S. Department of Energy, with additional support from the U. S. Army Ballistic Missile Defense Advanced Technology Center and the U. S. Air Force Weapons Laboratory.

Vector scatter-gather routines were written by K. Fong; a vector reciprocal square root routine was written by L. Rudsinski.

REFERENCES

1. S. G. Mikhlin, The Numerical Performance of Variational Methods (Wolters-Noordhoff, Groningen, 1971).

2. B. A. Finlayson, The Method of Weighted Residuals and Variational Principals (Academic Press, New York, 1972).

3. H. R. Lewis, "Application of Hamilton's Principle to the Numerical Analysis of Vlasov Plasmas," Meth. Comput. Phys. 9, 307 (1970).

4. H. R. Lewis, "Variational Algorithms for Numerical Simulation of Collisionless Plasma with Point Particles Including Electromagnetic Interactions," J. Comput. Phys. 10, 400 (1972).

5. B. B. Godfrey and L. E. Thode, "Galerkin Difference Schemes for Plasma Simulation Codes," Proc. 7th Conf. Num. Sim. Plas., New York, 1975, p. 87.

6. B. B. Godfrey, "Application of Galerkin's Method to Particle-in-Cell Plasma Simulation Codes," Proc. 8th Conf. Num. Sim. Plas., Monterey, California, 1978, PE-3.

7. B. B. Godfrey, "Numerical Cherenkov Instabilities in Electromagnetic Particle Codes," J. Comput. Phys. 15, 504 (1974).

8. L. E. Thode, B. B. Godfrey, and W. R. Shanahan, "Vacuum Propagation of Solid Relativistic Electron Beams," Phys. Fluids, to be published.

9. B. B. Godfrey, "Numerical Simulation of Autoresonant Ion Acceleration," IEEE Plasma Sci. 5, 223 (1977).

10. B. B. Godfrey, "The Localized Pinch Model as a High Energy Ion Collective Acceleration Mechanism," IEEE Plasma Sci. 6, 256 (1978).

11. R. J. Faehl, B. S. Newberger, and B. B. Godfrey, "Simulation of Cyclotron Wave Growth in a Helical Slow Wave Structure," Phys. Fluids, to be published.

12. B. B. Godfrey, "Canonical Momenta and Numerical Instabilities in Particle Codes," J. Comput. Phys. 19, 58 (1975).

13. F. H. McMahon, L. J. Sloan, and G. A. Long, STACKLIB (Lawrence Livermore Laboratory, 1977).

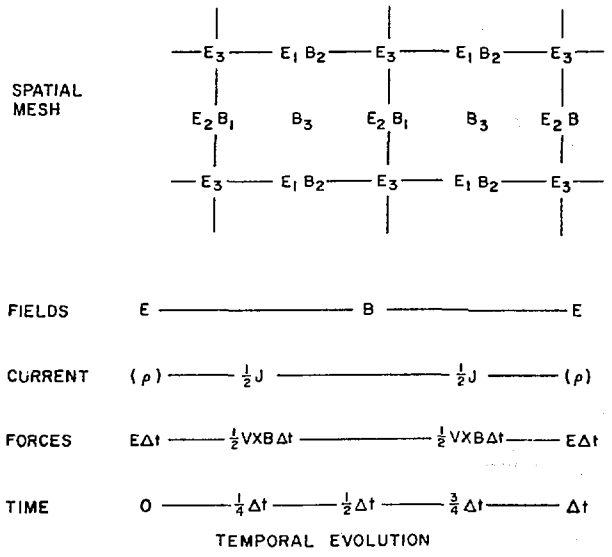

Fig. 1

CCUBE employs a field mesh staggered in both space and time. Corresponding components of J and E are collocated in space. The temporal evolution illustrates an N = 2 quadrature.

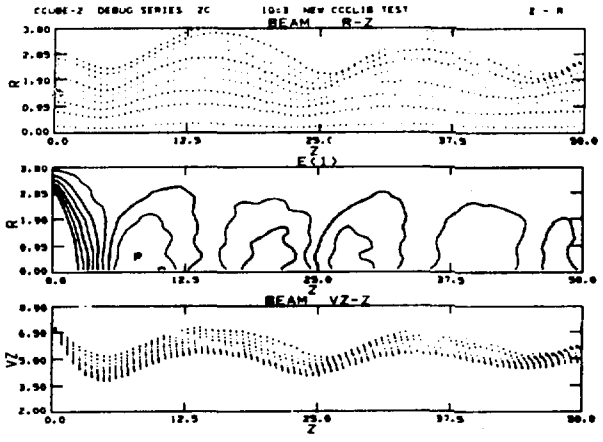

Fig. 2

Typical movie frame from test simulation of beam propagation in cylindrical drift tube, showing electron positions, contours of the axial electric field, and electron axial momenta.

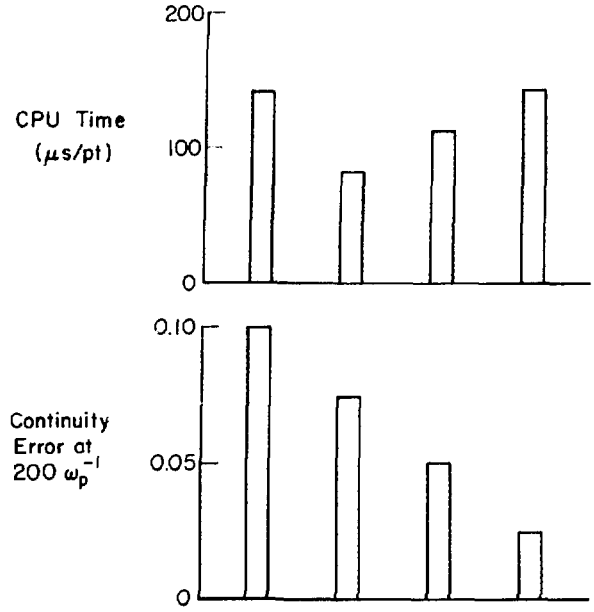

Fig. 3

Compared to conventional algorithms, the Galerkin method is reasonably fast and accumulates continuity errors slowly.

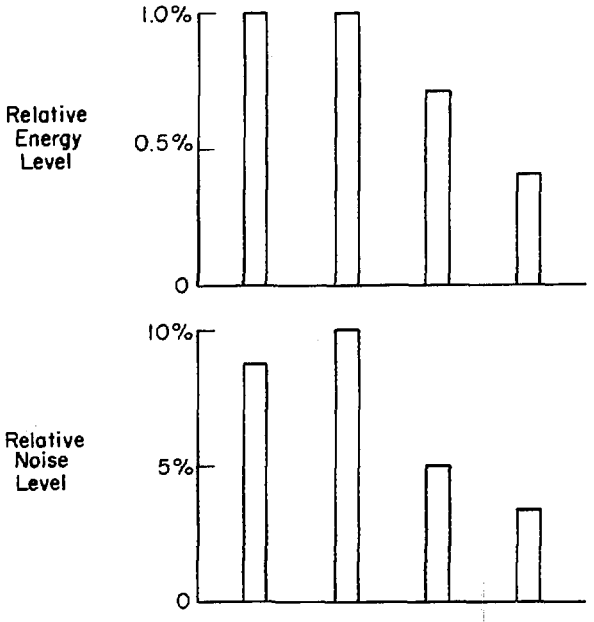

Fig. 4

Energy conservation and noise suppression are good with the Galerkin algorithm.

☆ U.S. Government Printing Office: 1979 – 677-013/136